UNIVERSIDAD AUTÓNOMA DE MADRID
Programa de Doctorado en Biociencias Moleculares

Doctoral Thesis

Differential roles of vesicle trafficking modulators RAB7 and RAB27 in melanoma progression and metastasis

RAÚL MARTÍNEZ HERRANZ

Madrid, 2018

UNIVERSIDAD AUTÓNOMA DE MADRID

Facultad de Medicina
Departamento de Bioquímica

Doctoral Thesis

Dissecting the role of the vesicle trafficking modulators RAB7 and RAB27 in melanoma progression and metastasis

RAÚL MARTÍNEZ HERRANZ

Licenciado en Biotecnología

Thesis Director
Dr. María S. Soengas

Melanoma Group (Molecular Oncology Program)

Spanish National Cancer Research Center

Madrid, 2018

Dr. María S. Soengas, Head of the Melanoma Group at Molecular Oncology program of the Spanish National Cancer Research Center (CNIO)

CERTIFIES:

That the study **"Differential roles of vesicle trafficking modulators RAB7 and RAB27 in melanoma progression and metastasis."** developed by **Raúl Martínez Herranz** meets the necessary requirements to obtain the **PhD Degree** and, to this purpose, will be presented at the Universidad Autónoma de Madrid. This work has been carried out under my direction and hereby I authorize its defense to a specific PhD Committee assembled for this purpose.

I hereby issue this certification in Madrid on March 5th 2018.

María S. Soengas
PhD, Thesis Director

The work in this doctoral thesis was carried out in the Melanoma Group at the Spanish National Cancer Research Centre (CNIO) from April 2013 to March 2018 under the supervision of Dr. María S. Soengas.

This work has been supported by the following fellowships and grants:

- "Formación de Profesional Investigador" (FPI) Fellowship, awarded by the Spanish Ministry of Economy and Competitiveness. SAF2011-28317 (20013-2017)
- RETOS Program. María S. Soengas (2017-2018)

A los pacientes.

ACKNOWLEDGEMENTS

AGRADECIMIENTOS

Nunca olvidaré el primer día que crucé la puerta del CNIO, esta tesis representa el final de una etapa, que ha sido a la vez la más enriquecedora y difícil de mi vida, a pesar de que sé que esto solo me coloca en el punto de partida. Sin embargo, una tesis doctoral nunca es un trabajo individual hay mucha gente involucrada, por lo tanto quiero aprovechar estas páginas para daros las gracias por todo el apoyo, amistad y compañerismo que han permitido sacar adelante este trabajo.

En primer lugar, me gustaría agradecer a mí directora de tesis **Marisol** por confiar en mí y darme la oportunidad de unirme a su maravilloso grupo, y llevar a cabo este apasionante proyecto que me ha permitido desarrollarme tanto personal como profesionalmente.

Dentro del Melanoma lab, quiero daros las **GRACIAS** a todos por vuestro apoyo y a mistad durante estos años ¡y los que nos quedan! **Estela**, tu labor es clave en el grupo, como lab manager, psicóloga, consejera, amiga, muchísimas gracias por todo tu apoyo durante estos años, voy a echar de menos los cafés por la mañana, y las "chapas" que me caían de vez en cuando (estas no tanto). **Cristina**, "la princesita", tu llegada al labo fue como un rayo de alegría tu siempre tan modesta y callada, ;) gracias por estar ahí. ¡sabes que contar todas las anécdotas darían para otra tesis! Así que lo resumiremos en gracias por las meriendas, por las largas horas de cultivos, las cenas en el labo a las 23. Trabajar con amigos así es un placer, no cambies nunca. **Susana**, cuando me vaya podrás expandirte y por fin ocupar mi sitio para que nadie te haga sombra en el 306. ¡Es broma! Muchísimas gracias por ser tan crack y portodos tus consejos con los experimentos y con la tesis. **Tonan**, gracias por toda tu ayuda con los experimentos con los ratones y por obligarme a mantener bajo control mi "pequeño caos". **Daniela**, mi compañera de tesis, mucha suerte en la recta final y muchas gracias por todos los dibujos de células y tu saber enciclopédico del sistema inmune, sin olvidar tu "humor especial" durante estos años. **David**, el senior del lab, muchas gracias por tu ayuda con los experimentos de ratones, el odioso IVIS y todo tu conocimiento sobre la metástasis, mucha suerte con el proyecto de MDK, no siempre se tiene la oportunidad de hacer la tesis junto a un proyecto de primer nivel **Paula,** ¿Te he dicho alguna vez que me

encanta el dulce de leche? Muchas gracias por tu ayuda con las pieles y por ser una magnífica compañera de laboratorio, tan organizada y tranquila, a ver si se me pega algo ¡Tenemos pendientes más salidas nocturnas! **Xavi**, nuestro independentista–anarquista vacilón, tenemos que volver a salir a correr, mucha suerte con esas dendríticas e immunofluorecencias y nunca cambies tu sentido del humor. **Marta**, la chica más dulce (y cabezota, con cariño) de todo el CNIO, mucha suerte con el doctorado, con tu constancia estoy seguro de que te va a ir genial, nunca pierdas la ilusión. **Davide**, el napolitano, sigo esperando la pizza eh? Ha sido un placer conocerte y te desea lo mejor en tu estancia. Por último, **Dani**, un placer tenerte como predoc-adoptado estos meses, suerte con todo que el final está ya cerca.

No quiero dejar de mencionar a todos aquellos compañeros con los que coincidí **Direna**, muchas gracias por empezar este proyecto que ha sido un placer y un honor continuar. **Eva,** gracias esos ribeiros en el Ondiñas y tu ayuda en mis primeros años**. Metehan,** el gran analista del laboratorio, no hay problema que no puedas resolver ni análisis que no puedas realizar, **Takis,** ánimo, no todo es tan malo como lo pintas, siempre negativo, gracias por tu ayuda durante todos estos años, **Lisa**, la alemana más marchosa ¡tenemos que volver a Hombrados! pero con **María,** la super-mami postdoc, era increíble ver como podías con todo y **Ana**, la valenciana con mejor gusto culinario, ¡mucha suerte con la tesis! Por último una mención especial a **Ángel** y **Alicia** por guiarme en los primeros pasos en el camino del doctorado en melanoma lab. No quiero dejar de mencionar a todos los estudiantes que hemos tenido brevemente en el laboratorio: **Jesús, Miguel Ángel, Bea, Celia, Lucía, Sandra Paula y Luna.**

También me gustaría agradecer a todos los trabajadores del CNIO, con muchos de ellos he desarrollado una relación más allá del mero compañerismo y saludos sin palabras al cruzarnos en los pasillos muchas GRACIAS. **Montero,** sobran las palabras, **Tim, Isidoro, Cristina Balbás** y **Almudena,** Escuelab ha sido una de las mejores cosas de esto años, ¡gracias por darme la oportunidad de participar! También a **Teresa, Leire y Miguel Ángel** entre otros, porque sería imposible nombrarlos a todos. Un agradecimiento especial a esa gente molona de

Estructual**: Chevi, Marta y Paco,** nunca perdáis vuestra alegría. Y a la gente del grupo de **Héctor Peinado** por esos lab meetings y las tardes eternas en el Nanosight: **Ana, Teresa, Lucía Susana y Marina**.

Y también a las unidades técnicas por su profesionalidad, simpatía y todo lo que he aprendido durante estos años: Microscopía Confocal **Diego Manu** y **Jesús**. A toda la Unidad de Proteómica, en especial a **Javier, Nuria** (sin ti este trabajo habría salido Adelante) y **Fernando**. Microscopía electrónica, **Jaska**, y por último Histopatología, muchas gracias a **Patricia** y **Zaira** y el resto del equipo ¡sobre todo en la recta final! También quiero agradecer a **Lucía** el hacernos la vida más fácil cuando se trataba de tareas burocráticas y a **Gloria** por venir a alegrarnos las tardes y dejar el laboratorio impoluto.

También quiero mencionar la suerte de haber conocido a una serie de personas, que aunque no son del laboratorio me han brindado su apoyo y amistad durante estos años En especial, **David y Carlos,** por todas esas fiestas. **Amaia**, "la tranquila navarra" **Luisa, Olaya** y **Alba** por nuestro "Piso Libertario**"** y **Leila y Lola por** todas esas tardes de cervezas.

Por último, pero no por ello menos importantes a mi familia, por que ha pesar de sus rarezas y excentricidades es la mejor que podía tener. En primer lugar a mi **padre** y a mi **madre**, por su apoyo incondicional y animarme para no rendirme nunca, por su paciencia y por estar siempre ahí cuando les necesito. También a todos mis tíos y primos, y por último una mención especial a Hombrados, el "paraíso" y a la mejor cuadrilla que se puede tener: **Ruth Itzi Gema Daniel** y **Juan Carlos.**

Lo importante no es la meta sino disfrutar el camino

CONTENTS

ÍNDICE

I.

ABBREVIATIONS

ABREVIATURAS

ACN	Acetonitrile
ALM	Acral Lentiginous Melanoma
ALR	Autophagic Lysosome Reformation
AKT	v-Akt murine thymoma viral oncogene homolog
ALDH	Aldehyde Dehydrogenase
ANOVA	Analysis of Variance
ARID1/2	AT-Rich Interaction Domain 1 and 2
ARL8B	ADP Ribosylation Factor Like GTPase 8B
ASAH1	N-Acylsphingosine Amidohydrolase 1
ATG	Autophagy Related Genes
BCL2	B-cell lymphoma 2
BIRC7	Baculoviral IAP Repeat Containing 7
BRAF	v-raf murine sarcoma viral oncogene homolog B
BrdU	Bromodeoxyuridine
BSA	Bovine Serum Albumin
C6	6 Carbons
CBE	Confutirol B Epoxide
CCND1	Cyclin D1
CCZ1	CCZ1 Homolog, Vacuolar Protein Trafficking And Biogenesis Associated
CD	Cluster of Differentiation
CERS	Ceramide Synthase
CI-M6PR	Cation Independent Manose 6 Phosphate Receptor
CID/CAD	Collision-Activated Dissociation/Decomposition
CM	Conditioned Medium
CMT2B	Charcot-Marie-Tooth type 2B
CNIO	Centro Nacional de Investigaciones Oncológicas
CNS	Central Neural System
COP9S	Constitutive Photomorphogenic Subunit 9
CORVET	Class C CORe Vacuole/Ensosome Tethering Comples
CPEB4	Cytoplasmic Polyadenylation Element Binding Protein 4
CUBP1	CUGBP Elav-Like Family Member 1

CTS	Cathepsins
DAPI	4,6-diamidino-2-phenylindole
DEK	DEK Oncogene
DMEM	Delbucco´s Modified Eagle´s Medium
DMSO	Dimethyl sulfoxide
DN	Dominant Negative
DRM	Detergent Resistant Membranes
DTT	Dithiothreitol
E1A	Adenovirus early region 1A
EC	Endothelial Cells
ECM	Extracellular Matrix
EEA1	Early Endosome Antigen 1
EGF	Epithelial Growth Factor
EGFR	Epithelial Growth Factor Receptor
ER	Endoplasmic Reticulum
ERBB4	Erb-B2 Receptor Tyrosine Kinase 4
ETV1	ETS Variant 1
ESCRT	Endosomal Sorting Complex Required for Transport.
EZH2	Enhancer Of Zeste 2 Polycomb Repressive Complex 2 Subunit
FACS	fluorescence-activated cell sorting
FA	FA Lysis Buffer
FASP	Filter Aided Sample Preparation
FBS	Fetal Bovine Serum
FDR	False Discovery Ratio
FYCO1	FYVE and collected domain containing 1
GAP	GTPase Activating Proteins
GBA	Glucosylceramidase
GDP	Guanosine Diphosphate
GEF	Guanine Exchange Factor
GNAQ	G Protein Subunit Alpha Q
GO	Gene Ontology
GSEA	Gene Set Enrichment Analysis
GTP	Guanosine Triphosphate

H&E	Hematoxylin and Eosin
HNSCC	Head and Neck Squamous Cell Carcinoma
HOPS	Homotypic fusión and Sorting Complex
HRAS	v-Ha-ras Harvey rat sarcoma viral oncogene homolog
HRP	Horse Radish Peroxidase
HSPA5	Heath Shock Protein A5
IF	Immunofluorescence
IAA	Indoleacetic Acid
IgG	Immunoglobulin G
IHC	Immunohistochemistry
iTRAQ	isobaric Tag for Relative and Absolut Quantification
JNK	c-Jun N-terminal Kinases
KEGG	Kyoto Encyclopedia of Genes and Genomes
KIT	Proto-Oncogene Receptor Tyrosine Kinase
LAMP	Lysosomal membrane protein
LBPA	lysobisphosphatidic acid
LC3	Microtubule-associated protein 1 light chain 3
LC-MS/MS	Liquid Chromatography Tandem-Mass Spectrometry
LDLR	Low Density Lipoprotein Receptor
LMN	Lentigo Malignant Melanoma
LRP	Low density lipoprotein-Related Protein
LRO	Lysosomal Related Organelle
MAPK	Mitogen-Activated Protein Kinase
MDM	Mouse double minute 2
MEFS	Mouse Embryonic Fibroblasts
MET	Mesenchymal Epithelial Transition (MET) Proto-Oncogene
MITF	Microphtalmia-associated Transcription Factor
MM	Mucosal Melanoma
MMP	Matrix Metalloproteinase
MON1	MON1 Homolog A, Secretory Trafficking Associated
miR	microRNA
mRNA	messenger RNA
MTP1-MMP	Membrane Type Matrix Metalloproteinase

mTOR	mechanistic target of Rapamycin
MSH	Melanocyte-Stimulating Hormone
MVB	Multivesicular Body
MYC	v-Myc Avian Myelocytomatosis Viral Oncogene Homolog
NBD	Nitrobenzoxadiazole
NEDD9	Neural Precursor Cell Expressed, Developmentally Down-Regulated 9
NES	Normalized Enrichment Score
NF1	Neurofibromin 1
NF-KB	Nuclear Factor Kappa-light-chain-enhancer of activated B cells
NK	Natural Killer cells
NM	Nodular Melanoma
NRAS	Neuroblastoma RAS viral oncogene homolog
NT	Non Treated
OCR	Oxygen Consumption Rate
OIS	Oncogene Induced Senescence
ORP1L	Oxysterol Binding Protein
OS	Overall Survival
OXPHOS	Oxidative phosphorylation
PBS	Phosphate Buffer Saline
pH	Potential of Hydrogen
PCR	Polymerase Chain Reaction
PI3K	Phosphatidylinositol-4,5.biphosphate 3-Kinase
PINK1	PTEN Induced Putative Kinase 1
PPP6C	Protein Phosphatase 6 Catalytic Subunit
PTEN	Phosphatase and Tensin Homolog
qPCR	quantitative Polymerase Chain Reaction
RAB	Ras-related in brain
RabGGT	Rab Geranylgeranyl Transferasa
RAC1	Rac Family Small GTPase 1
RAS	at sarcoma viral oncogene homolog
RB	Retinoblastome
RGP	Radial Growth Phase

RILP	Rab7-interacting Lysosomal Protein
RIP	Regulated Intramembrane Proteolysis
RT	Room Temperature
S1P	Sphingosine 1 Phosphate
SDS-PAGE	Sodium dodecyl sulfate-polyacrylamide gel electrophoresis
SEM	Standard Error of estimate mean
shRNA	short hairpin RNA
siRNA	small interfering RNA
SLAC2	Slp Homolog Lacking C2 Domains A
SLP2	Synaptotagmin-Like Protein 2
SMPD1	Sphingomyelin Phosphodiesterase 1
SNARE	Soluble N-ethylmaleimide-sensitive factor attachment protein receptor
ssGSEA	single sample Gene Set Enrichment Analysis
SSM	Superficial Spreading Melanoma
STRING	Search Tool for the Retrieval of Interacting Genes/Proteins
TBC1D15	TBC1 Domain Family Member 15
TCGA	The Cancer Genome Atlas
TBC1D15	TBC1 domain family member 15
TEM	Transmission Electron Microscopy
TERT	Telomerase Reverse Transcriptase
TGN	Trans Golgi Network
TRP2	tyrosinase-related protein 2
TP53	Tumor Protein P53
TYR	Tyrosinase
TYRP1	Tyrosinase-related protein-1
UM	Uveal Melanoma
USA	United States of America
UVRAG	UV irradiation Resistance-Associated Gene
VGP	Vertical Growth Phase
VPS34	Vacuolar Protein Sorting 34
VSVG	Vesicular stomatitis virus glycoprotein

SUMMARY

II. *PRESENTACIÓN*

Melanoma is a prime example of an aggressive tumor that accumulates a plethora of changes in the transcriptome and the proteome. This accumulation of mutations makes this tumor the most aggressive form of skin cancer. The aggressive nature of this disease is shown by the fact that lesions of barely 2 mm in depth already bear a high metastatic potential. Our group has focused on lineage-specific oncogenic dependencies as a strategy to identify unique or melanoma-enriched proteins that distinguish this tumor from other cancer types. In particular, we previously identified a melanoma-specific rewiring of vesicular trafficking characterized by a cluster of lysosomal genes differentially expressed in melanoma compared with other 35 tumor types. Within this cluster, we demonstrated a dependency of melanoma cells on the small GTPase RAB7. Curiously, RAB7 levels were not constant during tumor progression: high levels favor proliferation, tuned-down expression of RAB7 was associated with an increased metastasis. Instead, downregulation of RAB27, another RAB protein also related to vesicular trafficking and regulated in a lineage-restricted manner in melanoma cells, inhibited melanoma metastasis

Therefore, this PhD thesis was set to (1) Assess the differential impact of RAB7 and RAB27 in vesicular trafficking, (2) Perform a global proteomic analysis of intracellular and secreted fractions of melanoma cell lines upon RAB7 and RAB27 depletion and (3) to define functional differences RAB7 vs RAB27 in invasion and metastasis. To this end, we have observed how RAB7 and RAB27 have non-equivalent roles in cell invasion in auto-and paracrine ways and we have performed a global proteomic analysis of cell extracts and conditioned medium upon RAB7 and RAB27 depletion that allowed us to identify a rewiring of the sphingolipid metabolism pathways upon RAB7 depletion towards ceramide production. Moreover, analysis of the secretome allowed us to identify a cluster of lysosomal proteins specifically secreted. Within this cluster we identified LRP2, a transmembrane protein with unexpected prometastatic roles downstream RAB7 whose subcellular location is ceramide-enriched vesicles which are later secreted. Taken together, the results of this PhD thesis deepens the knowledge of vesicular trafficking in melanoma and establish a novel crosstalk between sphingolipid metabolism and vesicle trafficking modulators.

En la actualidad, el melanoma cutáneo es una de las neoplasias más agresivas y se caracteriza por la manifestación de una masiva acumulación de cambios tanto a nivel transcripcional como proteómico. Esto confiere al melanoma una agresividad intrínseca, por la cual lesiones de una profundidad ínfima presentan un elevado potencial metastásico. Investigaciones recientes desarrolladas en este laboratorio, han dilucidado la relevancia de oncogenes de linaje celular específico como posibles reguladores oncogénicos. Concretamente, se ha identificado una regulación específica del tráfico vesicular en melanoma caracterizada por grupo de genes cuya función está referida al tráfico lisosomal, y cuya expresión en melanoma en comparativa frente a 35 tumores diferentes es diferencialmente elevada. Dentro de este agrupamiento de genes se demostró la dependencia que presentan las células de melanoma en referencia a la pequeña GTPasa de membrana RAB7. En particular, los niveles de RAB7 no se presentan constantes durante la progresión tumoral, sino que presentan una oscilación en su patrón de expresión. Esto es, altos niveles de RAB7 correlacionan con alta tasa proliferativa celular, mientras que una reducción de la expresión de RAB7 se asocia con un incremento en la capacidad metastásica. Esto se debe a que la maquinaria de degradación lisosomal desvía las vesículas hacia un proceso secretor, donde curiosamente otra de las proteínas de la familia de las RABs tiene un papel perfectamente descrito RAB27. Precisamente RAB27 es comúnmente aceptado como un efector de factor de transcripción MITF, uno de los oncogenes de linaje celular específicos en melanoma más ampliamente estudiados.

Por todo eso, esta tesis doctoral se fundamenta en el estudio de (1) las diferencias en tráfico vesicular regulado tanto por RAB7 como por RAB27 en melanoma. (2) Análisis proteómico global de los cambios en el proteoma inducidos por el silenciamiento de RAB7 o RAB27 en el interior celular o en la fracción secretada. (3) Caracterización de las diferencias en la capacidad invasiva y metástasica controladas por RAB7 o RAB27. En el transcurso de esta tesis se han definido las diferencias de forma autocrina y paracrina en cuanto al potencial invasivo celular, siempre fundamentándose en la expresión de RAB7 y RAB27 como objeto de estudio. Además, tras la depleción de RAB7 o de RAB27 se han llevado a cabo experimentos de análisis proteómico masivo partiendo tanto de extractos

celulares como de medio celular condicionado, y su análisis han permitido la identificación de una novedosa vía de señalización metabólica esfingolipídica. Este reciente hallazgo es debido a la dependencia de RAB7 en la producción de caramida. Por otro lado, el análisis del secretoma celular nos ha permitido identificar nuevamente un grupo de genes implicados en el tráfico lisosomal específicamente secretado; dentro del cual encontramos LRP2, una proteína de transmembrana. En un estudio más detallado en referencia a RAB7 y LRP2 se ha establecido un inesperado efecto prometastásico, donde LRP2 se presenta como un efector de RAB7 específicamente localizado en dominios enriquecidos en ceramida de vesículas que son posteriormente secretadas.. A la luz de estos resultados, se establece que esta tesis doctoral profundiza en el conocimiento del tráfico vesicular en melanoma, y además revela una novedosa intercomunicación mediada por la modulación del tráfico vesicular y el metabolismo esfingolipídico en el melanoma cutáneo

III. *INTRODUCTION*

INTRODUCCIÓN

1. Melanoma: A XXI century global challenge

Cutaneous melanoma is a malignancy that arises from the transformation of the pigment-producing cells that reside on the skin called melanocytes[1]. Although it accounts for less than 3% of skin cancer cases[2], it is responsible for approximately 90% of skin cancer related deaths[3].

Even though the overall cancer incidence has declined worldwide in the last decades[4], this is not the case for melanoma. The number of new cases of this disease has constantly increased during the last 30 years [2,4] . In 2017, more than 74000 new cases of cutaneous melanoma were diagnosed in USA[4]. Numbers almost doubled compared to the 40000 cases diagnosed in 2012[5]. This tumor is also the 5th and the 6th most common cancer type in males and females, respectively[4] (**Figure 1**). Curiously, incidence rates are 60% higher in men than in women, while death rates are more than double[4]. Several studies have shown that sex is an independent predictor of survival[6,7] , although the ultimate cause of this difference is not clear.

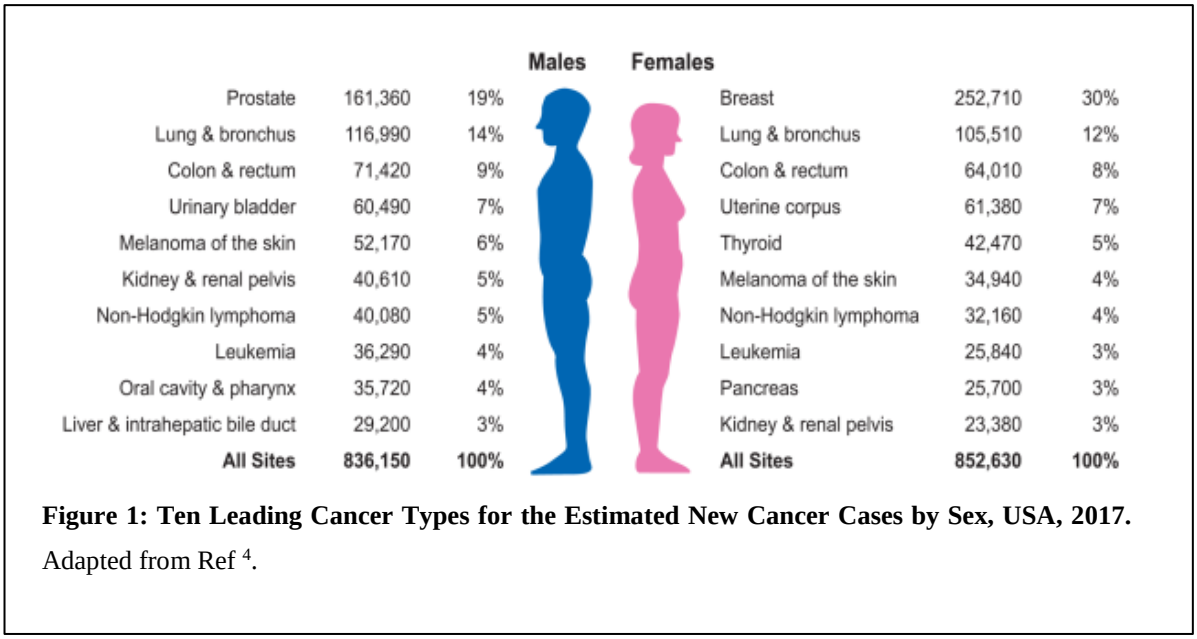

Figure 1: Ten Leading Cancer Types for the Estimated New Cancer Cases by Sex, USA, 2017. Adapted from Ref [4].

One of the main features of cutaneous melanoma is its intrinsic capacity to metastasize [8,9] and high resistance to traditional chemotherapy[10]. One reason is because melanoma is the solid tumor with the most complex (epi)genetic background, with over 80,000

mutations[11]. This high mutational load has been a hurdle for the rational design of therapies against it. Until recently, apart from surgical resection at early stages, no therapeutic approach has been shown to be effective in increasing patient survival[12]. However, in the last years our knowledge about this disease has improved dramatically leading to important scientific milestones[13] that have increased the 5-year overall survival of metastatic melanoma patients to 50%[14]. However, the past decade have witnessed critical scientific achievements/milestones that ultimately have led to the increase of the survival rates.

Nevertheless, despite all the progress in the last years, there is still an unmet need of achieving a better understanding of melanoma biology and the mechanisms this tumor exploits to metastasize in order to find new biomarkers and targets for melanoma treatment.

2. Melanocyte: The starting point

Melanocytes are dendritic cells that migrate from the neural crest to the skin during embryogenesis[1]. Specifically, they reside in the basal layer of the epidermis and in the hair folicules[15]. There, melanocytes establish contact with surrounding keratinocytes, typically in a ratio 1:10[1,16], giving rise to the so-called epidermal-melanin unit[17]. This structure is essential for cutaneous melanocytes function, which, briefly, is to provide melanin pigment to their neighbor keratinocytes[18] by the means of specialized membrane vesicles termed melanosomes[19]. Melanosomes are a type of Lysosome-related-organelles (LROs) specific from pigmented cells, such as melanocytes and melanoma, that accumulate melanin pigments[20]. Upon UV light stimulation, keratinocytes produce Melanocyte-Stimulating Hormone (MSH) which leads to the induction of Microphtalmia-associated Transcription Factor (MITF) to promote melanin synthesis[21]. Melanin provides hair and skin pigmentation, photoprotection and thermoregulation[18,22,23].

Unlike keratinocytes, melanocytes divide very unfrequently (less than twice a year)[24]. Thus, genomic alterations in these cells accumulate during very long periods and give

rise to both benign and malignant proliferative and pigmentation disorders. (They will be discussed in the next section).

In addition to the skin, melanocytes also migrate to other organ sites such as eyes[25] and, to a lesser extent, heart[26], ears[27], leptomeninges[28] and oral and genital mucosal membranes[29]. Depending on the place of origin, their malignant transformation gives rise to distinct types of melanocytic neoplasms, with different etiological and histopathological characteristics[30,31].

3. Classification of melanocytic lesions: Benign Neoplasms

Benign neoplasms of melanocytic lineage are termed nevi. Nevi are proliferations of melanocytes originated by gain of function mutations in oncogenes, which show a mutually exclusive pattern[31] (**Table 1**). However, nevi do not generally progress to melanoma due to the mechanism of Oncogene Induced Senescence[32].

Nevi Subtypes	Frequent Oncogene
Common Acquired	BRAF
Congenital	NRAS
Spitz	HRAS
Blue	GNAQ

Table 1: Most Common Nevi Subtypes and their most frequently associated mutated oncogene. Adapted from Ref[36,39,42,45]

Multiple type of nevi have been described. Among them, the most abundant are the **Common Acquired Nevi**, which are approximately 2mm in diameter. Caucasian individuals have between 20-30 of these nevi.[33,34] **Congenital Nevi** are those acquired shortly after or present at birth[35]. These two type of nevi can be stratified into junctional dermal, compound or dysplastic nevi according to their growth pattern, and specific location within the skin[36]. Of particular interest is the case of patients with dysplastic nevi, since they appear to have higher risk of developing melanoma[37–39]. However, whether dysplastic nevi are benign lesions or melanoma precursor is a long-standing debate [38,40]. Other less frequent benign nevi are **Spitz nevi** and **Blue nevi**[41,42].

Currently there is extensive research in nevi diagnose and classification[43,44]. Because some mutations observed in nevi are also frequently observed in melanomas[45–47] and

are histologically similar to them[48]. this resemblance may lead to misdiagnose and medical malpractice[49].

4. Malignant Neoplasms: Melanoma

Melanomas have been classified following several criteria such as: anatomical location, histopathological type and sun exposure level[41]. Wallace Clark[50] developed a proposal four decades ago, in which cutaneous melanoma can be subdivided into several categories: superficial spreading melanoma (SSM)[51], lentigo malignant melanoma (LMN)[52], nodular melanoma (NM)[51] and acral lentiginous melanoma (ALM)[53]. However, it is becoming clear that cutaneous melanomas should be sub classified attending to their genetic profile rather than any other classification[54].

Melanocytes from non-cutaneous tissues can also give rise to rare forms of melanoma, such as uveal melanoma and mucosal melanoma in the eye and genitourinary track, respectively. These melanomas are genetically very different to the cutaneous ones[55] and have different impact in patient prognosis and survival[30,56].

3.1 Clark model of stepwise-progression

The traditional multi-step model of melanoma progression involves a linear model of evolution from melanocytes to primary melanoma based in histological criteria[57,5858]. Five different steps were proposed attending to the lesion depth of invasion.

Melanocytic Nevi: It refers to the proliferation of common melanocytes. These melanocytes stop proliferating due to mechanisms of oncogene-induce-senescence (OIS)[32] and more than 80% of them have mutations in BRAF gene[45].

Dysplastic Nevi: This phase is characterized by aberrant growth of melanocytic nests, which can arise from a preexisting nevus or as a novel lesion[54].

Radial Growth Phase (RGP): Horizontal proliferation of melanoma cells, generally confined into the epidermis. They have to overpass the OIS barrier by acquiring novel mutations that lead to active proliferation but not invasive capacity yet[57,59]. The most frequent genetic alterations are: CDKN2A[60], PTEN[61] and NF1[62].

Vertical Growth Phase (VPG): In this phase, the tumor starts growing vertically to invade the dermis. VGP melanoma cells have increased motility and interact with the surrounding stroma to promote metastasis[63,64] and generate an immunosuppressive environment[65]. Several transcriptomic analysis have unveiled that the transition from RGP to VGP has the highest level of molecular changes[66,67]. Important alterations in this phase are mutations in the MAPK pathway, as well as TERT and SWI/SNF chromatin-remodeling complex[38].

Metastatic Melanoma: this phase occurs when melanoma cells have disseminated through the body and colonized distant organs[57]. Cutaneous melanoma metastasizes more frequently to the lymph nodes first[68,69] and later , to distal organs such as brain, liver, bones and lungs[70,71], while uveal melanoma metastasis occurs almost always in the liver[72]. This difference in tropism has opened a new lines of research focused on how tumor cells from the primary tumor can secrete soluble and vesicle-associated proteins that prepare the premetastatic niche[73–75].

Although the Clark model of melanoma progression has been the gold rule for melanoma clasification[76], its application has been hampered by the fact that only 20-30% of the melanomas follow a linear progression[77]: Up to 80% of cutaneous melanomas and all of mucosal melanomas lack the histopathological features of pre-existing nevus[31,78–81]. Therefore, this tumors may rise from primary melanocytes or precursor cells[70], although the exact contribution of melanocytes or stem cell precursors to melanomagenesis is controversial.[82,83]. Moreover, lesion thickness is very prone to measurement error, sentinel lymph node excision has not showed a beneficial for patient survival[84,85] and there are no clear molecular markers to distinguished between the different categories.

3.2 Nonlinear progression: Genetic classification

In an attempt to unravel melanoma complexity, several genomic studies using parallel sequencing over hundreds of melanoma cases from different stages have shed light about the most prevalent oncogenes and have helped to define patient subgroups[55,86,87]. One of the most extensive studies was performed by The Cancer Genome Atlas (TCGA)[87], which characterized 333 cutaneous melanomas at DNA, RNA and protein level to establish a genomic/transcriptomic framework of melanoma classification with potential biological and clinical significance.

Cutaneous Melanoma TCGA Consortium revealed four main subgroups of patients attending to the prevalence of the most predominant mutated genes (**Figure 2**):

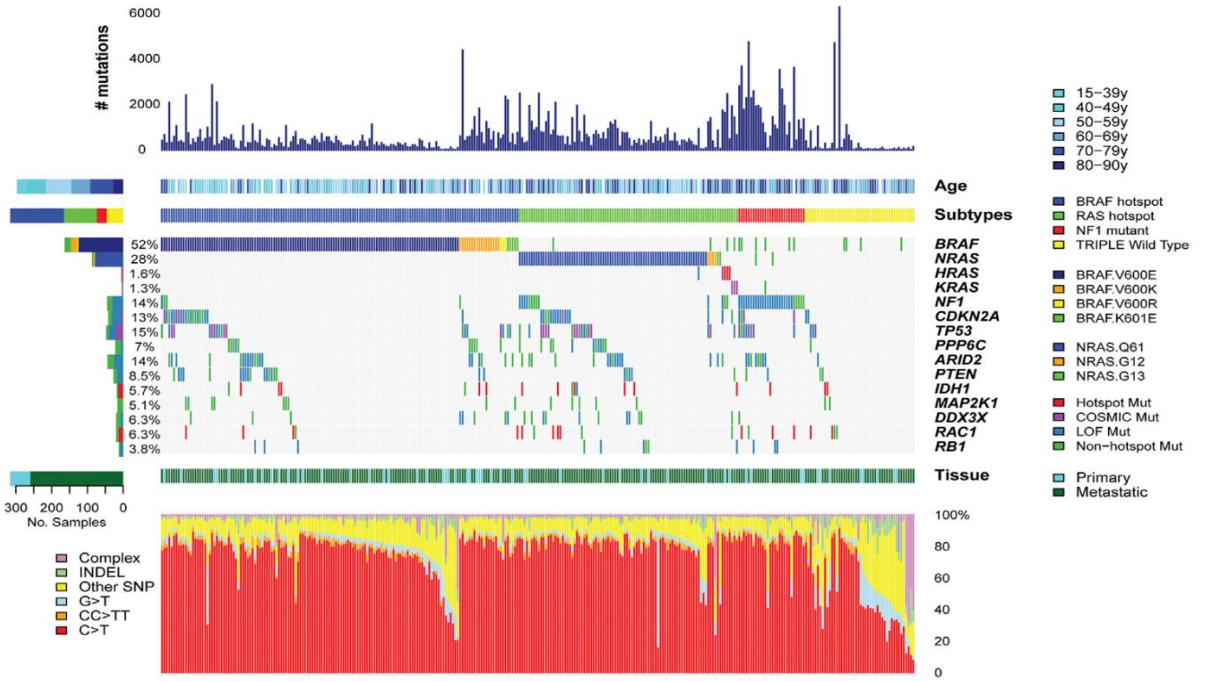

Figure 2: Landscape of driver mutations in TCGA-melanoma. Total number of mutations, age at melanoma accession, and mutation subtypes are indicated for each sample. Color-coded matrix of individual mutations (specific BRAF and NRAS mutations indicated) (middle), type of melanoma specimen (primary or metastasis), and mutation spectra for all samples (bottom) are indicated. Adapted from Ref[87]

1. **BRAF mutant:** 52% of patients harbored BRAF somatic mutations and of those, the most frequent was V600E, followed by V600K and V600R mutations. This subtype is also characterized by MITF amplifications and is more frequent in younger patients.

2. **RAS mutant:** Hot-spot mutations in any of the three RAS family members (N,H, K, and H) give rise to the second largest subset of patients, 28% of patients. Of those, the immense majority harbor NRAS somatic mutations, the most abundant are Q61R and Q61L. This subtype also has increased MAPK activity and AKT3 overexpression.

3. **NF1:** About 14% of melanoma patients show loss of function of the NF1 gene, which results in a non-canonical activation of the MAPK pathway. These patients have higher mutational burden and they tend to be older than average.

4. **Triple Negative:** This is a heterogeneous group of patients characterized by a lack of alterations in the above-mentioned genes. They also have higher genomic rearrangements.

3.3 Cutaneous vs Non-Cutaneous Melanomas

Acral and mucosal melanomas have different histological and genetic characteristics to cutaneous melanoma. These two melanoma subtypes are more common in non-Caucasian populations[88–90] and are frequently localized in the body cavities (mucosal melanoma) and palms soil and nails (acral melanoma)[31]. Unlike cutaneous melanoma, acral and mucosal melanomas have lower somatic mutation burden but higher large-scale genomic rearrangements[55,91,92].

5. Melanoma dependency: "Oncogenic" Vs "Non-Oncogenic" Addiction.

As melanoma is the solid tumor with the highest rate of somatic mutations[11], one of the most challenging areas of research has been the identification of tumor dependencies such as genes and pathways that can be exploited for cancer therapy.

Multiple melanoma oncogenes have been identified so far[87], and some of them have been exploited for targeted therapy, which paved the way for personalized medicine[13]. However, it is becoming increasingly accepted that tumor cells hijack multiple cellular

programs to allow them to survive in deleterious circustances[93]. Although these pathways are not intrinsically oncogenic themselves, they may be exploited therapeutically[93].

4.1 Melanoma Oncogenic Dependencies: Classical vs Lineage-Specific

The majority of oncogenes involved in melanoma development have impact on MAPK and PI3K pathways, as well as cell cycle checkpoints (**Table 2**). These factors are termed "classical oncogenes"[94] since they are shared by many tumor types[95].

However, there are also some genes, which are activated in a lineage-specific manner, i.e. they are unique to a particular tumor type. In melanoma, the best characterized lineage-specific oncogene is MITF[96]. By promoting the transcription of several genes involved in proliferation (CDK2), pigmentation (TYR, TYRP1, TRP2 or RAB27[97,98]) and survival (BCL2A1, BCL2 and BIRC7[99,100]) it is considered the master regulator of melanocytic development and function. Around 20% of melanoma patients show MITF amplification[96]. Similarly pro-oncogenic functions have been identified or proposed for some genes regulated by MITF such as: RAB27[101] and BCL2A1[99]. But surprisingly, primary tumors and melanoma cells with low or none MITF levels are highly invasive and metastatic[102–104]. This contradiction led to the proposal of the rheostat model, in which MITF-low cells are more stem cell like and invasive, whereas MITF-high cells are more proliferative[105].

Importantly, our group has recently identified several lineage-specific genes involved in mechanisms of regulation in melanoma, both acting in an MITF-independent manner, such as RAB7[104]and CUGBP1[106], or directly regulating MITF levels/activity, as is the case of CPEB4, which regulates MITF post-transcription modifications[107].

Gene	Alteration	Frequency	Pathway	Function
Primary Alterations				
BRAF	Point Mutation	50%	MAPK	Signaling kinase
NRAS	Point Mutation	20%	MAPK, PI3K	Signaling kinase
KIT	Point Mutation	1% overall[a]	MAPK, PI3K	Tyrosine kinase
GNAQ	Point Mutation	<1% overall[b]	MAPK, PI3K	G protein-coupled receptor
ERBB4	Point Mutation	15-20%	PI3K	Tyrosine kinase
CCND1	Amplification	10-18%	Cell cycle	G1 entry
CDK4	Mutation/Amplification	5-37%	Cell cycle	G1 entry
Secondary Alterations				
MITF	Amplification	20%	Melanocyte lineage	Transcription factor
ETV1	Amplification	15%	MITF, MAPK	Transcription factor
AKT1/3	Mutation/Amplification	25%	PI3K	Signaling kinase
PTEN	Mutation/Deletion	50-60%	PI3K	Tumor suppressor
CDKN2A	Mutation/Deletion	30%	Cell cycle	Tumor suppressor
TP53	Point Mutation	5-19%	Cell cycle	Tumor suppressor
RB	Point Mutation	6-14%	Cell cycle	G1/S transition
MDM2/4	Amplification	3-5%	Cell cycle	S phase
PPP6C	Point Mutation	9%	Cell cycle	Tumor suppressor
NEDD9	Amplification	36%[c]	Focal adhesion	Cell-cell interaction, Invasion
RAC1	Point Mutation	5%	Rho	Adhesion/Migration/Invasion
ARID1/2	Point Mutation	13%	SWI/SNF complex	Chromatin remodeling
EZH2	Point Mutation	3%	Histone modification	Chromatin remodeling
DEK	Amplification	6%	Histone modification	Chromatin remodeling

Table 2: Melanoma Oncogenes and Tumor Suppressors. a: 10% acral and mucosal; b: 70-80% uveal; c: metastatic. Adapted from Ref[22,95,108–110]

4.2 Melanoma Non-Oncogenic Dependencies

In addition to the aforementioned role of oncogenes in melanoma, tumors might have "non-oncogenic addictions", which are pathways non-intrinsically oncogenic per se, but that can act as facilitators of the tumorigenic process[93]. Our laboratory recently identified a novel non-oncogenic dependency of melanoma involving the lineage specific wiring of the vesicular trafficking machinery to foster tumor progression and metastasis [104].

6. Vesicular Trafficking: A novel Melanoma Non-Oncogenic Dependency

Autophagy, together with endocytosis and exocytosis are the three main vesicle-mediated pathways involved in the intracellular transport of proteins across the cell cytoplasm. In the tumoral microenvironment, cancer cells are anchored to the extracellular matrix and surrounding cells by transmembrane proteins. Some of this cell surface proteins might also function as receptors, and once engaged by their ligand in order to trigger downstream signaling they are endocytosed and targeted for lysosomal degradation [111–115]. Additionally, by exocytosis, cells also secrete macromolecules to influence behavior of the surrounding environment in order to make it more supportive[116]. Finally, in order to maintain cell homeostasis, damaged organelles and proteins are degraded by a process termed Autophagy (**Figure 3**). A fine tuning of the intracellular trafficking is so important that alterations in the sorting of growth factor receptors, unbalanced recycling of integrins, dissolution of cell-cell junctions and abnormal secretion has emerged as a multifaceted hallmark of cancer[117–119].

5.1 The Troika: Endocytosis, Exocytosis and Autophagy

Endocytic pathways comprise the uptake of material from the extracellular space and its retrograde transport to the lysosomes[120]. This process begins with the inward budding of vesicles from the plasma membrane that progress to form endosomes, which move from the cell periphery towards the perinuclear region. The molecular actors involved in endosome maturation change during the transport: Early endosomes are positive for the small GTPase RAB5[111,121]and EEA1[122,123], among others, but during maturation these trafficking regulators are substituted by new ones such as RAB7[120,124,125] RILP[126] and VPS34[127], which are late endosomal markers. Finally, these vesicles fuse with lysosomes, which are the major degradation site of eukaryotic cells. Cargo is subsequently degraded by acidic enzymes[104,116,128–130] contained in these organelles and used to generate ATP or utilized for biosynthetic pathways. Lysosomes are the end-point of both, the endolysosomal pathway and autophagy (**Figure 3**)

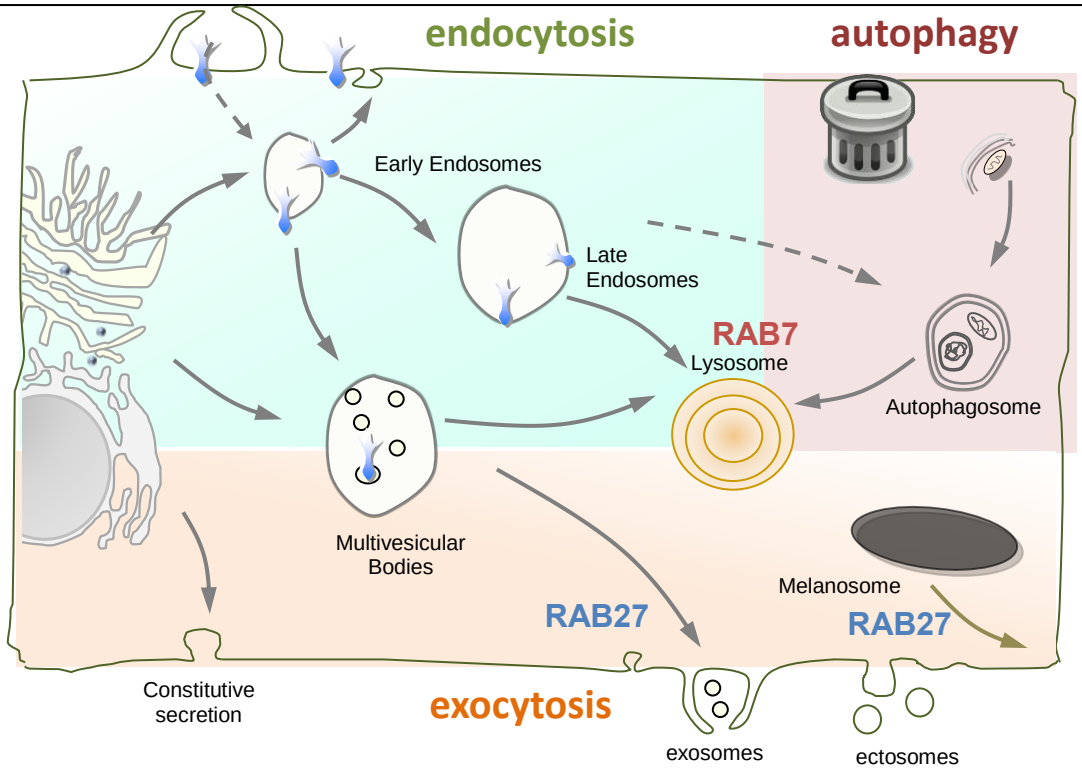

Figure 3: Schematic representation of vesicular trafficking pathways inside a cell. Endocytosis (green) exocytosis (orange) and autophagy (red). Note the central roles of RAB7 for endocytic and autophagy pathways and RAB27 role in exocytosis

Exocytosis is the reverse mechanism to endocytosis. It involves the anterograde transport of intracellular vesicles or newly synthesized extracellular proteins outside the cell in order to exert "extra-cellular signalling"[118,119,131–133]. As in the case of endocytosis, there are several mechanisms of secretion: The recycling of endocytic material back to the plasma membrane[133,134], constitutive secretion of newly synthesized proteins from the Trans Golgi Network (TGN)[135,136] and exovesicle secretion[118,137] (**Figure 3**). The secretome englobes all soluble proteins or exovesicles secreted by cancer cells. Cancer derived secretome is emerging as a critical player in cancer metastasis, particularly in the preparation of premetastatic niches[75,138], in which melanoma is no exception[71,74].

Autophagy is a regulated catabolic process that consists in the degradation of cytoplasmic material within doubled-layered vesicles (autophagosomes) that fuse with the lysosomes (**Figure 3**). It is a dynamic recycling system essential for cell homeostasis

by regulating organelle and protein turnover[139]. Depending on the context[140], autophagy may have a tumor promoter[141,142] or anti-tumoral activity[143–145]. However, in the case of melanoma, autophagy has been proposed as an "Achilles' heel"[146–148]since this tumor type employs autophagy for growth and survival[149]. Inhibition of basal autophagy, or several components of the pathway[143,150], as well as lysosomal biogenesis, compromises melanoma viability[104,143].

5.2 Lipids, the invisible player

Metabolic reprogramming is a well stablished hallmark of cancer[117]. One of the pathways that is becoming well recognized as supportive of tumor growth and metastatic dissemination is lipid metabolism[151,152]. Highly proliferative tumors need to satisfy their lipids requirements for several biochemical purposes. For a long time lipids have been regarded as mere components of the plasma membrane and vesicles with only structural roles. However, some species of lipids such cholesterol and ceramide have been described to also play a role in several steps of vesicle formation, trafficking and secretion[153–157]. Nevertheless, more in-depth analyses of the role of lipids in vesicular trafficking to drive melanoma progression and metastasis needs to be performed.

5.3 Rab Proteins: the organizers

These three pathways are finely regulated by the (Ras-like-Rat-Brain) RAB proteins, the largest family of small GTPases[133]. Each Rab protein regulate a particular step of vesicular trafficking and control each of the four major steps in membrane traffic (namely vesicle budding, delivery, tethering, and fusion)[133]by assembling multiprotein machinery in the cytoplasmic surface of intracellular membranes. They have a cyclical mechanism of activation and inactivation depending on GTP or GDP binding. This switch is controlled by guanine nucleotide exchange factors (GEFs), which trigger GDP dissociation and GTP binding, and GTPase-activating proteins (GAPs), which accelerate hydrolysis of the bound GTP to GDP. After translation, RAB proteins also undergo a prenylation process by Rab geranylgeranyl transferase (RabGGT) in order to be anchored to vesicles membranes[158–160].

7. RAB7: Master regulator of vesicular trafficking

We have reported a cluster of lysosome-associated genes that distinguishes melanoma from over 35 different tumor types and among this cluster of genes, we identified the small GTPase RAB7 as the master controller of this gene set (**Figure 4**).

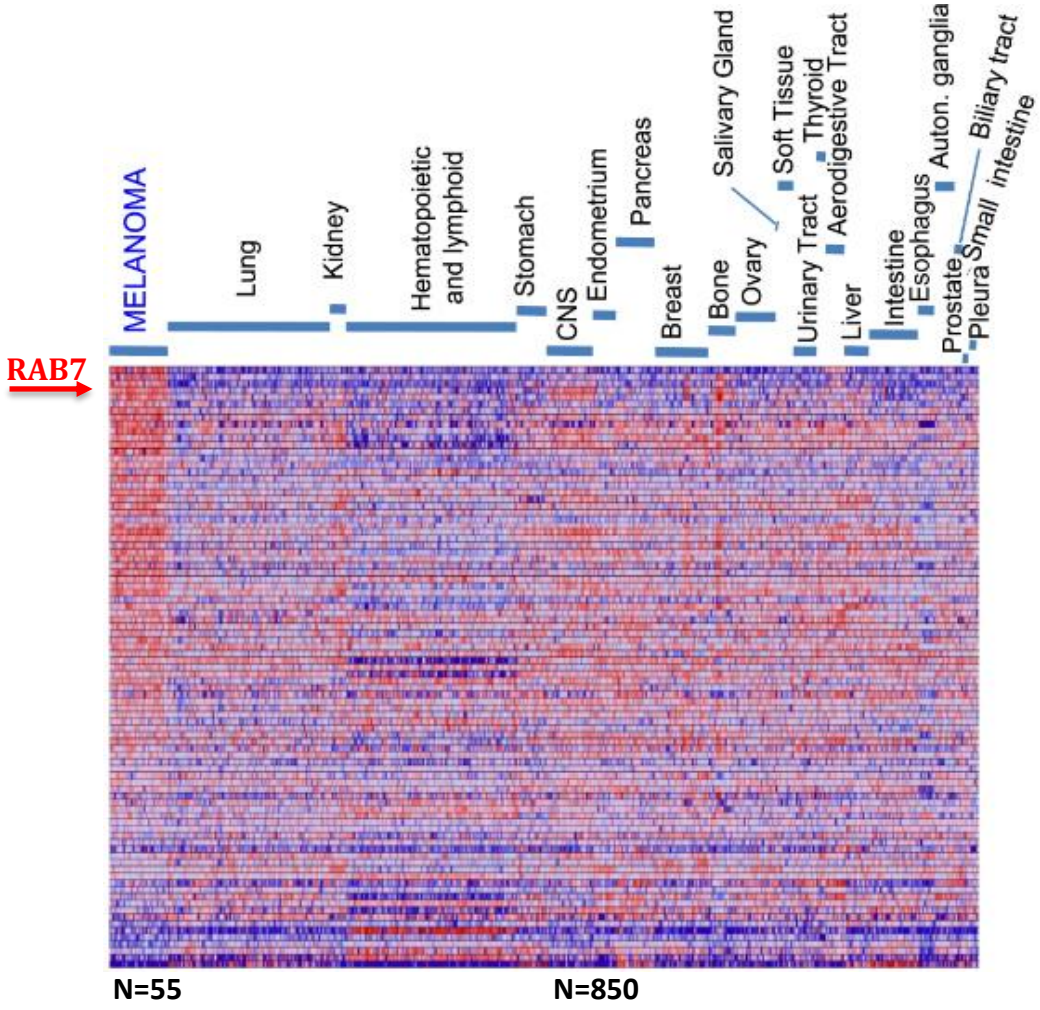

Figure 4: Melanoma Enriched Lysosomal Cluster. GSEA heat map showing a selective enrichment of the Lysosome Gene Ontology cluster (GO:0005764). RAB7 is highlighted. Adpated from Ref[104]

This small GTPase is one of the most characterized RAB proteins. It governs early-to-late endosomal maturation and late endosomes fusion with lysosomes[124]. Nevertheless, RAB7 has been shown to play a roles in several physiological processes[161]:

6.1 Role in Endocytosis

RAB7 is usually present on late endosomes after the generation of RAB7-domains[162,163] generated after the loss of RAB5, (early endosomal marker) in a highly coordinated switch [162,164]. Genetic loss of *rab7* results in embryonic lethality around E7-8 due to alterations in the endocytic compartiments[165]. The endocytic pathway begins with the initial recruitment of RAB5 to early-sorted endosomes. This process is mediated by Rabex-5[166,167], a RAB-GEF whose activity is promoted by the RAB5 effector Rabaptin-5[168]. These three proteins form a complex in the early endosomes membrane that triggers a positive feedback loop stimulating the rapid recruitment of RAB5 effectors to RAB5-positive organelles[169,170]. RAB7 replaces RAB5 when the feedback loop is inhibited or a RAB-GAP stimulate RAB5-GTP hydrolysis. SAND-1/Mon1 and Ccz1 play a key role in the RAB5 to RAB7 switch. SAND-1/Mon1 displace Rabex-5 to interrupt the positive feedback loop[164] and recruit and activate RAB7 by engaging RAB7 GEF on the Mon1-Ccz1 Complex [171,172]. Then, RAB7 is activated by this complex in the late endosomes membrane and dissociates once lysosome-late endosome fusion has ocurred[173]. Interestingly, it was recently reported that dephosphorylation of RAB7 by PTEN inhibits the complex RAB7 Mon1-Ccz1 and blocks its translocation to late endosomes[174].

Together with the RAB5-RAB7 switch, there are changes in the protein machinery that allow endosomes to recognize and fuse with other endosomes and lysosomes. The Homotypic fusion and Protein Sorting (HOPS) complex replaces the Class C CORe Vacuole/Endosome Tethering (CORVET) complex[175,176]. These two complexes play an essential role in the tethering and fusion machinery for early and late endosomes respectively. However, the mechanism of action of HOPS in mammalian cells is not fully understood as it differs from yeast[177–180]. The small GTPase Arl8b, but not RAB7 is essential for the assembly of the HOPS machinery and the recruitment of Vps41 to the lysosomal mebrane[180]. In addition an effector of RAB7, RILP, is able to recruit HOPS in a RAB7 independent manner[179] and by binding to ORP1L and the dynein motors allow the retrograde transport and fusion of late endosomes with lysosomes[178,181]. There are currently three proposed models: (1) Maturation of late endosomes to lysosomes(2)

"Kiss and run" model, continuous fusion and fission events between late endosomes and lysosomes and (3) direct fusion of both organelles to create a hybrid one termed endolysosome[182,183].

However, which steps of the endocytic pathway are specifically regulated by RAB7? This question has been addressed by using loss-of-function experimental models, particularly dominant negative mutant (DN) of RAB7. In the presence of DN-RAB7, VSVG protein[184], CTSD and CI-M6PR[185] are trapped in early endocytic compartments, suggesting that RAB7 mediates the transport of early to late endosomes. But RAB7also exerts functions downstream late endosomes/Multivesicular Bodies (MVB) since RAB7-DN decrease the degradation rate of EGF.EGFR complex in the lysosomes and induces accumulation of late endosomes[186,187]. Furthermore, RAB7 also plays a role in lysosomal biogenesis by regulating the retromer transport of newly synthetized cathepsins from the Golgi apparatus to the lysosomes[188–190]. RAB7-DN expression causes missorting of the acid hydrolases[191], dispersal of the perinuclear late endosomal and lysosomal compartment, and block cargo trafficking to lysosomes[104,124,192]. Also lysosomal acidification is severely perturbed, therefore affecting at the well-functioning of acid hydrolases[193–195]. Actually RAB7 regulates activity of the vacuolar ATPase through RILP interaction[196–198] but optimal pH also depends on lysosomal positioning in the cytoplasm[198]. On the other side, expression of a constitutively active mutant causes formation of large endocytic structures in the perinuclear region, and accelerates EGF lysosomal degradation[104,124,186].

6.2 Autophagy

Rab7 plays a key role in macroautophagy (hereafter autophagy) specifically in the final step, which leads to autophagosome maturation. In fact, autophagosomes fuse initially with early endosomes to form amphysomes, a "hybrid" organelle that lack lysosomal hydrolases but is able to fuse with late endosomes also[199,200]. As in the case of endosomes, during maturation, autophagosomes move towards the perinuclear region while undergoing pH acidification. RAB7 regulates this movement by the action of RILP[120,125,201]. The role of RAB7 in autophagy has been addressed in several cellular models. In cardiomyocytes ALDH2 activation induces RAB7 upregulation and increase

of the autophagic flux, with important implications in cardioprotection[202]. On the contrary, although RAB7 silencing or DN mutants do not affect early stages of autophagosome maturation[120,125] it does affect late stages of maturation: Actually increasing RAB7 labeling intensity and colocalization with LC3 was observed during vacuole maturation. However, RAB7 positive autophagosomes were detected before they acquire LBPA or LAMP1 staining[104,120,125]. Finally RAB7 was also shown to mediate the fusion of late autophagosomes with lysosomes: In cardiomyocites, ablation of the COP9S signalosome lead to an extensive accumulation of autophagosomes and downregulation of RAB7 levels[203]. In addition, after starvation, or mTOR inhibition RAB7 depletion leads to blockage of late endosomes and autophagosomes with lysosomes to accumulation of late autophagosomes. Similar to what occur upon treatments with drugs that block lysosomal fusion[104,120,204]. However, upon prolonged starvation, there is an mTOR reactivation needed to restore lysosomal homeostasis, process termed Autophagic Lysosome Reformation (ALR). RAB7 is located only in lysosomal fractions, and it must dissociate from the lysosomal membrane for ALR to occur. Expression of a constitutively active RAB7 mutant abrogates ALR resulting in enlarged autolysosomes[205]. Also, Rapamycin treatment inhibit ALR and blocks RAB7 dissociation from autolysosomes, suggesting RAB7 acting downstream mTOR to regulate ALR[205–207]. All this results reinforce the role for RAB7 in final maturation and fusion of late autophagic vesicles.

By interacting with different effectors, RAB7 also plays a role in a different type of autophagy: Mitophagy, which is the selective degradation of mitochondrias by autophagy. PINK1 and Parkin are they key controllers of this process. RAB7 together with TBC1D15/TBC1D17 (RAB-GAPs) and FIs1 are downstream effectors of Parkin. TBC1D15 binds to LC3 and Fis1 to coordinate RAB7 activity[208] RAB7-GTP forms and stabilizes mitochondrial-lysosomal contacts sites, while upon TBC1D15 mediated hydrolysis of RAB7-GTP, these contacts are no longer maintained[209]. RAB7 silencing in TBC1D15 KO cells prevent the accumulation of LC3 positive vesicles[210,211].

6.3 Cytoskeleton

RAB7 can regulate anterograde vesicle transport mediated by kinesin motors[211] and retrograde movement of organelles along microtubules[181]. However, it can also regulate the formation of intermediate filaments and actin cytoskeleton.

In RAB7 silenced cells, there is an increase in the amount of insoluble peripherin and vimentin (Intermediate Filaments components), while expression of the constitutively active RAB7 protein has the reverse effect[212,213] .

Actin cytoskeleton is in partly regulated by Rac1 small GTPase. It was recently described how RAB7 interacts with Rac1 by the action of Armus[214,215]. RAB7 overexpression increased Rac1 activity while RAB7 inactivation caused Rac1 inactivation[216]. Furthermore RAB7 overexpression induces the formation of circular dorsal ruffles, membrane protrusions enriched in actin filaments[216].

6.4 RAB7 in specialized cells

RAB7 controls late endosome and autophagosome fusion with lysosomes. However, it may play another role in particular cell types.

Osteoblast are a type of bone cells important for the degradation of bone matrix. In this cells RAB7 is mainly localized in the ruffle border of the plasma membrane[217], where It mediates secretion of lysosomal enzymes to the extracellular space important for the bone matrix degradation.

RAB7 is especially important in the immune system cells[218,219] as it also plays a critical role during phagocytosis. This is the process of internalization of particulate matter to phagosomes, and RAB7 mediates the fusion of phagosomes with late endosomes and lysosomes[126,220] in a similar manner as described above. Actually, some pathogenous microorganisms are able to bypass this cell defense mechanism by hijacking RAB7 or RAB7 interactors after being phagocytosed, blocking phagosomal maturation and acidification[221–223].

In neural cell cultures, RAB7 interacts with the Tropomyosin receptor kinase A (TrkA)[224] and a recently identified RAB7-effector, Protruding[225,226], to drive neurite and protrusion outgrowth. RAB7 coordinates with RAB5 to regulate retrograde axonal transport, RAB7 impairment induces a complete blockage in axonal transport[227]. Finally, together with other RABs, RAB7 regulates neural migration and dendritic morphology[228]. Hereditary heterozygous mutations in RAB7 are responsible of a peripheral neuropathy disease called Charcot-Marie-Tooth type 2B (CMT2B)[229,230]. The fact that mutations in RAB7 only cause neural symptoms even though RAB7 is ubiquitously expressed in all tissues might be explained by a neuronal specific function of RAB7.

Focusing in melanoma, RAB7 has been shown to play a role in melanosome biogenesis by directing TYRP1 protein to Type I melanosomes[231] and early melanosome motility[232]. Pigmentation-related pathways are of special importance in melanoma, since they are usually exploited by the tumor to foster progression: Melanosomes derived from early melanomas have been shown to influence the formation of tumor microenvironment[63]. Additionally, TYRP1 mRNA is able to sequester miR-16 to direct a specific gene expression program that favors melanoma growth[233]. These findings reinforce the idea of non-oncogenic addiction of tumors by hijacking a non-tumorigenic cellular program.

6.5 Oncogene or Tumor Suppressor?

The specific role of RAB7 in cancer is controversial, with several reports supporting its oncogenic role [104,234,235], while others state it is a tumor suppressor[236–239].

RAB7 was found necessary to maintain prosurvival signaling in cancer cells[234]. Furthermore, invasion and migration were found to be inhibited by RAB7 inactivation in HeLa and HT-1080 fibrosarcoma cells[235], but favored in prostate cancer cell lines[237,239], also, in fibroblasts, RAB7 silencing induces survival upon growth factor withdrawal by blocking lysosomal degradation of glucose transporters[236]. Actually, upon starvation RAB7 is activated on lysosomal membranes triggering apoptosis[240]. Also, dominant-negative Rab7 cooperated with E1A to promote the transformation of

p53(-/-) mouse embryonic fibroblasts (MEFs)[236]. Regarding the role of RAB7 in the microenvironment, Endothelial cells (ECs) from a lysosomal acid lipase KO mice, facilitate melanoma growth and metastasis and display higher RAB7 levels RAB7 inhibition revers the tumor supportive role of the ECs[241].

However, our group recently identify RAB7 as the master regulator of a cluster of lysosomal proteins that differentiate melanoma from other 35 tumor types (figure 4). Further characterization studies showed that RAB7 levels were modulated during tumor progression, being induced at early stage, but undergoing partially downregulation in invading melanomas (**figure 5A**). Actually, lower RAB7 levels was a predictor of poor prognosis (**figure 5B**) [104].

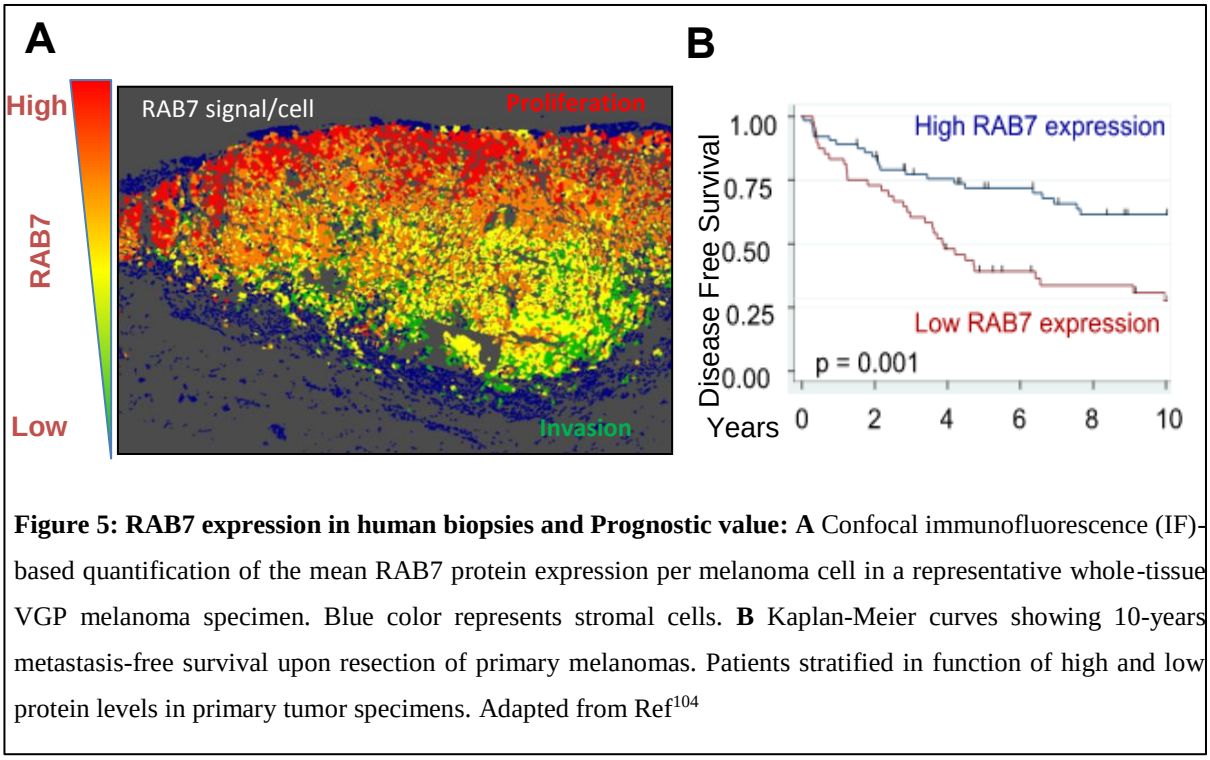

Figure 5: RAB7 expression in human biopsies and Prognostic value: A Confocal immunofluorescence (IF)-based quantification of the mean RAB7 protein expression per melanoma cell in a representative whole-tissue VGP melanoma specimen. Blue color represents stromal cells. **B** Kaplan-Meier curves showing 10-years metastasis-free survival upon resection of primary melanomas. Patients stratified in function of high and low protein levels in primary tumor specimens. Adapted from Ref[104]

Functional analyses showed that when RAB7 levels were diminished in melanoma cell lines, they became more metastatic due to changes in the cytoskeleton, translocation of lysosomal hydrolases to the plasma membrane and modulation of gene expression profiles[104]. We also demonstrated the pro-oncogenic role of RAB7 in melanoma initiation by showing the requirement of RAB7 to delay PI3K driven OIS in primary

melanocytes[242], supporting the non-equivalent role of RAB7 in melanoma compared to other systems.

Nevertheless, the mechanism behind RAB7-dependent increased metastasis, and relation with other mechanism of vesicular trafficking is not fully understood.

8. RAB27 a new player downstream RAB7?

RAB7 is not the only RAB protein that has been characterized in melanoma. The small GTPase RAB27a (hereafter referred as RAB27) was previously identified as a melanoma driver by bioinformatics approach[101]. RAB27 is an MITF[97] effector and CPEB4[107] target, two melanoma lineage-specific factors.

RAB27 was the first RAB protein identified whose mutations were linked to a disease. Type 2 Griscelli syndrome is a hereditary disease characterized by partial albinism and immunodeficiency caused by mutations in the RAB27 gene. RAB27 is involved in exovesicle secretion[232,243]. Thus, mutations in this gene make the protein unable to bind and secrete melanosomes, causing pigmentary dilution[244,245] and affects the exocytic capacity of several cell types such as lytic granule secretion of NK cells and CD8+ T cells[245] producing immunodeficiency.

7.1 RAB27 role in specialized cell types

RAB27 is highly expressed in secretory cell types, especially in melanocytes, immune system and pancreatic beta-cells. In melanocytes, RAB27, together with its adaptor proteins Myosin Va and Slac2-a, regulates the anterograde transport of melanosomes in F-actin filaments to the plasma membrane[232,246,247], where Slac2-a is replaced by Slp2 to allow membrane docking of melanosomes[248]. The RAB27-mediated secretory mechanism is not as well understood in other secretory cells, mainly because many RAB27 effectors are simultaneously present on secretory granules and they might be tissue specific as well[249,250].

Although RAB interactors are known to bind to RAB proteins when they are GTP-bound, in the case of RAB27, Coronin-3 was identified as a RAB27-GDP bound effector that controls endocytosis of pancreatic-beta cells[251].

7.2 Role in cancer

Deregulation of RAB27 expression has been reported in several tumor types, acting as an oncogene in pancreatic cancer[252], hepatocellular carcinoma[253], glioma[254], breast cancer[255], bladder cancer[256] and melanoma[74]. However, RAB27 is often downregulated in advanced prostate cancer[257] and colorectal cancer[258].

RAB27 plays a role in several tumor types by regulating exosome secretion. Exosomes derived from cancer cell lines have been shown to prepare the niche for distal metastasis[74,75], participate in the establishment of a tumor-promoting microenvironment and increase resistance to therapeutic agents[259]. In melanoma[74] breast[260] and kidney cancer[261] cell lines, RAB27 depletion abrogates exosome secretion and decreases tumor progression and metastasis.

It was recently reported that the role of RAB27 in cancer progression might not be only limited to exosome secretion as it was found to be involved in glutamate-driven recycling of MTP1-MMP-containing vesicles back to the plasma membrane[262] and might regulate NF-KB signaling to promote tumor growth[256].

In the case of melanoma, RAB27 levels increase during melanoma progression, unlike RAB7, which behaves as a rheostat favoring either proliferation or invasion (**figure 6**). Whether RAB27 plays a role in RAB7-mediated increase in metastasis[104] is unknown. Therefore, this PhD thesis will focus in expanding the knowledge of vesicle trafficking machinery in melanoma pathogenesis in the context of RAB7 and RAB27.

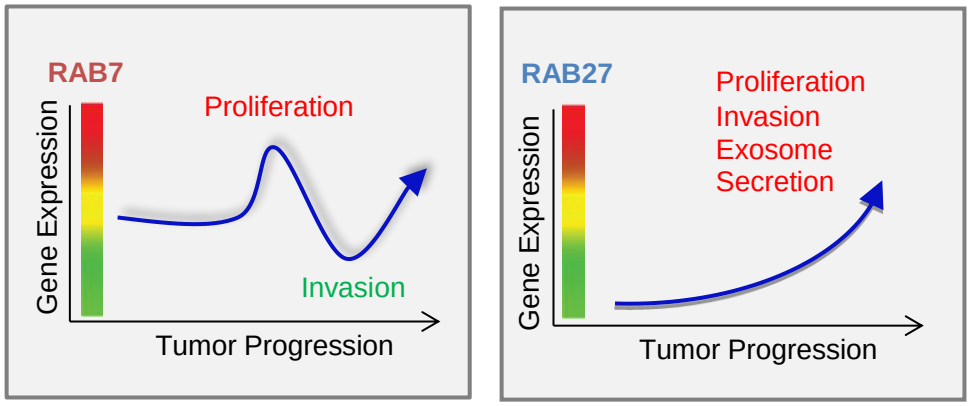

Figure 6: Model of expression levels and functions of RAB7 and RAB27 in melanoma progression. RAB7 has an oscillating pattern of expression during tumor development while RAB27 has an increased expression during melanoma progression.

IV.

OBJECTIVES

OBJETIVOS

Melanoma is a paradigm of histopathologically complex tumors, proceeding with the highest mutational rate known to date. Our laboratory has shed light on how melanoma cells exploit a lineage-specific wiring of the endolysomal pathway to sustain and acquire cancer hallmarks. We identified a cluster of Lysosomal genes differentially upregulated in melanoma. Of those genes, RAB7 plays a key role in favoring melanoma growth and metastasis. However, whether there is a cross-talk between RAB7 and other vesicular trafficking modulators such as RAB27, both melanoma lineage specific oncogenes, and the mechanism of RAB7-dependant increase in metastatic potential is still unknown. Therefore, the **Specific Aims** of this PhD thesis study are as follows:

1. To analyze cytoplasmic alterations and cellular fitness induced by depletion of vesicular trafficking modulators RAB7 and RAB27
2. To perform a global proteomic analysis of intracellular and secreted fractions of melanoma cell lines upon RAB7 and RAB27 depletion
3. To define the functional differences between RAB7 and RAB27 increase in melanoma metastasis.

V. *MATERIALS AND METHODS*

MATERIALES Y MÉTODOS

1. Cell culture

The human melanoma cell lines SK-Mel-28, SK-Mel-103, SK-Mel-147, UACC-62, WM-164, YUHOIN and YUHEF were selected for their genetic background, recapitulating the most frequent genetic alterations cutaneous melanoma (**Table 3**) and the mouse melanoma cell line B16F1 and B16F10 for their metastatic capacity. These cells were cultured in Dulbecco's modified Eagle's medium (DMEM, Lonza, cat. no. BE12-604F/U1) supplemented with 10% fetal bovine serum (FBS, Lonza, cat. no. DE14-801F) and 100 µg/mL Penicillin/Streptomycin (Invitrogen, cat. no. 15070-063) or Gentamicin (Sigma Aldric, cat. no. G1272) 50 µg/mL. YUHOIN and YUHEF were cultured in Opti-MEM® (Thermo Fisher, cat. no. 51985026) supplemented with 5% FBS and 100 µg/mL Penicillin/Streptomycin.

Cell Line	BRAF	NRAS	PTEN*	TP53	NFI
SK-Mel-28	V600E	WT	+	R273H	WT
SK-Mel-103	WT	Q61R	+	WT^R	WT
SK-Mel-147	WT	Q61R	+	WT^R	WT
UACC-62	V600E	WT	-	WT	WT
WM164	V600E	WT	+	WT	WT
YUHOIN	WT	WT	nd	nd	WT
YUHEF	WT	WT	+	WT	Q853/FS-indel

Table 3: human melanoma cell lines used in this PhD thesis study.
(*: protein levels, WT: wild type, ^{R}: repressed and nd: not determined)

2. Vector cloning

2.1 LRP2 shRNA

For LRP2 gene silencing, sense and antisense synthetic oligos were designed following TRC Laboratory Protocols: Forward Primer (CCGGCGGGATTTGTTAATTGGTGATCTCG AGATCACCAATTAACAAATCCCGTTTTTG). Reverse Primer (AATTCAAAAACGGGATTTGTTAATTGGTGATCTCGAGATCACCAATTAACAAATCCCG). Briefly, pLKO vector was digested using AgeI and EcoRI at 37ºC for 4 hours in the presence of NEBuffer Cutsmart (NEB Inc, cat. no. B7204S). Oligos were annealed in the presence of NEBuffer 2 (NEB Inc, cat. no. B7002S) incubated for 4 min at 95ºC and

allowed to cool to room temperature. For the ligation, annealed oligos were diluted 100 fold and 1 ul was used for the reaction with T4 DNA Ligase (NEB Inc, cat. no. M0202). For bacterial transformation Stbl3 cells were used (Thermo Scientific, cat. no. C737303). Plasmid isolation was performed following manufacturer instructions (QIAGEN-tip 500, cat. no. 10063). Insertion was checked by DNA sequencing.

3. Gene Silencing

3.1 Lentiviral transduction of shRNAs

RAB7 and RAB27 expression was inhibited by lentiviral-driven gene silencing using two previously reported shRNAs, Target sequences were; shRAB7a: GAAACAAGATTGACCTCGAAA (Sigma-Aldrich-TRCN0000007998) and shRAB27a: GCTGCCAATGGGACAAACATA (Sigma-Aldrich-TRCN0000005297). For genetic inactivation of human LRP2, target sequences were: shLRP2 CGGGATTTGTTAATTGGTGAT. As control, non-targeting shRNA from Sigma: CAACAAGATGAAGAGCACCAA was used. Viruses were produced in HEK 293FT cells and infections were performed as previously described[263]. Downregulation efficiency was determined after puromycin selection (1µg/mL) (Sigma-Aldrich, cat. no. P-8833) by protein immunoblotting. Unless otherwise indicated, cells were plated for expression and functional assays after puromycin selection (1µg/mL), at day 6 post-lentiviral infection.

3.2 siRNA mediated gene silencing

Cells were transfected with specific short interfering RNA (siRNA) molecules using Lipofectamine 3000 Transfection Reagent (Invitrogen, cat. No. L3000008) according to manufacturer´s protocol. Specifically, for downregulation of LRP2[264]. at a final concentration of 100nM ON-TARGETplus SMART pools were used (Dharmacon Thermo Scientific, cat. no. L-003714-00-0005 and L-012673-00-0020, respectively). *100nM final concentration* siGENOME Non-Targeting siRNA #1 (cat. No. D-001210-01-20) was used as control siRNA. Expression analyses were performed at 72 hours for LRP2, by protein immunbloting.

4. Protein Immunoblotting

Cells were harvested and total cell lysates were obtained using 1X Laemmli buffer (62.5 mM Tris-HCl pH 6.8, 2% SDS, 10% glycerol and 5% β-mercaptoethanol) and boiled at 99°C for 10 minutes. Protein concentrations were determined using the Bio-Rad Protein Assay (Bio-Rad Laboratories) according to manufacturer's protocol. Protein immunoblots were performed by standard SDS-PAGE electrophoresis in 6, 8, 10 or 12% polyacrylamide gels and subsequently transferred to Immobilon-P membranes (Millipore) using Mini Trans-Blot Cell system (Bio-Rad Laboratories). Transfer was performed at 100V during 1 hour at 4°C. Membranes were blocked with 5% milk in tris-buffered saline with 0.05% Tween-20 (TBS-T) for 1 hour at RT. Primary and secondary antibodies were diluted in 5% milk TBS-T incubated overnight at 4°C or 1 hour at room temperature. Primary antibodies used were: RAB7a (Sigma-Aldrich, cat no, R8779), RAB27a (Sigma-Aldrich, cat no, HPA001333), LRP2 (Proteintech Group, cat no, 19700-1-AP), SMPD1 (Santa Cruz Biotechnology, cat no, SC-293189), GBA (Sigma-Aldrich, cat no, G4171), FLOT1 (Abcam, cat no, ab133497), Rho-GDI (Santa Cruz Biotechnology, cat no, SC-360) Tubulin (Sigma-Aldrich, cat no, T9026) and Actin (Sigma-Aldrich, cat no, A5441). HRP-conjugated secondary antibodies used were anti-mouse and anti-rabbit (GE Healthcare, cat no, NA934) or anti-mouse (GE Healthcare, cat no, NA931). When indicated, image J software was used to quantify protein band intensities.

5. Cell Immunofluorescence

5.1 Immunofluorescence on fixed cells

Cells were cultured on coverslips and fixed with 4% paraformaldehyde in PBS at room temperature for 15 min. Then, cells were then washed twice with 0.1M glycine in PBS for 10min each, permeabilized with 0.1% Triton X-100 in PBS for 10 min, washed twice with PBS and incubated with 1% BSA in PBS at room temperature for 30 min. Fixed cells were incubated with primary antibody diluted in blocking buffer (1% BSA in PBS) over night at 4ºC Cells were then washed three times with PBS and incubated with Invitrogen´s Alexa-conjugated secondary antibodies at room temperature for 1h. Cells were washed 3 times with PBS and counterstaining of nuclei with 4,6-diamidino-2-phenylindole (DAPI) and mounting of the cover slips were done with Prolong Gold

(Invitrogen, cat. No. P36930) 20 minutes before imaging. Negative controls were obtained by omitting the primary antibody. The following primary antibodies and reagents were used: LRP2 (Proteintech Group, cat no, 19700-1-AP), Lysenin (Sigma-Aldrich, cat no, S7651), and lysenin Antiserum (Peptanova, cat. no. 14802-v). Lysenin and Lysenin antiserum were used for sphingolipid staining . Alexa Fluor 555 anti-rabbit IgG (Invitrogen, cat no, A-31572) Alexa Fluor 555 anti-goat IgG (Invitrogen, cat no, A-21432) and Alexa Fluor 488 anti-mouse IgG (Invitrogen, cat. No. A-21202) were used as secondary antibodies.

5.2 Visualization of cellular organelles: Lysosomes, Mitochondrias, and Ceramide Positive Vesicles

In order to asses changes in subcellular compartments after depletion of RAB7 or RAB27 in live cells several fluorescence probes were employed: LysoTracker Red (Invitrogen, cat no, L-7528) , Mitotracker Red (Invitrogen, cat no, M-7512) and NBD-C6-Ceramide complexed with BSA (Thermo Scientific, cat no, N1154) For the visualization of lysosomes mitochondria and ceramide positive vesicles respectively.

Briefly, fluorescence probes were added to live cells for 1 hour, then medium was change before imaging under a Nikon ECLIPSE TiE fluorescence microscope (Izasa, Barcelona, Spain) or TCS-SP5-WLL (AOBS-UV) spectral microscope (Leica Mycrosystems, Wetslar, Germany) or fixing with 4%PFA for 15 minutes at room temperature. All experiments were performed in duplicates and were repeated at least twice.

For double immunostaining NBD-C6-Ceramide and LRP2. Regular protocol for live cells visualization was followed by cell fixation and regular protocol of immunofluorescence on fixed cells but without permeabilization.

6. Transmission Electron Microscopy

$2*10^5$ cells with their corresponding shRNA were rinsed with PBS, fixed in 3% glutaraldehyde buffered to pH 7.4 PBS1X for 1 hour at room temperature, and subsequently postfixed in osmium 1% ferricyanide 0.8% and kept at 4ºC for 1 hour. Fixed samples were dehydrated in a series of graded ethanol and embedded in LX 112

resin (Ladd Research Industries). Then, the block was sectioned at 60-100 nm ultrathin sections and allocated on copper grids. Sections were stained with 2% uranyl acetate and lead citrate. Electron micrographs were acquired with a JEOL-1230 transmission electron microscope at 80KV (JEOL, USA) and a 16x16 TVIPS TemCam-F416 CMOS camera.

7. Cell Proliferation Assays

7.1 Growth Curves

$2x10^3$ cells were plated in 96-well optical bottom plates at day 6 after lentiviral transduction of the indicated shRNAs. At the indicated time intervals (Day 0 is the following day after seeding), cells were fixed with 4% paraformaldehyde (Electron Microscopy Sciences, cat no, 15750) and stained with DAPI (Sigma-Aldrich, cat no, D9542). For each time point, total cell number was quantified in triplicates by automated high throughput confocal detection of DAPI-stained nuclei using the OPERA HCS platform and the Acapella Analysis Software (Perkin Elmer).

7.2 Colony Formation

High and low confluency colony formation assays were performed by seeding $5X10^4$ and $5x10^3$ cells per well respectively onto 6-well plates. Cells were allowed to grow for 5-14 days, for subsequent fixation with cold methanol for 10 minutes. Colonies were stained with 0.4g/L crystal violet (Sigma-Aldrich, cat no, C3886). The number of colonies were quantified from micrographs of the plates using the ImageJ software. Unless otherwise indicated, all proliferation, assays were done in triplicates and were repeated at least twice. Pooled data are presented as means ± SEMs of two independent experiments performed with three replicates each.

7. 3 Cell Cycle Analysis by Flow Cytometry

For Cell Cycle analysis, exponentially growing control or shRAB7 and shRAB27 depleted human melanoma cell lines cells were incubated with 10μM BrdU (Sigma-Aldrich, cat no, B9285).for one hour. Cells were fixed with ice cold 70% ethanol and processed following the acidic protocol described before[265]. S-phase BrdU positive

cells were stained with FITC-conjugated anti-BrdU antibody (BD Biosciences, cat no, 556028), and DNA was counterstained with 50μg/mL propidium iodide (Sigma-Aldrich, cat no, P4170). Data was acquired using a FACS Calibur flow cytometer (Becton Dickinson). Cell aggregates were excluded using pulse processing and a minimum of 10000 single events were measured. Data were analyzed using FlowJo 9.6.4 software (Treestar).

9. TMRE Apoptotic Assay

Supernatants and cells were collected, pelleted by 5 minutes centrifugsation at 1200 rpm. Then, resuspende pellet in TMRE 40nM (Sigma Aldrich, cat no. 87917) Incubate 10 min at 37ºC, add pbs, centrifuge,aspirate supernatant and resuspend pellet in 400ul of PBS and 2ul of DAPI (Sigma-Aldrich, cat no, D9542) just before Flow Cytometry analysis with FACS Calibur flow cytometer (Becton Dickinson). Data were analyzed using FlowJo 9.6.4 software (Treestar).

10. Animal Experiments

Mouse xenograft models were generated by subcutaneous implantation of $1x10^6$ B16F1 cells in C57BL/6 female mice (Charles Rivers). Cells were harvested at day 6 after infection with control or RAB7/RAB27 shRNAs, resuspended in PBS at 1:3 ratio and injected in the back of the animals (n=7 per group). Tumor growth was measured blinded to the experimental conditions at the indicated time intervals. Tumor volume was estimated using a caliper and calculated as $V= axb^2x\pi/6$, where "a" stand for the bigger and "b" for the smaller diameter of the tumor. All experiments with mice met the Animal Welfare guidelines and were performed in accordance with protocols approved by the Institutional Ethics Committee of CNIO.

11. Mitochondrial Respiration

$5x10^3$cells of RAB7 and RAB27 deficient SK-Mel-103 and UACC-62 cells with the corresponding shControl cells were plated per well in XF 96-well microplates and incubated for 24 hr at 37 °C in 5% CO_2. Respiration was measured under basal

conditions, and in response to Oligomycin an ATP synthase inhibitor; 0.5 µM (Sigma Aldrich, cat. no. 75351) and the electron transport chain accelerator ionophore FCCP (Trifluorocarbonylcyanide Phenylhydrazone); 0.5 µM (Quimigen S.L., cat. no. SC-203578). Finally, respiration was stopped by adding the electron transport chain inhibitors Rotenone and Antimycin A (Sigma Aldrich, cat. no. R8875 and A8674 respectively); 1 µM each. Oxygen consumption rate (OCR) and extra-cellular acidification rate (ECAR) were measured with a XF96 Extracellular Flux Analyzer (Seahorse Biosciences) following manufacturer instructions OCR and ECAR values were normalized to cell number. Four technical replicates per condition were used in three independent experiments.

12. Detergent Resistant Membrane Isolation

A confluent 15 cm dish was scrapped with DRM Buffer (25Mm MES, Sigma Aldrich cat no. M-8250) pH7.2 0.15M NaCl, Triton X-100 1%, Sigma Aldrich, cat. no. T9284 and protease inhibitor, Roche Diagnostics GmbH, cat no, 11836170 001) and centrifuged 10 mins at 13000 rpm 4ºC. A continuous sacarose gradient 5-40% was formed in an adaptor tube of a 40 Ti rotor and 1 ml of the protein extracts was layed in the bottom part. Gradient was centrifuged overnight at 200.000g and 12 fractions were collected by pipetting into a 2 ml eppendorf, 1 volume of acetone was added to each tube and samples were left at -20ºC 4hr for protein precipitation. Samples were centrifuged 10 mins at 13000 rpm 4ºC, supernatant discarded and tubes were left opened for air-dry overnight. Next day each fraction was resuspended in 80 ul of Laemmli buffer and run in a precast gel (Bio-Rad Laboratories, cat no. 161-1123).

13. Drug Treatments

SMPDI inhibitor, Siramesine was used as a concentration of 4µM (Sigma Aldrich, cat. no. SML0976) for 24 hr. Cell Titer Kit (Promega cay. no. G7571) was used to determine a sublethal concentration of this drug at mentioned time point. GBA inhitor, Condutirol B Epoxide (Santa Cruz Biotechnology cat. no. SC-201356) was used as a concentration of 500µM for cell line UACC-62 and 100µM for cell line SK-Mel-28.

14. Protein Secretion Assays

Conditioned media was prepared by plating 1.5x10^6 cells of each condition and 6hr later incubate with serum-free DMEM for 24 hours. Conditioned media was harvested, clarified by centrifugation 2000g for 10 minutes, and then concentrated in Amicon Ultra-15 centrifugal filter devices with Ultracel-3 membrane 3kDa NMWL (Millipore, Bedford, MA, USA) by centrifugation at 5000g for 2h in a swinging bucket rotor. For matrigel invasion assays with conditioned medium the final concentrated volume, 500ul was used when indicated, Protease inhibitor (Roche Diagnostics GmbH, cat no, 11836170 001) was added to the serum-free DMEM to avoid protein degradation only in the conditioned medium concentrated for proteomic analyses or ELISA.

For LRP2 detection in the concentrated secretome from melanoma cells depleted of RAB7 or RAB27 a commercial Sandwich ELISA Kit was obtained (LSBio, cat no. LS-F11978) and manufacturer instructions were followed.

15. Exosome Purification

Exosome purification form cell culture supernatants after RAB7 and RAB27 depletion was performed following a protocol described before[266]. Briefly, cells were cultured in media supplemented with 10% exosome-depleted FBS. FBS was depleted of bovine exosomes by ultracentrifugation at 100,000*g* for 16 hour. Supernatant fractions collected from 24 hour cell cultures were pelleted by centrifugation at 2000*g* for 10 min. The supernatant was centrifuged at 10,000*g* for 30min. Exosomes were then harvested by centrifugation at 100,000*g* for 70 min using SW28 rotor. The exosome pellet was washed in 12 ml of PBS and collected by ultracentrifugation at 100,000*g* for 70 min using SW40Ti rotor. The exosome pellet was resuspended in 40ul PBS and collected for further assays. The LM10 nanoparticle characterization system (NanoSight) was used for size characterization of the vesicles. Next, LRP2 content in those exosomes was determined by ELISA.

16. Matrigel Invasion Assays

Cells were serum-starved overnight and were seeded in serum-free DMEM or (concentrated serum-free conditioned medium from cells infected with shRAB7 or shRAB27) onto the upper Boyden Chamber (0.8µm BD BioCoat™ Matrigel™ Invasion Chambers; from BD Biosciences, San Jose, CA, USA cat. no. 354234). DMEM containing 10% FBS was placed in the lower chamber. After incubation for the indicated time intervals, invading and non-invading cells were first fixed with 4% paraformaldehyde and then stained with DAPI. Single cells were visualized by confocal detection of DAPI-stained nuclei through the 20x objective of a TCS-SP5-WLL (AOBS-UV) spectral microscope (Leica Mycrosystems, Wetzlar, Germany). The transwell membrane was also visualized by laser reflection. LAS AF Matrix screening Software was used for an automated high-throughput acquisition across the total width of the matrigel membrane in 4 different fields per experimental condition. IMARIS 6.3 Software was used to quantify the % of invading cells (normalized to the total cell number per field). Data are presented as means ± SEMs of three independent experiments performed in duplicates.

17. Reconstructed Skins

The reconstructed skins in vitro were prepared in two steps. First, the dermal compartment was prepared using type-1 collagen gel and 20 × 104 human fibroblasts/dermis. After polymerization, 25 × 104 human keratinocytes, 0.83 × 104 human melanocytes and 10 × 104 melanoma cells (WM164) were seeded on top of each lattice and the skins were kept submerged in the culture medium for 24 h. Subsequently, theculture was raised and maintained at the air–liquid interface for 11 days to allow complete keratinocytes stratification and differentiation[267–270].

The reconstructed skins containing melanoma cells were treated with concentrated conditioned medium obtained from melanoma cell lines Sk-Mel-28 or UACC-62 silenced for Rab7 or Rab27 every 72 h.

For Hematoxilin & Eosin visualization, skin samples were fixed in bufferen formalin, followed by dehydration, cleaning for paraffin inclusion and stained with H&E for

morphological analysis. All images were obtained by optical microscopy and analyzed by the NISElements software (Nikon Instruments, Melville, NY, USA). Measurement of melanoma area thickness was carried out with five measurements per skin from three independent samples.

18. Proteomics

18.1 Secretome

Cell culture supernatants from two melanoma cell lines (SK-Mel-103 and UACC62) at 6 days upon RAB7 or RAB27 genetic inactivation were collected as described above, and subjected to MS analysis.

18.2 LC-MS/MS analysis

Concentration of secreted proteins was determined using the Pierce® 660nm Protein Assay (Bio-Rad) using BSA as standard. Then, the samples were diluted in UT buffer (8M urea in 100 mM Tris-HCl, pH=8.01) and digested by means of the standard FASP protocol[271]. Briefly, samples were reduced with 10 mM DTT, alkylated using 50 mM IAA for 20 min in the dark. Secreted proteins were digested with Lys-C (Wako) (1:50) overnight, and then, diluted in 50 mM ammonium bicarbonate to reduce the urea concentration less than 1M and subsequently digested with Trypsin (Promega) (1:100) o/n at 37 °C during 6h. Resulting peptides were desalted and dissolved in 30 µL of 0.1% formic acid (FA).

18.3 Peptide analysis by nanoLC-MS/MS.

Peptides were separated by reversed-phase chromatography using a nanoLC Ultra system (Eksigent), directly coupled with a LTQ-Orbitrap Velos instrument (Thermo Fisher Scientific) via nanoelectrospray source (ProxeonBiosystem). Peptides were loaded onto the column (RP ReproSil Pur C18-AQ 1.9 µm 400 x 0.075 mm home-made column), with a previous trapping column step (NS-MP-10 BioSphere C18 5 µm 120 Å 360/100 µm, L=20 mm, Nanoseparations), during 10 min with a flow rate of 2.5 µl/min of loading buffer (0.1% FA). Elution from the column was made with a 120 min

linear gradient (buffer A: 4% ACN, 0.1%FA; buffer B: 100% ACN, 0.1%FA) at 300 nL/min. The peptides were directly electrosprayed into the mass spectrometer using a PicoTip emitter (360/20 OD/ID µm tip ID 10 µm, New Objective) a 1.4 kV spray voltage with a heated capillary temperature of 325°C and S-Lens of 60%. Mass spectra were acquired in a data-dependent manner, with an automatic switch between MS and MS/MS scans using a top 20 method with a threshold signal of 800 counts. MS spectra were acquired with a resolution of 60000 (FWHM) at 400 m/z in the Orbitrap, scanning a mass range between 350 and 1500 m/z. Peptide fragmentation was performed using collision induced dissociation (CID/CAD) and fragment ions were detected in the linear ion trap. The normalized collision energy was set to 38%, the Q value to 0.25 and the activation time to 10 ms. The maximum ion injection times for the survey scan and the MS/MS scans were 500 ms and 100 ms respectively and the ion target values were set to 1E6 and 5000, respectively for each scan mode.

18.4 Data analysis of Secretome

Raw files were analyzed either with Proteome Discoverer (version 1.4.1.2), and with by MaxQuant (v 1.5.1.2)[272,273], against a forward-reverse concatenated database including human proteins (UniProtKB/Swiss-Prot, December 2013, 20.584 sequences) and common contaminants. MaxQuant was used for protein quantification using Label free approach, while Protein Discoverer was used only for protein identification. Carbamidomethylation of cysteines was considered as fixed modification whereas oxidation of methionines was set as variable modifications in both Sequest HT and Andromeda search engine (v2.2). Sequest HT, in conjunction with Percolator provided the list of proteins for Proteome Discoverer. Minimal peptide length was set to 6 amino acids and a maximum of two missed-cleavages were allowed. Peptides were filtered at 1% FDR. For protein assessment in MaxQuant, at least one unique peptide provided by Andromeda search engine3 with a FDR = 1% was required for both identification and quantification, other parameters were set as default. Afterwards, the "proteingroup" file was uploaded in Perseus (v1.5.1.6)4. After removing proteins annotated as contaminants, only identified by site and/or reversed, the missing values of the matrix were imputed as a normal distribution assuming low intensity values. Then, a two-sample Student's T-Test (FDR≤ 0.05, s0 >0.1) was

performed on proteins containing 100% of valid values in at least one group. Only significant proteins were considered as regulated.

18.5 Intracellular Fraction (iTRAQ)

Melanoma cell pellets from two melanoma cell lines (SK-Mel-103 and UACC62) were collected 6 days upon RAB7 or RAB27 genetic inactivation and subjected to proteome analysis by iTRAQ.

18.6 Sample Preparation

Pellets were lysed using 7 M urea, 2 M thiourea, 100 mM Hepes pH 7.5, 1:1000 (v/v) of benzonase and 1:100 (v/v) of HaltTM phosphatase and protease inhibitor cocktail 100x. Samples were vortexed, sonicated and clarified by centrifugation at 4 °C and 16,100 × g for 15 min. Protein concentration was determined using the Pierce® 660nm Protein Assay (Bio-Rad) using BSA as standard.

Samples were digested using the filter aided sample preparation (FASP) protocol[271]. Briefly, the equivalent to 60 µg of each sample was loaded on the filter, reduced with 10 mM DTT 1 h at 37ºC in UTEAB and alkylated using 55 mM iodoacetamide for 20 min in the dark. The excess of reduction and alkylation reagents were washed out with UTEAB (8M urea in 100 mM triethylammonium bicarbonate, pH=8.01). The proteins were digested overnight using endoproteinase Lys-C (Wako) with 1:50 enzyme to protein ratio. Finally, trypsin (Promega) dissolved in 0.05M TEAB was added and samples were subjected to a second digestion for 6 h. Each tryptic digest was labeled according to the manufacturer's instructions (AB Sciex) with one 8-plex isobaric amine-reactive tag per cell line (iTRAQ® Reagent 8plex kit). After two hours of incubation, labeled samples were pooled, and evaporated to dryness in a vacuum centrifuge. The iTRAQ sample was cleaned up using a Sep- Pak C18 cartridge for SPE (Waters Corp., Milford, MA). Eluted peptides were vacuum-dried.

Peptides were fractionated using high pH reverse phase technique)[203]. Peptides were dissolved in 100 µl of phase A (10mM NH4OH) and eluted at a flow rate of 500 µl/min onto an XBridge BEH130 C18 (3.5 µm, 4.6 x 250 mm) column (Waters) during 60

minutes using the following gradient of phase B (10mM NH4OH, 90% CH3CN): 0-50 min 25% B, 50-54 min 60% B, 54-61 min 70% B. 40. Fractions were collected, and concatenated into 15 fractions and evaporate in the speed vac. Peptides were resuspended in 15µl 0.1% FA.

18.7 Peptide analysis by nanoLC-MS/MS

The LTQ Orbitrap Velos mass spectrometer (Thermo Scientific, Bremen) was coupled to an Eksigent nano LC system (Eksigent technologies) through a nanoelectrospray ion source (Proxeon Biosystems). Peptides were loaded from a cooled nanoLC AS-2 autosampler (Eksigent technologies). In order to pre-concentrate and desalt the samples before switching the pre-column in line with the separation column, 5 µL from each sample was loaded onto a trapping cartridge (NS-MP-10 BioSphere C18 5 µm 120 Å 360/100 µm, L=20 mm, Nanoseparations) during 10 min with a flow rate of 2.5 µl/min of loading buffer (0.1% FA). The peptides were eluted from a RP ReproSil Pur C18-AQ 1.9 µm 400 x 0.075 mm home-made column by application of a binary gradient consisting of 4% ACN in 0.1% FA (buffer A) and 100% ACN in 0.1%FA (buffer B), with a flow rate of 300 nL/min. Peptides were separated using the following gradient: 0-2 min 4% B, 2-133 min 30% B and 133-143 min 98% B. The column was operated at a constant temperature of 55ºC. The LTQ Orbitrap Velos was operated in positive ionization mode. The MS survey scan was performed in the FT analyzer scanning a window between 350 and 1500 m/z. The resolution was set to 30 000 FWHM at m/z 400. The m/z values triggering MS/MS with a repeat count of 1 were put on an exclusion list for 60 s. The minimum MS signal for triggering MS/MS was set to 5000 counts. In all cases, one microscan was recorded. HCD was used for fragmentation, up to the 15 most abundant isotope patterns with charge ≥2 from the survey scan were selected for fragmentation in the HCD collision cell. Normalized collision energy was set to 38.0, the Q value to 0.25 and an activation time to 0.10 ms. Waveform filter was activated. The resulting fragments were detected in the Orbitrap system with a resolution of 7500 FWHM at m/z 400. The maximum ion injection times for the survey scan and the MS/MS scans were 500 ms and 250 ms respectively and the ion target values were set to 1E6 and 7E4, respectively for each scan mode.

18.8 Data Processing

All files were analyzed using Proteome Discoverer 1.4 (Thermo Scientific) with Sequest HT as the search engine against a concatenated Uniprot database of Homo sapiens (UniProtKB/Swiss-Prot, December 2013, 20.584 sequences and common contaminants), iTRAQ 8plex tag labelling in lysine and peptide N-termini were included as fixed modifications, together with carbamidomethylation of cysteine. Oxidation of methionine and iTRAQ 8plex labelling of tyrosine were included as variable modifications. Precursor mass tolerance was 20 ppm and fragment mass tolerance was 0.05 Da. The integration of reporter ions was performed using the most confident centroid with a tolerance of 50 ppm. PSMs were filtered using Percolator (v2.04) with a FDR of 1%. Quantification results at the PSM level were exported for further analysis.

18.9 Statistical and Data analyses

Quantification and statistical analysis was performed using Isobar (version 1.10)[274,275], in R (version 3.1.2 "Pumkin Helmet"), using a noise model that accounts for the technical variation and a second biological variability model using the two independent digestions of the control samples. Proteins with a p-value of less than 0.05 and with a log2 ratio > 0.3 or < - 0.3 were classified as up- or down- regulated, respectively.

19. GSEA, Heatmaps and Venn diagrams

Gene Set Enrichment Analysis (GSEA) or Single Sample GESA were performed using annotations from the KEGG or REACTOME pathways. Genes were ranked using the t statistic. After Kolmogorov-Smirnoff correction for multiple testing, only those pathways bearing a FDR <0.25 were considered significant[276]. Heatmap and correlation graphs for RNA and protein levels were created by Perseus v1.5.1.6. Protein networks were created by using Search Tool for the Retrieval of Interacting Genes/Proteins (STRING)[277] . Venn diagrams were created by using online tools Venny v2.0[278].

20. Statistical Analysis

Difference on growth and invasion capacity of melanoma cells after genetic depletion of RAB7 and RAB27 was analyzed by ANOVA $p<0.05$ was considered significant and p-values were represented in figures as follow: "***" for $p<0.001$, "**" for $p<0.01$, "*" for $p<0.05$ and "ns" for not significant.

VI.

RESULTS

RESULTADOS

1. RAB7 and RAB27 are required to sustain melanoma growth.

Previous studies have shown that RAB7[104] and RAB27[101] are required to maintain melanoma cell proliferation. However, to our knowledge, a parallel comparison of their role in melanoma has not been performed. Therefore, we silenced the expression of these genes in a panel of melanoma cell lines (**Figure 7**) with different genetic background (**Table 3**).

Cells monitored at day 6 after infection by DAPI-based nuclei count (see Methods) showed a marked inhibitory effect of bothRAB7 and RAB27 shRNA in cell viability (**Figure 7B**). Interestingly, albeit to different extends, all melanoma cell lines tested responded to RAB7 and RAB27 shRNA with decrease in inhibited proliferative capacity (see **Figure 7C** for colony formation assays). To further confirm the physiological relevance of these results, control, RAB7- and RAB27-depleted mouse melanoma cells (B16F1) were injected subcutaneously into the flanks of 8-week-old BL6 female mice as a syngeneic mouse model. The same observations described in vitro were recapitulated in an immunocompetent mouse model (**Figure 7D**). Next, in order to characterize cell cycle alterations, control RAB7- and RAB27-depleted human melanoma cells were stained with BrdU and propidium iodide, flow cytometry analysis of total DNA revealed that RAB7- and RAB27- shRNA cells accumulated at the G1 phase, with the concomitant reduction in S-phase proliferating cells in comparison with shControl cells (**Figure 7E**). Together, these in vitro and in vivo results support a relevant role of RAB7 and, in particular, of RAB27 on the tumorigenic potential of melanoma cells,

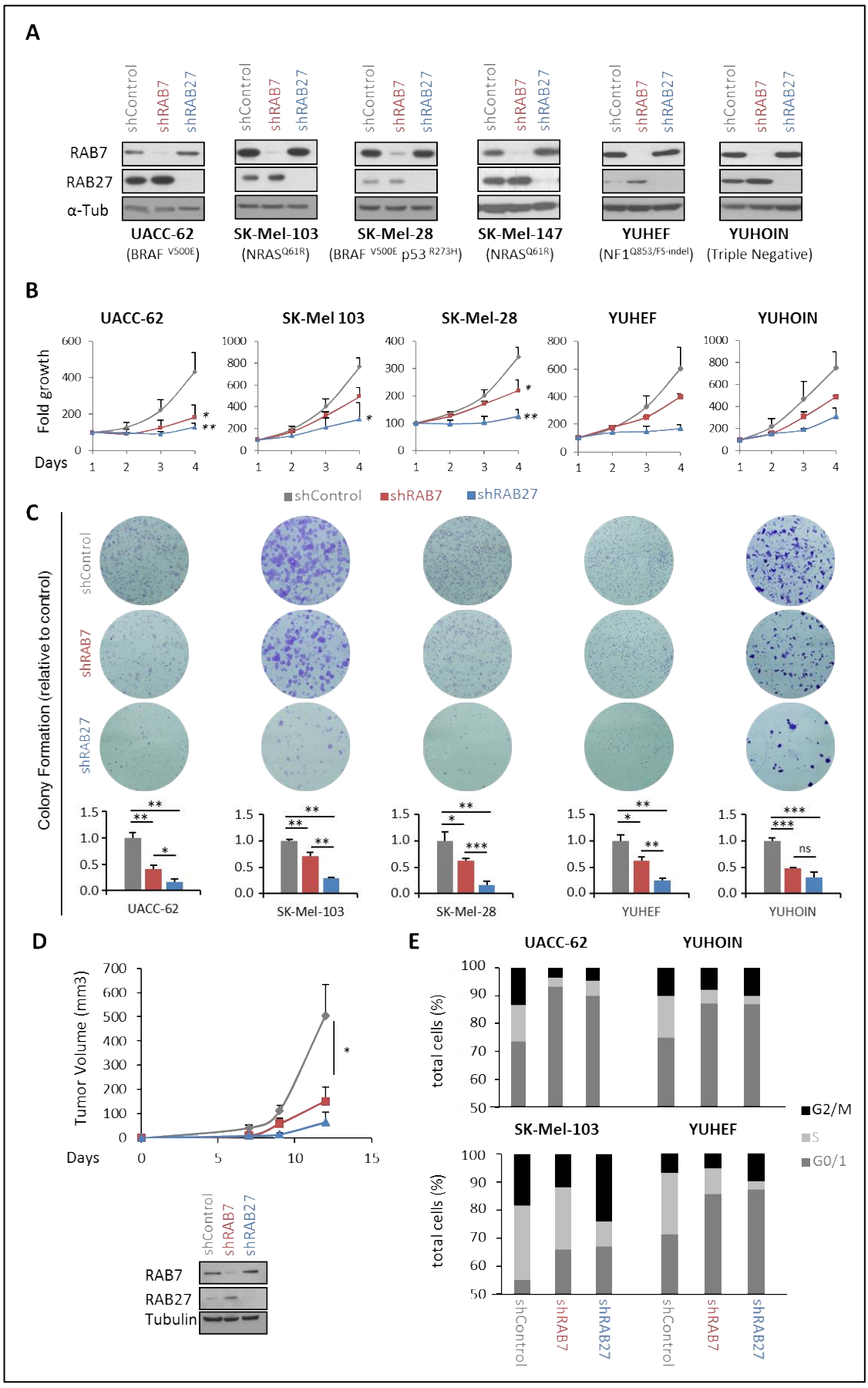
A
shControl
shRAB7
shRAB27
RAB7
RAB27
α-Tub
UACC-62
(BRAF V500E)
SK-Mel-103
(NRASQ61R)
SK-Mel-28
(BRAF V500E p53 R273H)
SK-Mel-147
(NRASQ61R)
YUHEF
(NF1Q853/FS-indel)
YUHOIN
(Triple Negative)
B
UACC-62
SK-Mel 103
SK-Mel-28
YUHEF
YUHOIN
Fold growth
Days
shControl
shRAB7
shRAB27
C
Colony Formation (relative to control)
UACC-62
SK-Mel-103
SK-Mel-28
YUHEF
YUHOIN
ns
D
Tumor Volume (mm3)
Days
RAB7
RAB27
Tubulin
E
UACC-62
YUHOIN
SK-Mel-103
YUHEF
total cells (%)
G2/M
S
G0/1

2. Non-equivalent roles of RAB7 and RAB27 in melanoma cell invasion and migration

Interestingly, although RAB7 and RAB27 are required for cell proliferation, opposite roles in cell invasion has been described for them[74,104]. Therefore, we performed a parallel comparison of the effect of silencing both genes in invasion and proliferation. Matrigel invasion assays revealed that RAB7 downregulation enhanced the invasiveness of low-metastatic cell lines, while RAB27 silencing had no effect (**Figure 8A**). However, RAB7 silencing did not enhance the metastatic potential of highly metastatic cell lines, while RAB27 depletion decreased their invasive capacity (**Figure 8B**). Equivalent results were obtained in a wound healing assay with mouse melanoma cell lines (**Figure 8C**). These data confirms non-equivalent roles of vesicular trafficking modulators RAB7 and RAB27 in melanoma invasion and migration.

3. Different cytoplasmic alterations induced by RAB7 or RAB27 silencing

Invasion capacity is directly linked to the cell ability to migrate. Since there is a corollary of studies suggesting that vesicular trafficking is essential for cell migration[279–281], we hypothesized that depletion of RAB7 or RAB27 might be affecting vesicular trafficking pathways in a different manner and, in turn, affecting the cellular invasion capacity. As expected, microscopy-based cell observation showed marked morphological changes in RAB7-depleted melanoma cells, most frequently leading to dendrification or to prominent cytosolic vacuolization. However, alterations induced by RAB27 downregulation were very different: cells were more rounded and had lost their dendrification. (**Figure 9A**).

Figure 7 (Page 64). RAB7 and RAB27 are required to sustain melanoma growth.
A, Downregulation of RAB7 and RAB27 in a panel of human melanoma cell lines, by lentiviral-based transduction of shRNA constructs visualized by immunoblotting compared to cells expressing control shRNA. **B,** Impaired growth of human melanoma cell lines upon RAB7 or RAB27 depletion. Time points indicate the days after seeding. **C**, Colony formation of the cell lines in (A) determined by crystal violet 14 days after seeding. Quantification shown below, (ratio of inhibition with respect to control shRNA-transduced cells). **D,** Growth of allografts generated with the indicated mouse melanoma cell line after subcutaneous implantation in B16 mice. **E,** Relative cell numbers at different phases of the cell cycle of the cell lines in (A) upon RAB7 or RAB27 depletion compared to control cells. Error bars correspond to SEM of at least two experiments. "***"$p<0.001$, "**"$p<0.01$, "*"$p<0.05$ and "ns" not significant.

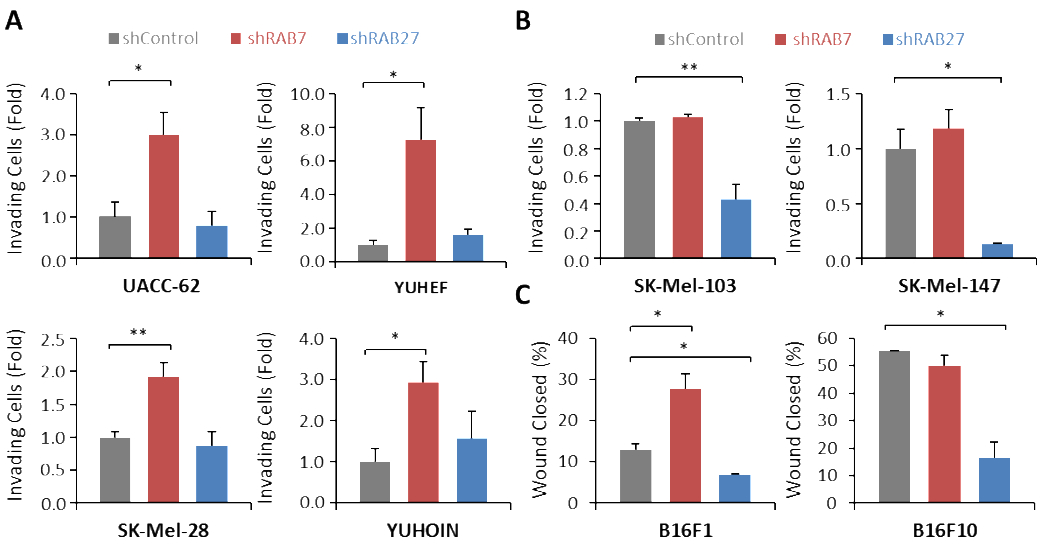

Figure 8. Non-equivalent roles of RAB7 and RAB27 in melanoma cell invasion and migration. **A,** Invasiveness of low invasive cell lines expressing Control shRNA or an shRNA directed against RAB7 or RAB27, evaluated by Matrigel invasion assay (72 hr). **B,** Invasiveness of highly invasive cell lines expressing Control shRNA or an shRNA directed against RAB7 or RAB27, evaluated by Matrigel invasion assay (12 hr). **C,** Total area covered in 10 hr in a wound healing assay by two mouse melanoma cell lines upon RAB7 or RAB27 depletion compared with shControl cells.

Subsequently, we took advantage of Transmission Electron Microscopy (TEM) to acquire a global view of the morphological changes induced by either RAB7 or RAB27 depletion on two melanoma cell lines silenced for either gene. We chose SK-Mel-103 and UACC-62 as representative cell lines for the different genetic background and because of the differential changes upon RAB7 or RAB27 depletion (**Figure 8A and B**). As expected, we observed different ultrastructural changes: RAB7 depletion caused large vacuolization and lysosomal accumulation in the cell cytoplasm. On the other hand, RAB27 depletion caused increased microvesicle formation and general membrane disruption (**Figure 9B**).

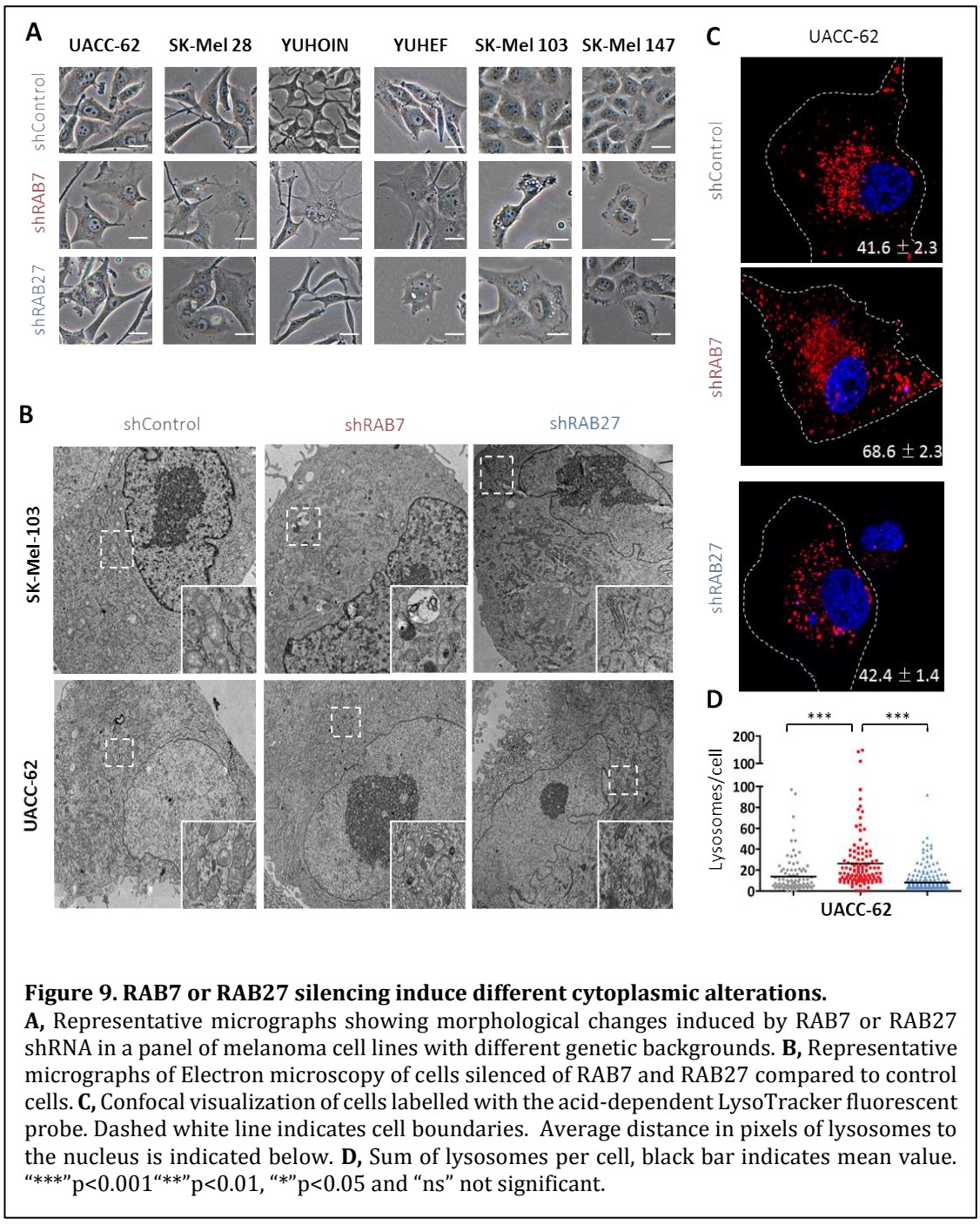

Figure 9. RAB7 or RAB27 silencing induce different cytoplasmic alterations.
A, Representative micrographs showing morphological changes induced by RAB7 or RAB27 shRNA in a panel of melanoma cell lines with different genetic backgrounds. **B,** Representative micrographs of Electron microscopy of cells silenced of RAB7 and RAB27 compared to control cells. **C,** Confocal visualization of cells labelled with the acid-dependent LysoTracker fluorescent probe. Dashed white line indicates cell boundaries. Average distance in pixels of lysosomes to the nucleus is indicated below. **D,** Sum of lysosomes per cell, black bar indicates mean value. "***"p<0.001"**"p<0.01, "*"p<0.05 and "ns" not significant.

In order to confirm TEM results that suggest accumulation of lysosomes upon RAB7 depletion, we stained the cells with the acidic dye LysoTracker and observed different mobilization of lysosomes upon RAB7- but not upon RAB27-depleted cells compared to control. Lysosomes shifted from the perinuclear region towards the cell periphery upon RAB7 depletion (**Figure 9C**) being the

number of lysosomes also increased (**Figure 9D**). These results reinforced the non-equivalent function of these two RAB proteins in the regulation of vesicular trafficking pathways in melanoma.

4. Proteomic Analysis (iTRAQ LC-MS/MS) for the identification of deregulated pathways

Vesicle trafficking plays a critical role in maintaining cell homeostasis[282,283]. In order to have a global view of all pathways affected by the alterations introduced in the vesicular trafficking pathways we performed a global proteomic analysis of the intracellular fraction of two melanoma cell lines (UACC-62 and SK-Mel-103) upon RAB7 and RAB27 depletion.

The resulting proteomic data was filtered for proteins showing a 0.3 $\log_2$ fold change with respect to shRNA controls and $p<0.05$. 5135 proteins were detected, which rendered 385 and 738 distinct proteins (both downregulated and upregulated) in UACC-62 and SK-Mel-103, respectively, upon RAB7 depletion. More changes were observed upon RAB27 depletion, which might be a reflection of the drastic changes observed by TEM: 1483 and 1182 distinct proteins in SK-Mel-103 and UACC-62 (**Figure 10A**). We actually observed a significant overlap of protein changes induced by silencing of either gene in both cell lines: r=0.31 for shRAB7 and r=0.41 for RAB27. (**Figure 10B**). Full list of upregulated or downregulated genes in both cell lines upon RAB7 or RAB27 depletion are listed in **Annex 1** and **Annex2** respectively. Enrichment analyses using KEGG database revealed a preferential downregulation for biological processes related to proliferation, such as DNA replication and cell cycle, common to the depletion of both genes. (**Figure 10C top**). We also observed differential enrichment of pathways related to vesicle trafficking. Some of the pathways enriched upon RAB7 depletion, such as Cell Adhesion Molecules, ECM interaction, Focal adhesion and lysosomal proteins, were not altered upon RAB27 depletion. The opposite was observed in the case of other pathways such as proteosome and TOLL, NOD and RIG receptor pathways (**Figure 10C medium**). Interestingly, we also observed changes in lipid metabolism pathways. Particularly, a strong enrichment in sphingolipid metabolism pathways was observed upon RAB7 depletion, being the

pathway unaltered upon RAB27 depletion (**Figure 10C lower**). Full list of pathways enriched upon RAB7 or RAB27 depletion are listed in **Annex 3.** Gene Set Enrichment Analyses were performed to check that enrichments observed in Figure 10C were statistically significant and identify the genes in each category. (**Figure 10D**). Together these results support the non-equivalent role of RAB7 and RAB27 in controlling different cellular pathways with a particular focus in lipid metabolism pathways.

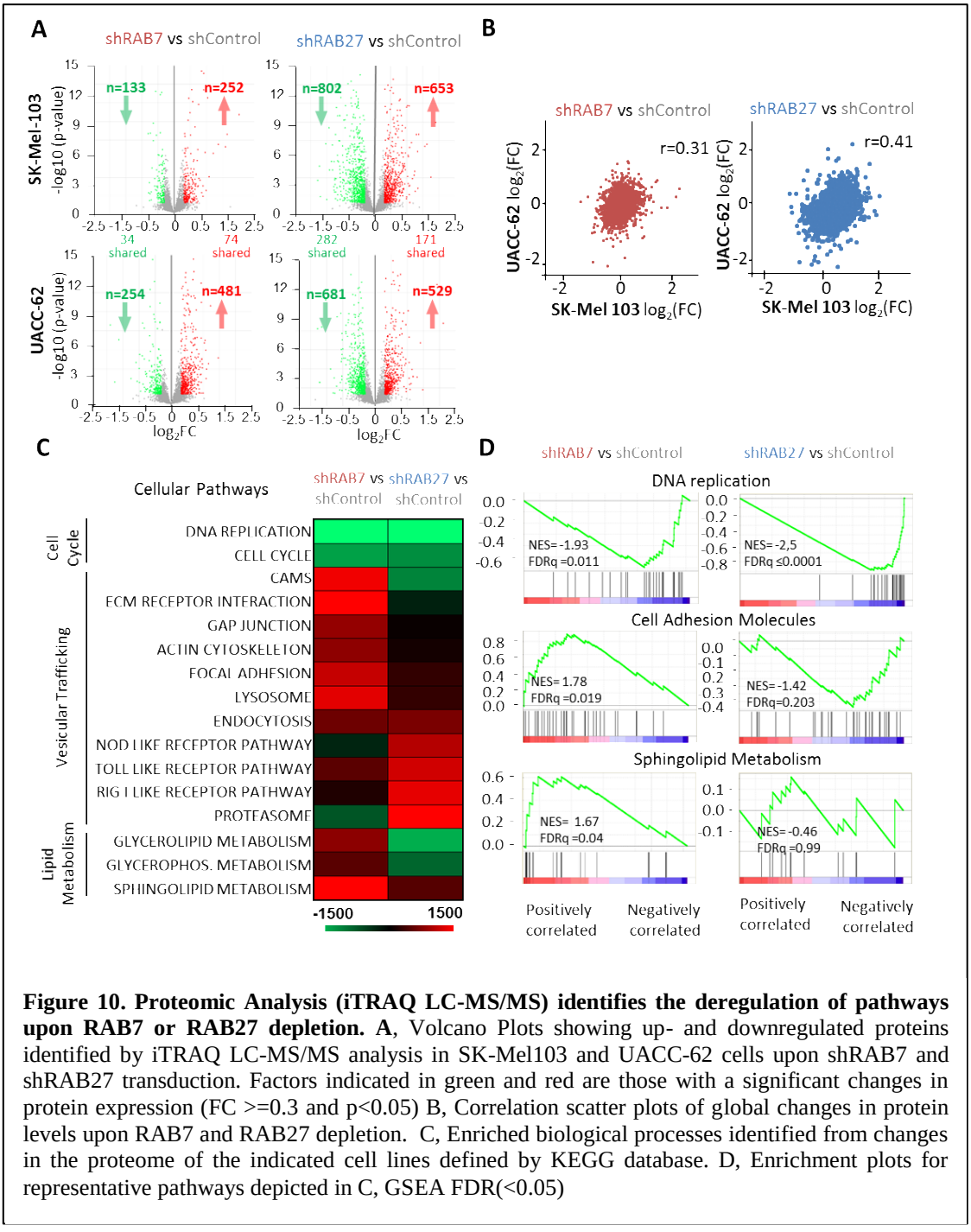

Figure 10. Proteomic Analysis (iTRAQ LC-MS/MS) identifies the deregulation of pathways upon RAB7 or RAB27 depletion. A, Volcano Plots showing up- and downregulated proteins identified by iTRAQ LC-MS/MS analysis in SK-Mel103 and UACC-62 cells upon shRAB7 and shRAB27 transduction. Factors indicated in green and red are those with a significant changes in protein expression (FC >=0.3 and p<0.05) B, Correlation scatter plots of global changes in protein levels upon RAB7 and RAB27 depletion. C, Enriched biological processes identified from changes in the proteome of the indicated cell lines defined by KEGG database. D, Enrichment plots for representative pathways depicted in C, GSEA FDR(<0.05)

5. RAB7-rewiring of sphingolipid metabolism towards ceramide production

We were intrigued by the alterations observedin sphingolipid metabolism caused by RAB7 depletion. Thus, we searched for proteins implicated in this pathway that were upregulated in both cell lines and we identified two lysosomal enzymes that mediate the transformations of sphingolipids into ceramide: Glucosylceramidase (GBA)[284] and Acid Sphingomyelinase (SMPD1)[285] (**Annex 4**).

Next, we confirmed proteomics results by evaluating the changes in the protein levels of SMPD1 and GBA upon shRAB7 and shRAB27 by immunoblot in a panel of melanoma cell lines. Despite some intrinsic-cell line variability we observed an increase in the levels of SMPD1 and GBA upon RAB7 depletion across all the cell lines tested, (**Figure 11A**). Next, we tested if those changes in protein levels

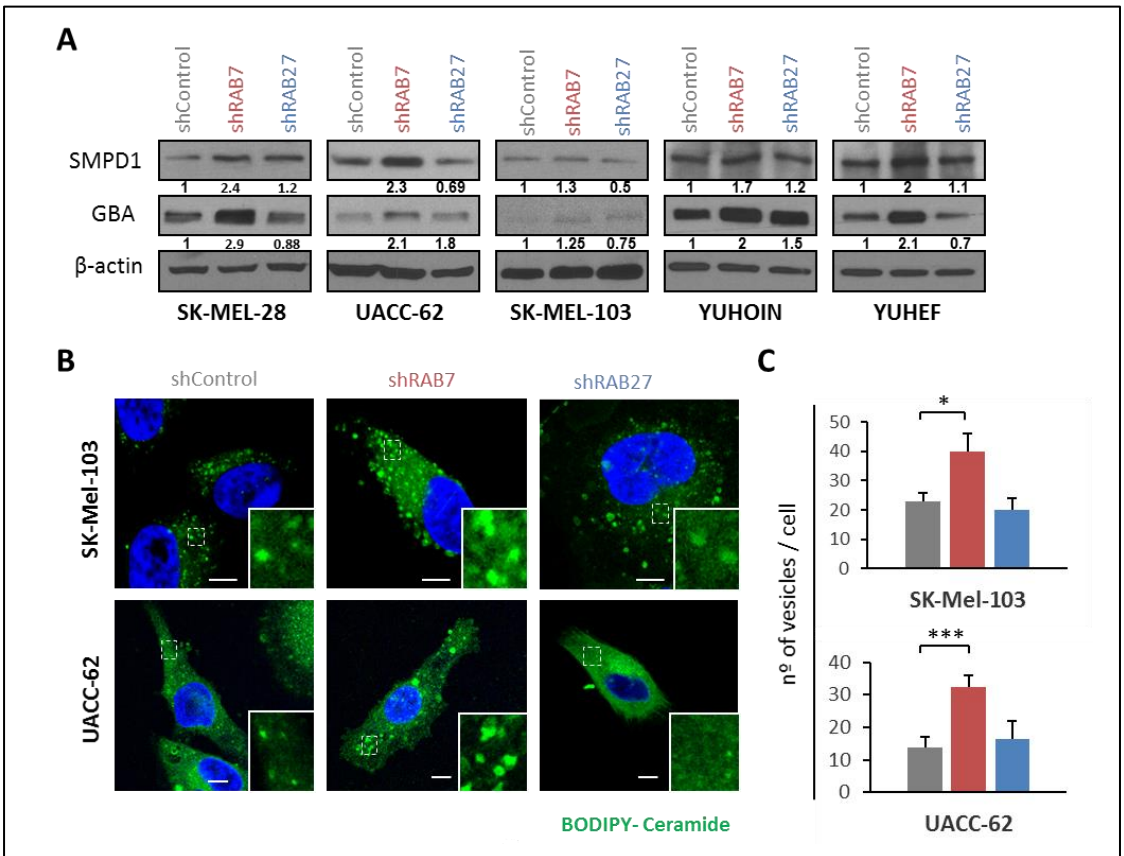

Figure 11 RAB7-rewiring of sphingolipid metabolism towards Ceramide production.
A, Immunoblots showing changes in SMPD1 and GBA upon RAB7 and RAB27 depletion in a panel of melanoma cell lines. **B,** Changes in intracellular ceramide content labeled with NBD-C6-ceramide. Scale bar 10um. **C,** Quantification of number of ceramide positive vesicles per cell in the melanoma cell lines SK-Mel-103 and UACC-62. Error bars correspond to SEM of at least two experiments in duplicates. "***"p<0.001, "**"p<0.01, "*"p<0.05 and "ns" not significant.

translated into alterations in ceramide levels by using the fluorescent probe C6-Ceramide and we observed an increase in the number of ceramide positive vesicles scattered throughout the cytoplasm caused by RAB7 depletion but not upon RAB27 depletion (**Figure 11B and C**).

6. RAB7-depletion does not induce melanoma cell death

As ceramide is considered a classical apoptosis inductor[286,287], we evaluated cell death by a flow cytometry based TMRE mitochondrial membrane potential assay. Interestingly, RAB7 depletion did not caused any difference in cell death compared with control cells, while there was a significant increase in apoptosis upon RAB27 depletion (**Figure 12A**). One of the mechanism described for ceramide-mediated induction of cell death is by triggering pore formation in the mitochondrial outer membrane, which causes the reduction of the membrane potential, leading in turn to cytochrome C release and apoptosis induction. In order to see if this increment in cellular ceramide is affecting mitochondrial homeostasis we stained the cells with the red fluorescent probe MitoTracker (**Figure 12B**). Although there were no changes in mitochondrial network in shRAB7 cells compared with the control, shRAB27 cells mitochondrial network was totally disorganized. Subsequently, we evaluated the mitochondrial OXPHOS activity using the Seahorse technology. As expected, mitochondrial potential and activity was not affected by shRAB7 but was reduced by shRAB27 (**Figure 12C** and **D**). Together, these data suggest that intracellular ceramide accumulation induced by RAB7 depletion is not triggering cell death, while depletion of RAB27 is inducing apoptosis, further reinforcing the non-equivalent role of these two proteins in melanoma.

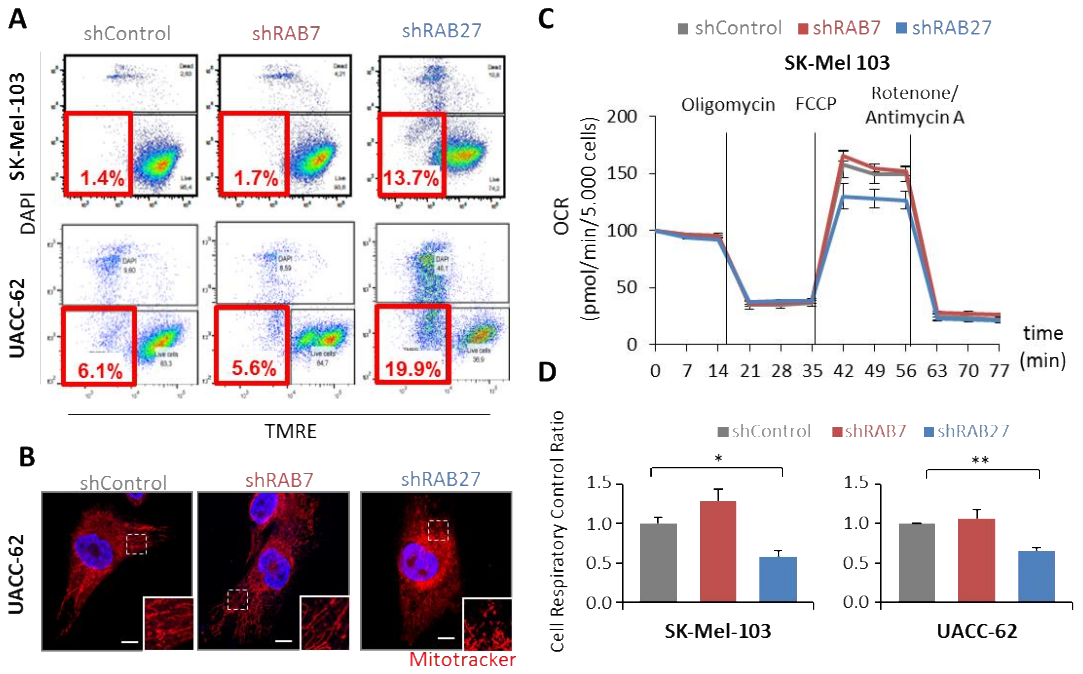

Figure 12 RAB7 depletion does not induce melanoma cell death. A, Flow cytometry TMRE analysis of cell death upon RAB7 and RAB27 depletion. Percentage of apoptotic cells is highlited in red. **B,** Mitochondrial network stained with red fluorescent probe mitotracker in melanoma cells upon RAB7 and RAB27 depletion. **C**, Mitochondrial activity in melanoma cells upon RAB7 or RAB27 silencing determined by oxygen consumption rate (OCR) utilizing the Seahorse XF96 Extracellular Flux Analyzer (Seahorse Bioscience). OCR was measured as pmol/min/cells ($5x10^3$) in four technical replicates at basal conditions and after the administration of the indicated compounds (n=3). **D,** Cell Respiratory Control Ratio from Seahorse experiment in (C). Results are mean ± SEM. Error bars correspond to SEM of three experiments in duplicates. "**"$p<0.01$, "*"$p<0.05$ and "ns"not significant.

7. shRAB7 rewiring of sphingolipid metabolism and invasion is dependent of SMPD1 and GBA

We were intrigued by the fact that melanoma cells silenced for RAB7 are more metastatic while having elevated expression of these enzymes and higher ceramide content. Recent studies have described novel functions of ceramide not related with cell death but with tumour progression, cell-cell communication and metastasis[153,288]. Therefore, we interrogated TCGA database and we observed that among cutaneous melanoma patients (n=486) those with higher mRNA levels of either SMPD1 or GBA had worse survival that those with lower expression levels of those genes. On the other hand, the reverse behaviour was observed in other tumour types such as Pancreatic Adenocarcinoma, or no

differences in overall survival in the case of breast and lung adenocarcinoma. (**Figure 13A**).

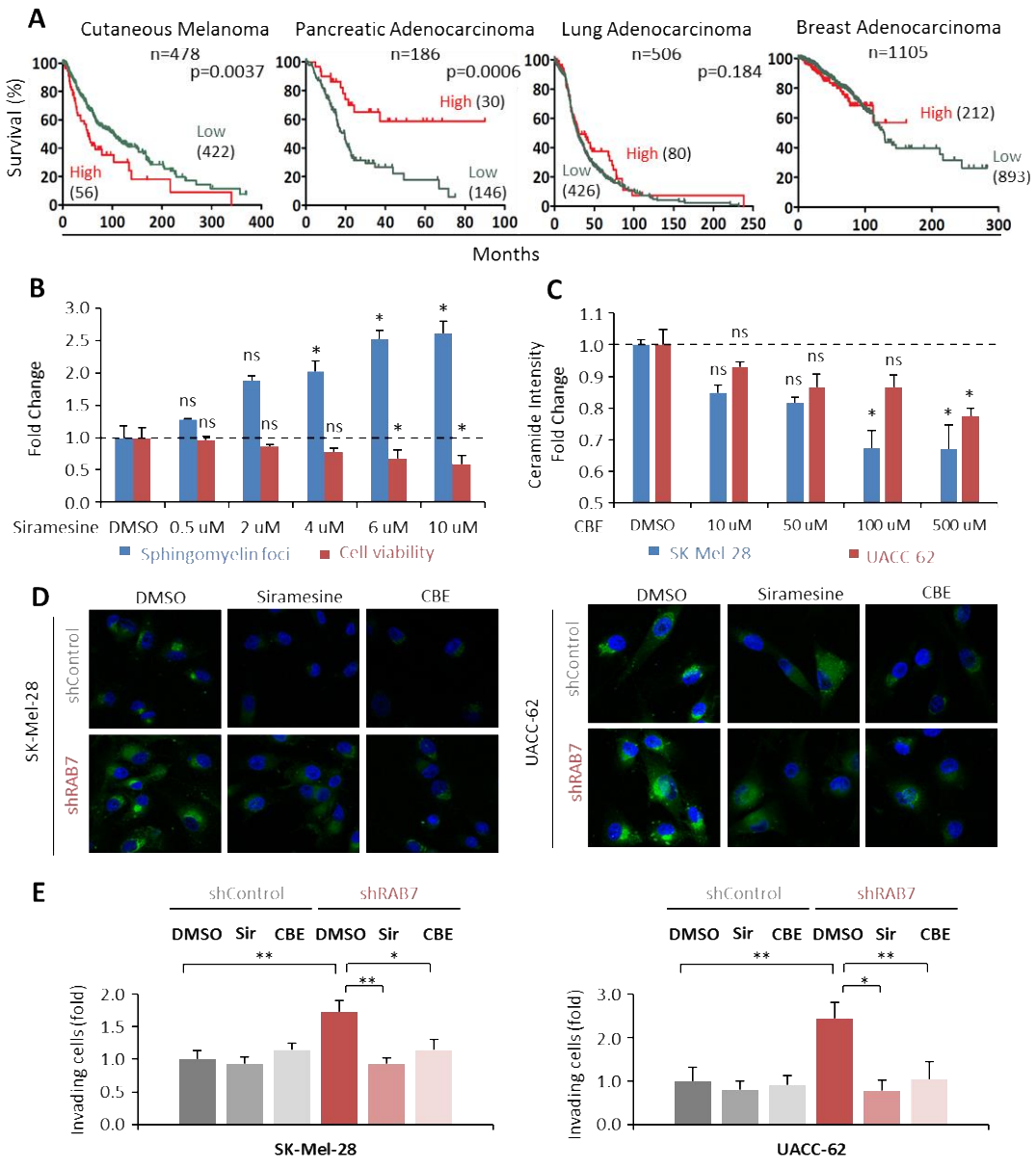

Fig 13 shRAB7 rewiring of sphingolipid metabolism and invasion is dependent on SMPD1 and GBA . A, Overall survival of patients from different tumor types separated as a function of high (10% highest expression) vs. low (remaining patients) *SMPD1 and/or GBA* mRNA . Indicated are *p*-values estimated with the Log-rank test **B,** Left panel, titration of siramesine drug, readout was cell viability determined by cell titer (red) and accumulation of sphingomyelin foci determined by immunofluorescence (blue). **C,** Titration of CBE determined by a decrease in intracellular ceramide intensity determined by IF of NBD-C6- ceramide. **D,** Ceramide staining by IF using NBD-C6-ceramide in two melanoma cell lines upon RAB7 silencing +/- Siramesine and CBE treatment for 24 hrs. **D**, Matrigel invasion assay of two melanoma cell lines upon RAB7 silencing +/- Siramesine and CBE pre-treatment for 24 hrs. Error bars correspond to SEM of two experiments in duplicates. "**"p<0.01, "*"p<0.05 and "ns" not significant.

Therefore, to determine if this increase in ceramide production was behind the increase in invasiveness observed upon RAB7 depletion, we used chemical inhibitors for each of these enzymes: Siramesine[289] for SMPD1 and Conduritol B Epoxide (CBE)[290] for GBA. In order to identify the optimal concentration that would block ceramide production without affecting cell viability we tittered Siramesine by assessing intracellular levels of sphingomyelin (**Figure 13B**) while CBE titration was done by measuring ceramide content (**Figure 13C**). Cell viability was not affected by CCBE even at the highest concentrations used, (data not shown). Moreover, treatment with both inhibitors caused a decrease in ceramide content as measured by immunofluorescence with C6-ceramide probe in two melanoma cell lines transduced with shRAB7 compared to control cells (**Figure 13D**). Curiously, 24hr treatment with either Siramesine or CBE reverted the increase in invasiveness observed by RAB7 depletion in a matrigel invasion assay. (**Figure 13E**). These results reinforce our findings of a RAB7-dependent lineage-specific wiring of the endolysosomal machinery in melanoma.

8. Conditioned medium of RAB7-and RAB27-depleted cells have opposite effects on cell invasion.

Since ceramide has also been described to influence cell-cell communication[153,157], and some studies have described how the secretion of prometastatic proteins with paracrine functions are regulated by RAB proteins[291,292], we tested whether the condition medium of cells depleted of RAB7 and RAB27 would influence the invasiveness of other melanoma cell lines. Thus, we performed a matrigel invasion assay with a non-invasive cell line treated with conditioned medium obtained from cells depleted of RAB7 and RAB27 respectively. Surprisingly, cells treated with conditioned medium from shRAB7 cells were more invasive than cells treated with medium from control cells, and the opposite happened when cells were treated with conditioned medium from shRAB27 cells (**Figure 14A**). This observations recapitulate changes in invasiveness observated in (**Figure 8A and B**).

In addition, similar results were observed in an "in vitro" model of reconstructed human skin: WM164 cells treated with conditioned medium from shRAB7 cells were able to migrate deeper through the dermis while cells treated with conditioned medium from shRAB27 cells barely moved not being able to disrupt the basal layer. (**Figure 14B**). And importantly, treatment of shRAB7 cells with either Siramesine or CBE abrogated the increase in invasion capacity (**Figure 14C**), while adding the inhibitor alone, did not influence invasiveness in WM164 cell line. (**Figure 14D**).

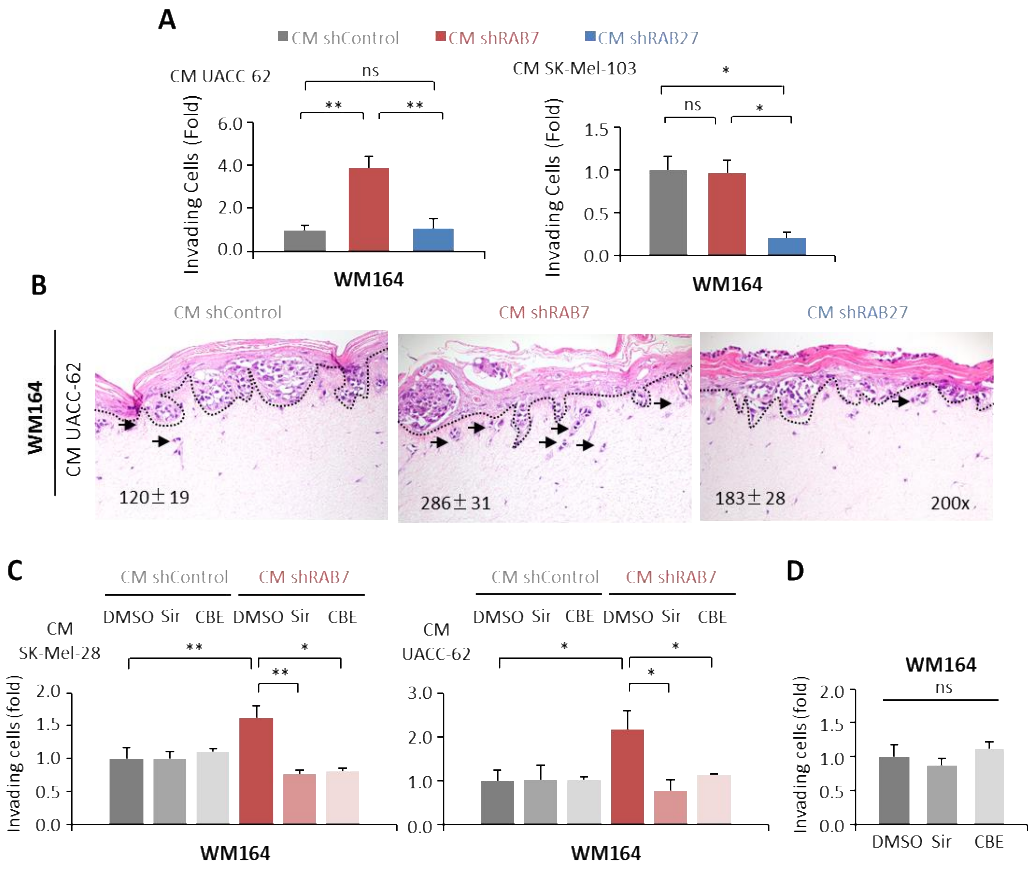

Fig 14 The conditioned media of RAB7- and RAB27-depleted cells has an opposed effect on cell invasion A, Matrigel Invasion Assay of WM164 treated with concentrated CM obtained from UACC-62 or SK-Mel-103 silenced of RAB7 or RAB27. (72 hr). **B,** H&E staining of reconstructed skins with WM164 melanoma cell line treated with concentrated CM of cell line UACC-62 silenced for RAB7 or RAB27 expression. Average invasion (pixels) of melanoma cells is indicated below. **C,** Matrigel Invasion Assay of WM164 treated with concentrated CM obtained from UACC-62 or SK-Mel-28 silenced for RAB7 and treated with DMSO Siramesine or CBE. (72 hr) **D,** Matrigel Invasion Assay of WM164 treated with DMSO Siramesine or CBE (72 hr). Error bars correspond to SEM of at least two experiments in duplicates. "***"p<0.001, "**"p<0.01, "*"p<0.05 and "ns"not significant.

9. Identification of a cluster of lysosomal proteins differentially secreted upon RAB7 depletion

We hypothesized that changes in vesicular trafficking upon RAB7 depletion would cause a secreted factor to be responsible of the paracrine increase in invasiveness of other melanoma cells treated with CM of shRAB7 cells. The secreted fraction was collected from the same cell populations in which iTRAQ experiment was performed, concentrated and analysed by MS/MS as well. 489 and 791 proteins were differentially secreted upon RAB7 depletion in SK-MEL-103 or UACC-62 respectively, and 677 and 1041 proteins in the case of RAB27 depletion in both cell lines (**Figure 15A**). However, we observed little overlap of secreted proteins induced by silencing of RAB7 gene in both cell lines (r=-0.13) while secreted factors changes had a more similar tendency in the case of shRAB27 in both cell lines (r=0.46) (**Figure 15B**). This difference explain why the CM of mildly invasive cells, RAB7-depleted, increase invasion while the CM of highly invasive cell lines. Did not have that effect.

Next, by comparing the secretome data with the intracellular proteomic results we identified 279 proteins that were absent in the cell extracts. Enrichment analyses of the specifically secreted proteins using Gene Ontology database revealed that this proteins are usually located in the extracellular space (Cellular Component GO) and are involved in ECM interactions (**Figure 15C**). Interestingly, focusing on the proteins that were more secreted in UACC-62 shRAB7 and not showing intracellular changes allowed us to identify a cluster of 52 proteins. Functional enrichment of this protein cluster was performed, and strikingly the most enriched categories are related to lysosomal function and location (KEGG and Gene Ontology category FDR >0.05) (**Figure 15D** Full list of functional enrichments is listed in **Annex 5**). Many lysosomal proteins such as Cathepsins and MMP have been linked with tumour metastasis[293]. Therefore, our findings support the prometastatic role of the conditioned medium of RAB7 depleted cells. Unexpectedly, the top scoring protein in that cluster was not a protease but a transmembrane protein termed LRP2/Megalin (Low density lipoprotein receptor type II). LRP2 is a multiligand endocytic receptor located in the plasma membrane, but it is also annotated as endolysosomal protein[294]. This protein was

of particular interest because secreted forms has been described to be involved in several diseases such neuropathies and nefropathies[294,295]. In melanoma, LRP2 expression was described to be increased during melanoma progression[296], but has not been linked to RAB7 mediated trafficking or to metastasis.

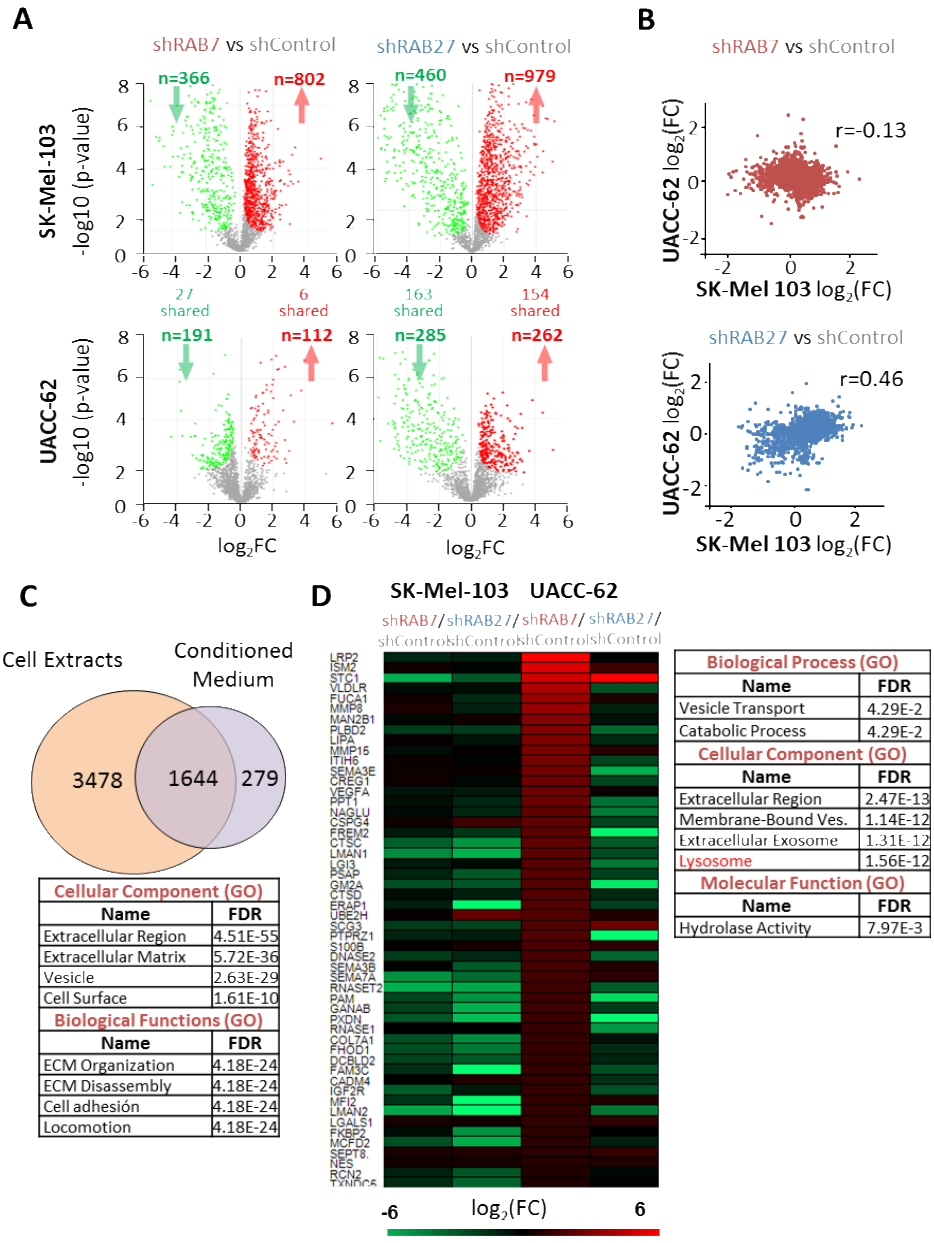

Fig 15 Identification of a cluster of lysosomal proteins differentially secreted upon RAB7 depletion A, Volcano Plots showing up- and downregulated proteins identified by Label Free MS analysis of the concentrated CM obtained from SK-Mel103 and UACC-62 cells upon shRAB7 and shRAB27 transduction. Factors indicated in green and red are those with a significant changes in protein expression (FC >=0.3 and p<0.05) **B,** Correlation scatter plots of changes in protein levels upon RAB7 and RAB27 depletion. **C,** Overlap between all proteins identified in the iTRAQ experiment of Cell extracts and those identified in the proteomic analysis of the conditioned medium. Below are shown the enriched biological process and biological functions of proteins exclusively identified in the concentrated conditioned medium **D,** Cluster of proteins specifically secreted upon RAB7 depletion in UACC-62. Right, panel enrichment analysis of those proteins. Lysosome GO category is highlighted in red

10. RAB7 depletion induces LRP2 secretion in vesicles

First we validated proteomics results by performing an ELISA of the CM from shRAB7 and shRAB27 melanoma cell lines. We observed higher levels of LRP2 secretion upon RAB7 depletion compared with control cells, and the other way around in the case of shRAB27 in several cell lines (**Figure 16A**). Curiously, although intracellular LRP2 was not detected in the iTRAQ we could see how LRP2 levels were also slightly increased upon RAB7 depletion while there was a clear reduction of LRP2 levels upon RAB27 depletion (**Figure 16B**).

Next, we focused on the mechanism behind intracellular trafficking of LRP2 from inside the cell to the extracellular space. By double IF in fixed cells we observed there was an increase in the colocalization of LRP2 with ceramide positive vesicles upon RAB7 depletion (**Figure 16D**). Since ceramide is a component of membrane lipid rafts we purified Detergent Resistant membranes by density gradient and observed a partial colocalization of LRP2 with Flotilin-1 a positive marker of lipids rafts, and no colocalization with the the cytoplasmic marker, Rho-GDI (**Figure 16E**). Since ceramide production by sphingomyelinases has been described as a mechanism of ESCRT-independent exosome secretion[153,157], we checked whether LRP2 colocalized by IF with the exosomal marker CD81 (**Figure 16F**). Furthermore, by ELISA we determined that LRP2 is found preferentially in exovesicles rather than in a soluble form (**Figure 16G**). Together, these results suggest the LRP2 decorates a subtype of intracellular vesicles that are secreted to the extracellular space upon RAB7 depletion.

11. LRP2 as a novel prometastatic protein downstream RAB7

Next, in order to unravel the connexion between ceramide production and LRP2 regulation we analysed the effect of chemical inhibition of GBA and SMPD1 on LRP2; treatment with either CBE or Siramesine caused a decrease in endogenous LRP2 protein levels, measured by immunoblot (**Figure 17A**) and IF (**Figure 17B**) in melanoma cell lines depleted for RAB7. Subsequently, LRP2 amount in purified exosomes was also decreased (**Figure 17C**). This data uncovers a novel link of

regulation between sphingolipid metabolism and transmembrane protein regulation.

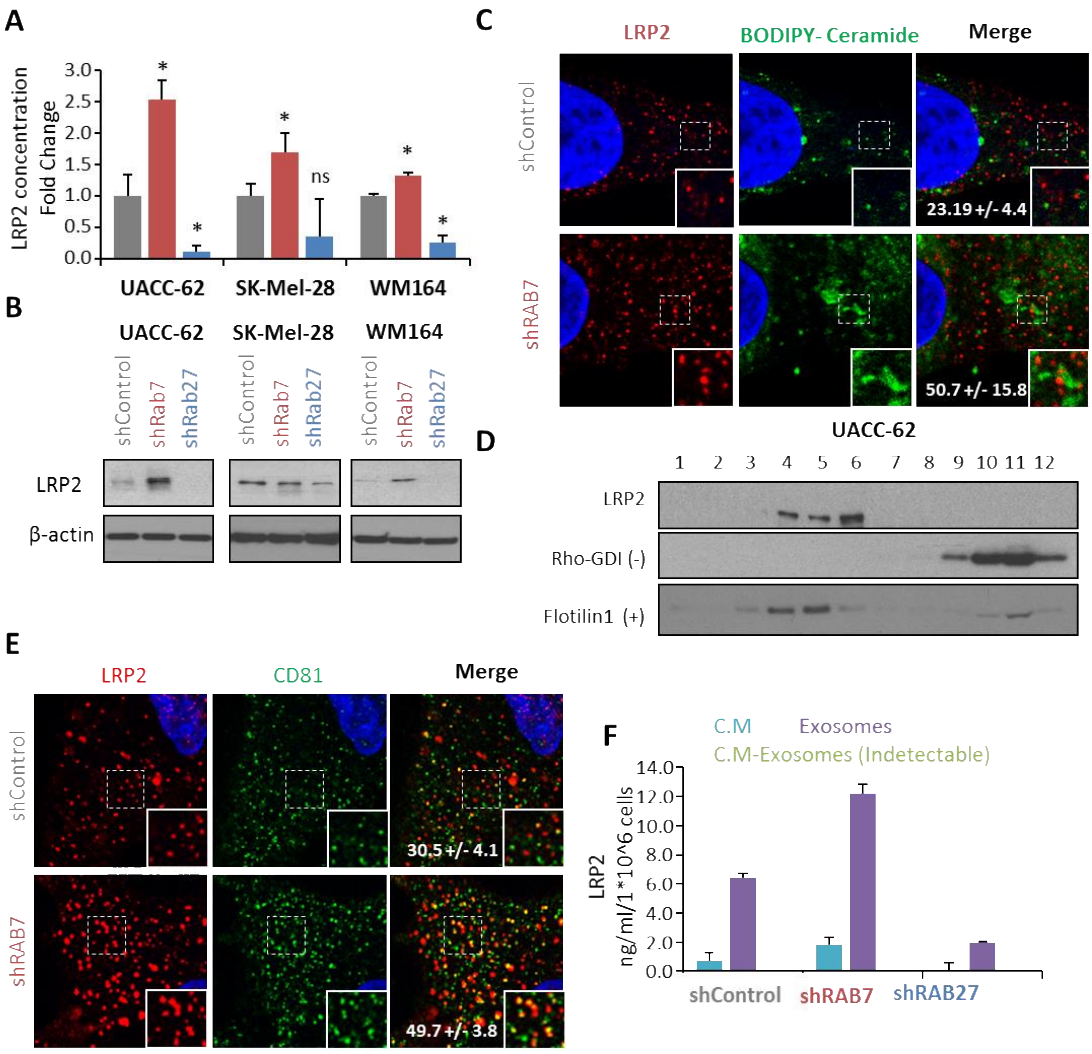

Fig 16 RAB7 depletion induces LRP2 secretion in vesicles
A, ELISA-based quantification of LRP2 in concentrated CM upon depletion of RAB7 and RAB27 in UACC-62, SK-Mel-28 and WM-164 melanoma cell lines. **B**, Immunoblots showing changes in LRP2 upon RAB7 and RAB27 depletion in a panel of melanoma cell lines. **C,** Colocalization of LRP2 and ceramide in UACC-62 silenced for RAB7. Below, green signal intensity in every red dot (arbitrary unit) **D,** LRP2, Rho-DGI and Flotilin1 Immunoblot of continuous fractions obtained from sucrose gradient centrifugation of cell lysates of UACC-62. **E** LRP2 (red) and CD81 (green) double IF upon RAB7 depletion in UACC-62. Percentage of colocalization is indicated below. **F,** ELISA-based quantification of LRP2 in exosomes or concentrated CM of UACC-62 silenced for RAB7 and RAB27 containing or depleted of exosomes (blue, purple and green bars respectively).

It has been described that melanomas acquire LRP2 expression during melanoma progression[296]. However, LRP2 mRNA levels did not predict patient prognosis or there were not significant changes comparing primary tumour and metastasis in the TCGA database[297]. Interestingly, patients harbouring BRAF mutations have

higher mRNA expression levels than patients with mutations in other oncogenes (**Figure 17D**)

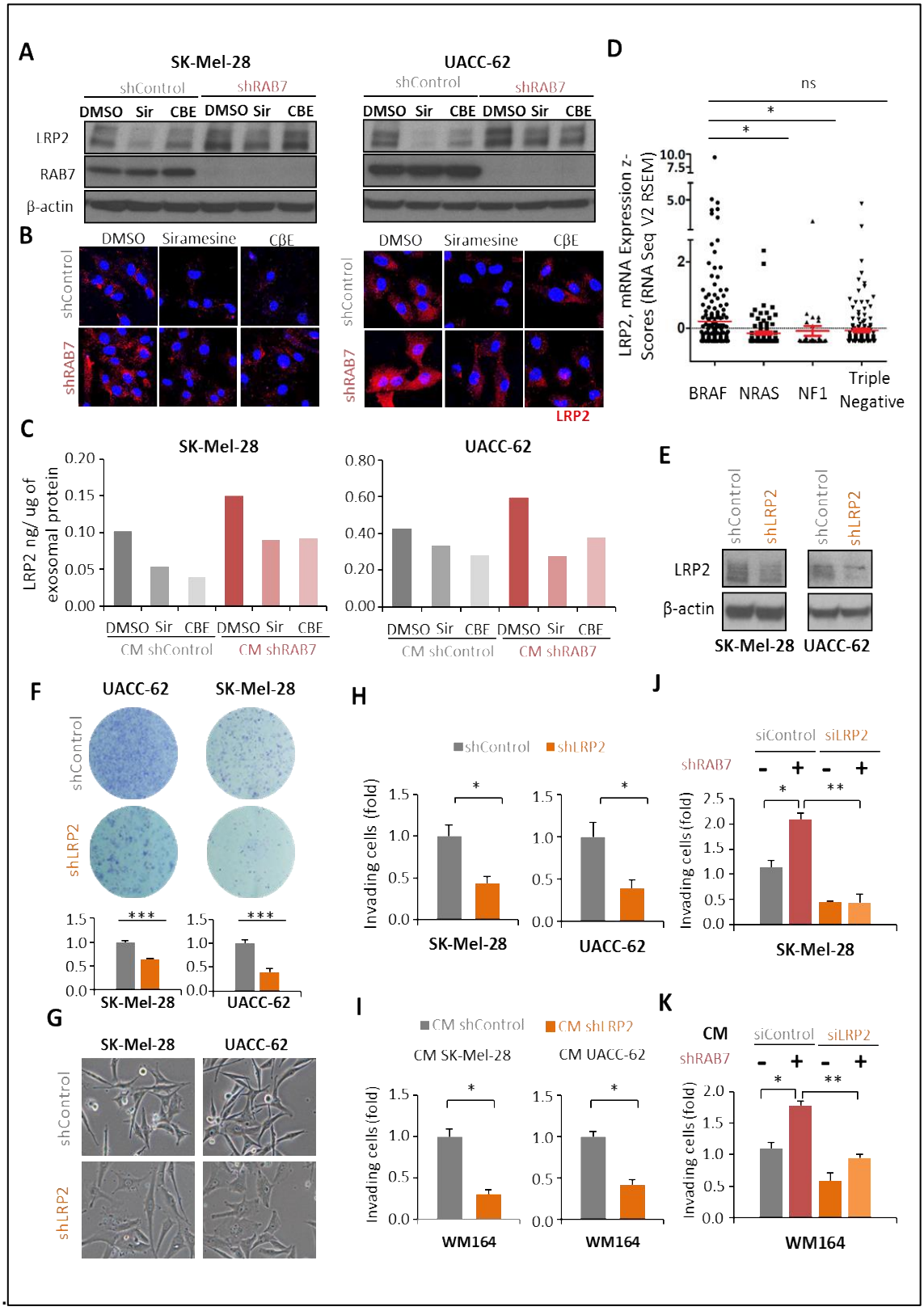

Therefore, we chose two BRAF mutant melanoma cell lines to perform loss-of function assays with a short hairpin RNA construct targeting the coding sequence of the LRP2 gene (**Figure 17E**). Consistent with reported results, LRP2 depletion inhibited melanoma cell proliferation (**Figure 17F**) and induced alterations in cell morphology (**Figure 17G**). Curiously, we also showed that LRP2 depletion (by both shRNA and siRNA) decreased melanoma invasion capacity assessed by matrigel invasion assays (**Figure 17H**). Supporting the paracrine pro-invasive role of LRP2, melanoma cells treated with CM from LRP2 depleted cells decreased their invasion capacity (**Figure 17I**). Moreover, shRAB7-mediated increase in invasion capacity is abrogated when LRP2 is depleted. The same effect was observed when a low invasive melanoma cell line was treated with CM of shRAB7 cells and LRP2 siRNA (**Figure 17J** and **K**).

12. Intracellular proteomic analysis (iTRAQ LC-MS/MS) upon LRP2 depletion identifies enrichment in cell cycle pathways.

In order to gain insight into the mechanism of metastasis driven by LRP2 we performed an unbiased global analysis of cell extracts depleted by LRP2 in two melanoma cell lines (SK-Mel-28 and UACC-62) upon LRP2 depletion (siRNA and shRNA). After performing enrichment analysis, we observed a decrease in

Figure 17. (Page 80) LRP2 as a novel prometastatic protein downstream RAB7 **A** Immunoblot of LRP2 and RAB7 levels upon DMSO, Siramesine or CBE treatment in UACC-62 and SK-Mel-28 melanoma cell lines silenced for RAB7. **B,** LRP2 (red) immunofluorescence in the same conditions that (A) **C,** ELISA-based quantification of LRP2 in exosomes of UACC-62 and SK-Mel-28 silenced for RAB7 upon DMSO, Siramesine or CBE treatment. **D,** LRP2 mRNA expression levels from TCGA melanoma samples categorized by oncogene subtypes. **E**, Downregulation of LRP2 in two melanoma cell lines by lentiviral-based transfer of an shRNA constructs visualized by immunoblotting with respect to cells expressing control shRNA. **F**, Colony formation of the cell populations in (D) determined by crystal violet 14 days after seeding. Left panel shows quantification, data are represented as the ratio of inhibition with respect to control shRNA-transduced cells. **G,** Representative micrographs showing morphological changes induced by LRP2 depletion in SK-Mel-28 and UACC-62. **H,** Invasiveness of two melanoma cell lines expressing Control shRNA or an shRNA directed against LRP2, evaluated by Matrigel invasion assay (72 hr). **I,** Matrigel Invasion Assay of WM164 treated with concentrated CM obtained from SK-Mel-28 or UACC-62 silenced of LRP2. (72 hr) **J,** Changes in invasiveness SK-Mel-28 expressing Control shRNA or LRP2 shRNA with or without siLRP2, evaluated by matrigel invasion assay. **K,** Matrigel invasion assay of WM164 treated with concentrated CM obtained from SK-Mel-28 silenced of RAB7 plus siControl or siLRP2 (72 hr). Error bars correspond to SEM of at least two experiments in duplicates. "***"$p<0.001$, "**"$p<0.01$, "*"$p<0.05$ and "ns" not significant.

pathways involved in cell proliferation, and protein secretion (**Figure 18A**). These results confirmed our previous findings upon LRP2 depletion (**Figure 17D**).

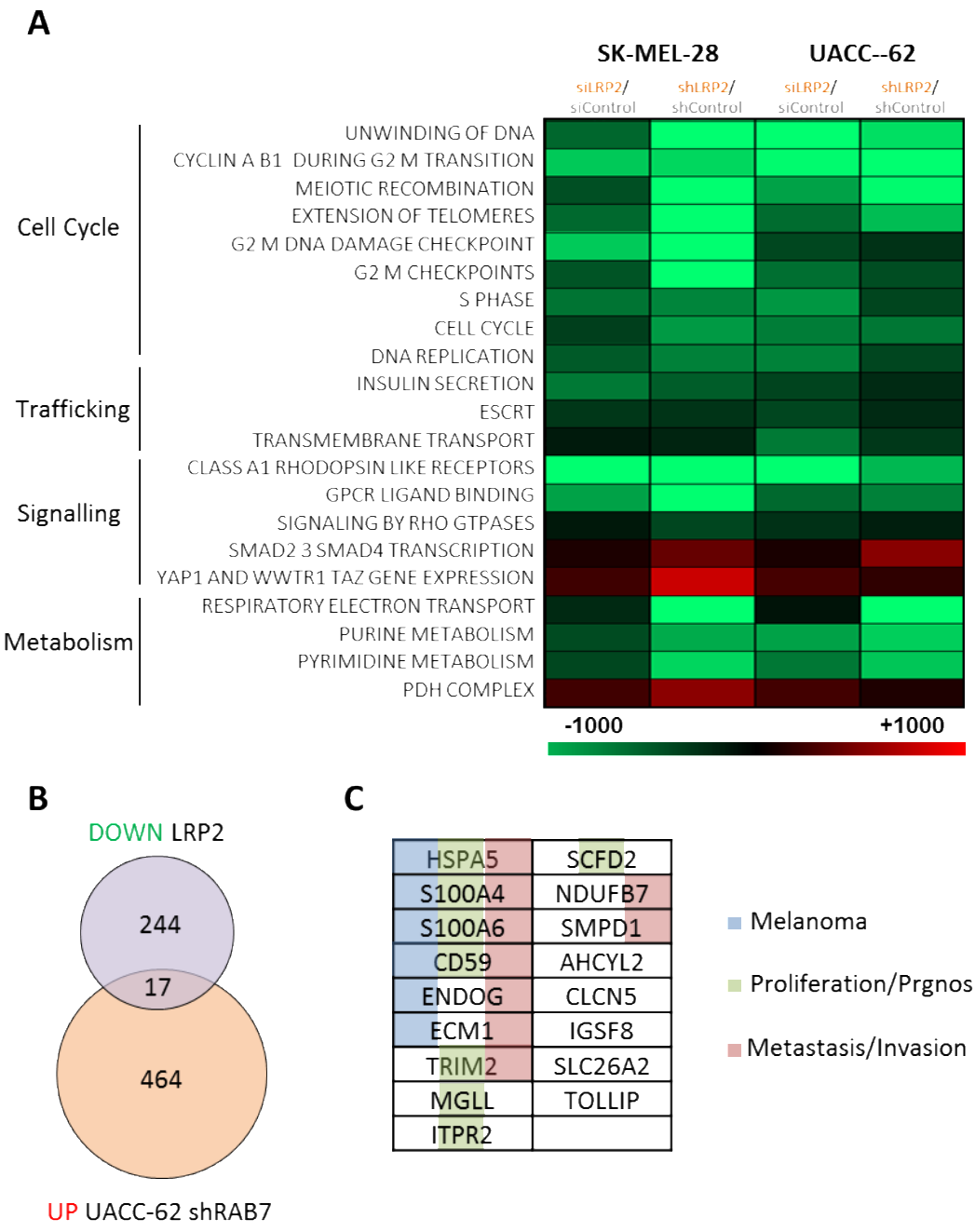

Figure 18. Intracellular proteomic analysis (iTRAQ LC-MS/MS) upon LRP2 depletion identifies enrichment in cell cycle pathways. A, Enriched biological process identified from changes in the proteome of the indicated conditions defined by REACTOME database by ssGSEA. **B**, Venn diagram showing overlap between downregulated genes obtained in both Proteomics experiment upon LRP2 or RAB7 depletion. **C,** List of shared proteins identified in (B). Proteins with a described role in melanoma are labeled in blue, those with role in cancer proliferation or prognosis in green and those with a prometastatic role in red.

Next, an overlap enrichment of the proteins downregulated upon LRP2 depletion and those overexpressed in UACC-62 shRAB7 (**Figure 10A**) was performed. This analysis allowed us to identified 16 proteins controlled by both LRP2 and RAB7 (**Figure 18B**). This cluster was composed by proteins implicated in melanoma proliferation and metastasis such as CD59[298], S100A4, S100A6[298–300] and HSPA5[301] among others (**Figure 18C**). All together, these results expand the knowledge of vesicular trafficking in melanoma and have provided new insight in the regulation of sphingolipid metabolism. Moreover, we have identified a novel prometastatic target of RAB7, LRP2 that open new venues of research in the endolysosomal and cancer metastasis fields.

VII.

DISCUSSION

DISCUSIÓN

Melanoma is prime example of aggressive tumor that proceeds with important changes in the transcriptome and proteome[11,66,67,87,302]. Its incidence has increased worldwide becoming a public health problem(ref9 dire). Nevertheless, last decade has witnessed an enormous advance in genomic subclassification of melanoma patients attending to mutations in multiple signaling cascades (ie BRAF, NRAS, NF1, p53 and PTEN)[55,87]. However, unlike other tumors, melanoma subgroups do not present differences in patient prognosis[303–305].

Therefore, there is an urgent need to dissect the mechanisms of melanoma progression and metastasis. Our laboratory recently described a melanoma unique wiring of the lysosomal pathway that fosters tumor progression[104]. The small GTPase RAB7 was also identified as an early induced melanoma driver[242] whose levels can be tuned to favor either proliferation or invasion[104]. Surprisingly, RAB7 regulation and expression in clinical specimens was unlike the small GTPase RAB27, a well-known target of MITF[94,306–308] (the best characterized melanocyte lineage-specific transcription factor), that is involved in exosome secretion and melanoma metastasis[74,243,309].

The objective of this PhD thesis was to deepen the knowledge of the alterations of vesicular trafficking induced by RAB7 and RAB27 in melanoma and its implications in progression and metastasis. In brief, (1) we have confirmed previous studies describing that both small GTPases have similar roles in cell proliferation, but non-equivalent roles in cell invasion. (2) We have described differential vesicular trafficking alterations induced by either RAB7 or RAB27 silencing, particularly alterations in lysosomal biogenesis and motility. (3) An unbiased proteomic analysis of cell extracts us to identify a RAB7-dependent rewiring of the sphingolipid metabolism pathways characterized by an increase in ceramide production driven by the lysosomal proteins SMPD1 and GBA. (4) Accumulation of intracellular was responsible of the increase in invasion capacity upon RAB7 depletion in an auto- and paracrine manner. (5) In addition, proteomic characterization of the secretome changes induced by RAB7 silencing has identified a cluster of lysosomal proteins differentially secreted that were unaltered intracellularly. (6) From this cluster of proteins, we identified LRP2 as a novel melanoma prometastatic factor that was located in ceramide enriched exovesicles and increase melanoma cell invasiveness in an auto-and paracrine way. All together, we have unveiled how

melanomas modulate sphingolipid metabolism, increasing ceramide synthesis and inducing secretion of LRP2, a protein not associated with melanoma metastasis before in a RAB7 dependent manner.

The **figure 19** illustrates the findings of this PhD Thesis, highlighting the mechanism that mediating the increased melanoma metastasis observed upon RAB7 depletion.

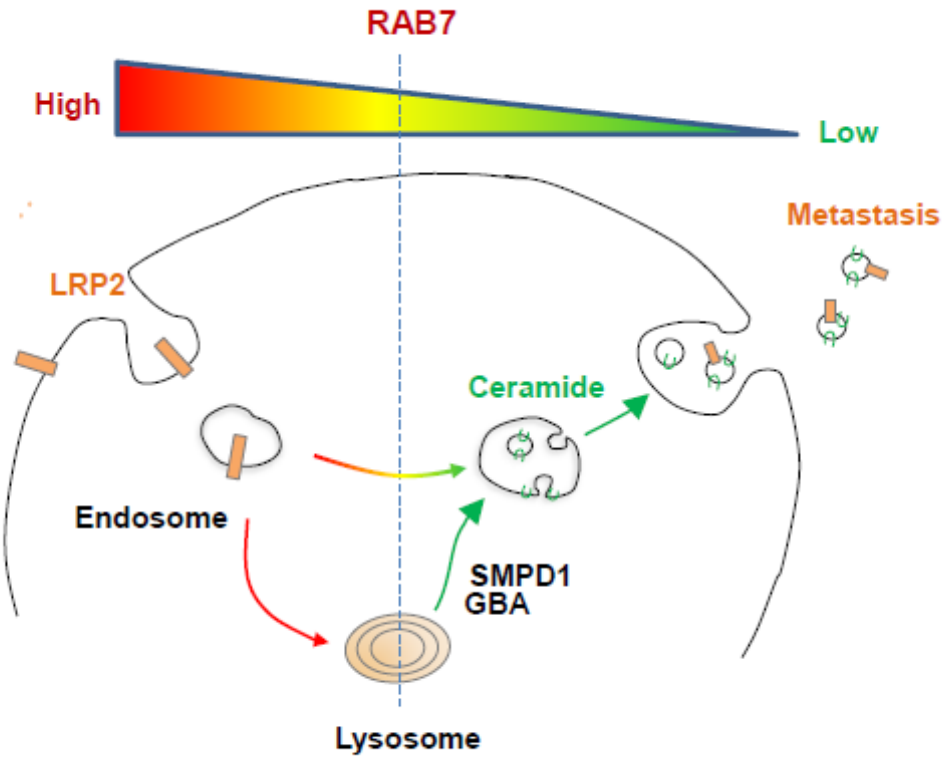

Figure 19. Proposed model illustrating RAB7-dependent metastasis through ceramide and LRP2, Upon RAB7 downregulation, there, LRP2 is no longer degraded, therefore it is secreted via exovesicles produced by an increase in ceramide mediated by SMPD1 and GBA. This increased secretion of vesicles loaded with LRP2 increase invasive potential in a paracrine way.

1. Non-equivalent roles of RAB7 and RAB27 in melanoma proliferation and invasion confirmed by proteomics

RAB7 and RAB27 dependency of melanoma to has been previously addressed by us and other groups[101,104]. However, even though they are the best characterized RAB

proteins in this tumor type, we are the first ones comparing their effect in proliferation in parallel, both in vitro and in vivo, We also extended the previous knowledge associated with the role of these two RAB proteins in proliferation: In vitro, we have use an extensive panel of melanoma cell lines representative of the most frequent genetic background identified in patients. In vivo, we have employed a syngeneic melanoma mouse model that allowed us to rule out involvement of the immune system in the proliferation defects observed upon RAB7 or RAB27 silencing. We have determined that growth arrest is due to an A an impairment in S phase entry, which has been confirmed by our proteomics data, However, whether it is a direct or indirect effect needs to be further elucidated. Furtheremore, although both proteins are required for cell proliferation, RAB27 depletion, unlike RAB7 depletion, triggers apoptosis by inducing mitochondrial membrane depolarization and, therefore, growth arrest.

In melanocytes, it has been shown that RAB7 and RAB27 control different steps in melanosome biogenesis and secretion[232,310–312]. Therefore, we initially hypothesized that RAB27 could be downstream RAB7 in promoting shRAB7 dependent increase in invasion capacity. However, this was not the case: Our proteomics experiment showed that vesicular trafficking pathways were modulated in different ways upon RAB7 or RAB27 depletion, and the observation was confirmed with Electron microscopy and lysoTracker fluorescent probes. It is important to mention that intracellular alterations in membrane trafficking are later translated to the secretory phenotype and invasion capacity[118,119]. We identified lysosomal alterations in the case of RAB7 depletion that promote melanoma invasiveness, but no with RAB27, actually enrichments in proteins secreted upon RAB27 depletion revealed pathways such as “proteasome” and “ER-stress” (Data not shown). Together, this data suggest that RAB7 and RAB27 has different downstream effectors regulating different pathways that in the case of proliferation have the same result but different outputs in invasion. However, further characterization of the trafficking machinery is required in order to identify effectors of the phenotypes observed.

2. Implications of the rewiring of sphingolipid metabolism mediated by RAB7 depletion

One of the most relevant findings of this thesis was the identification of the rewiring of the sphingolipid metabolism pathways towards a ceramide production phenotype with implications in auto- and paracrine invasiveness. The proteomic approach employed identified the overexpression of SMPD1 and GBA, two lysosomal enzymes that produce more ceramide upon RAB7 depletion. Ceramide is one the best described inductor of apoptosis in cancer[287,313,314], including melanoma[315], and the mechanism of induction has been extensively described[316].

However, more recent evidence challenges this long-established anti-tumorigenic role of ceramide and suggests it may favor tumor progression: In breast cancer there is an increase in Ceramide Synthases (CERS) and ceramides have been observed during progression[317]. Ceramide originated by CERS6 protects from apoptosis in HNSCC cells[318] and in Hela cells, overexpression of CERS2 protects cells from ionizing radiation[319]. Regarding ceramide-induced autophagy, it can also be cytoprotective[320,321], increase anoxia resistance[322] and it is necessary for lung colonization in a melanoma mouse model of metastasis[288]. Finally, ceramide also plays a role in vesicular trafficking: It regulates an ESCRT-independent mechanism of exosome secretion[153,157], which might be behind increased LRP2 secretion in RAB7 depleted cells. These exovesicles are enriched in ceramide compared to the parental cell line[323].

In our model, we ruled out that the increase in ceramide upon RAB7 depletion was triggering apoptosis. In line with the novel cancer-related ceramide function, it was very surprising to see that patients with the highest expression at RNA level of GBA or SMPD1 had worst prognosis than the rest. This might be a reflection of the lineage-specific wiring of the lysosomal pathways in melanoma. SMPD1 and GBA are two lysosomal proteins; mutations in those genes have been associated with the lysosomal storage disorders Niemann-Pick disease (types A and B)[324,325] and Gaucher disease[284,326], respectively. These two diseases together with CMTB2, disease caused by mutations in RAB7 have in common the appearance of

neuropathies[230,327–329]. Moreover, some subsets of patients suffering Gaucher disease or CMTB have higher risk of developing cutaneous melanomas[330–332], although whether this mutations could favor or hamper melanoma progression is unclear. As melanocytes are cells from neural origin[1], our data offer a mechanistic framework to close the gap between the melanoma-specific rewiring of vesicular trafficking and lysosomal storage diseases.

Although a connexion of GBA and melanoma has not been previously addressed, the role of SMPD1 in melanoma is controversial: it is been regarded as tumor suppressor, whose depletion induces melanoma growth and metastasis[113]. Nevertheless, other study performed in a mouse model of melanoma metastasis, suggest that is important for in vivo colonization[288]. In our model, some of the effects observed upon RAB7 depletion, such as a decrease in cell proliferation and pigmentation (data not shown) matches with those described for SMPD1 overexpression[113]. However, upon RAB7 depletion there is an increase in the invasive potential, abolished upon siramesine or CBE treatment. A possible reason of this difference, is because most of SMPD1 studies have been done with genetic downregulation or overexpression. However, in our model SMPD1 upregulation only occurs at protein level and not RNA level (data not shown) and in a more regulated location: the endo-lysosomal system. Actually, RAB7 is essential for lysosome biogenesis and its fusion with late endosomes and autophagosomes[120,125,161,187]. Therefore, the activity and turnover of lysosomal enzymes such as SMPD1 and GBA may be affected due to the impaired autophagic and endocytic flux and lysosomal biogenesis and homeostasis found upon RAB7 silencing[124]. Importantly, lysosomal membrane permeabilization can lead to the leakage of hydrolases and proteases into the cytoplasm leading to lysosomal mediated cell death[289,333,334] interestingly, in macrophages, SMPD1 activity is required for correct lysosome-endosome fusion[335,336]. Therefore, an increase in SMPD1 could be a compensatory mechanism to alleviate lysosomal instability induced by RAB7 depletion[337], an to avoid an excess in sphingomyelin levels, which can be deleterious for lysosomes[338]. Moreover, it is also required for the correct trafficking of MET receptor to the plasma membrane[339] a tyrosine kinase with well described roles in drug resistance and cancer progression including melanoma[74,340–342] . Thus, this study expands the knowledge of vesicular trafficking

by emphasizing its connection with ceramide production and reinforcing the non-canonical apoptotic role of ceramide that results in a proinvasive phenotype in melanoma.

3. **Paracrine effect of Conditioned Medium in other cell types: LRP2**

Another striking finding is that cells treated with the CM of RAB7 or RAB27 depleted cells could recapitulate the changes in invasion observed in the donor cells. A similar effect has been described for other proteins such as LAMC2[343], RAB3C[291], RAB37[292] and miRNAs[344] in several cancer models. This induced increase in invasiveness is not a direct consequence of the increased levels of ceramide themselves, since addition of exogenous ceramide could not recapitulate the changes in invasiveness observed (data not shown). Thus, we hypothesized that the paracrine effect of shRAB7 derived conditioned medium could be mediated by a different process.

Our lab and others have previously described that lysosomal proteins intracellular location can be regulated by RAB7 levels and translocated towards cell periphery and the extracellular space to favor metastasis[104,237–239]. However this conclusions were raised in the observation of individual proteins such as Cathepsins (refe direna) and XXX upon RAB7 depletion[104]. But no systemic assessment of changes in the secretome has been reported to date. However, we have performed an unbiased proteomic approach that led to the identification of a cluster of lysosomal proteins differentially secreted (without alterations in the intracellular fraction) upon RAB7 depletion. Many of those genes have been, individually, shown to have a pro-metastatic role in melanoma and other tumor types, such as SEMA3E[345], CTSD[346,347], MMP15[348], and GM2A[349]. Surprisingly the top scoring gene in the proteomic analysis of the conditioned medium was not a protein with degradative or chemoattractant roles, but as transmembrane receptor: LRP2/Megalin. LRP2 expression has been described to increase along melanoma progression, and to have an essential role in melanoma cell proliferation[296], results that were confirmed with our Loss-of-Function experiments and proteomic analysis. However, the positive effect here reported on metastatic or invasive potential of melanoma cells has not been previously observed. Curiously, RAB27 depletion also decreased LRP2 levels and

induced apoptotic cell death, suggesting that LRP2 may be downstream RAB7 and RAB27 but modulated in a different manner.

LRP2 is expressed during embryonic development in the neural tube, where it plays a role in forming brain structures[295,350,351]. In adults, LRP2 expression is generally restricted to the proximal tubes of the kidney, where it mediates the clearance of filtered molecules[352,353]. Interestingly, this protein has been identified in urine-derived exosomes[354] and altered expression of LRP2 has been described in several nephropathies[355,356] and neuropathies, such as Alzheimer Disease[357,358]. Curiously, although little is known about the mechanism of LRP2 intracellular trafficking, LRP2-mediated endocytosis has been described as an alternative pathway for lysosomal biogenesis[359]. LRP2 expression is widespread during embryonic development and later repressed[360] this switch resembles EMT process which is crucial for the reestablishing of migratory abilities in cancer cells. Alterations in LRP2 expression levels or mutational status have been identified in several tumor types such as: hepatocellular carcinoma[361], renal[362], prostate cancer[363] and Melanoma[296]. However, only in the melanoma study, functional experiments to address the physiological relevance of LRP2 were performed. Thus, the role of LRP2 in cancer is mostly unknown.

We have shown that LRP2 is secreted in melanoma-derived exosomes[356], which are small vesicles with crucial roles in metastasis[74,364,365] and derived from RAB7 regulated late endosomes (Multivesicular bodies)[187,366]. Those exosomes can be uptaken by recipient cells and their content (RNA and proteins) can confer changes in invasiveness[367–370] to the recipient cells. LRP2 has been identified in exovesicles purified from urine samples obtained from healthy[354,371,372], diabetic patients[356] or kidney cells in culture[373], although, this studies were descriptive and provide no mechanism of how is LRP2 translocated to the exosomes. Interestingly, LRP2 transmembrane domain has been described to be associated with lipid rafts in Madin-Darby canine kidney cells[374]. Lipid rafts are membrane microdomains, with important functions in cell signaling[375]. They are composed by several species of glycosphingolipids and glycoprotein, being ceramide one of them[376,377]. Thus, our data suggest that upon ceramide formation blockage with Siramesine or CBE,

ceramide abundance in lipid rafts is diminished and LRP2 can no longer be directed there. This suggest a novel mechanism of LRP2 regulation.

LRP2 is a transmembrane receptor with more than 50 ligands described so far[294]. However, there is nothing described regarding how can this protein increase cell invasion in a paracrine way. One hypothesis that may explain how LRP2 can increase invasiveness of other melanoma cells, would propose that LRP2 has a mechanism of action similar to Notch[112,358]: LRP2 can be cleaved in a process called regulated intramembrane proteolysis(RIP)[378], and the resulting intracellular cytoplasmic domain (ICD) might be translocated to the nucleus where it would alter gene expression[115,358,379]. Actually, a Notch-similar mechanism of action has been described for LRP1[380,381], another member of the LDLR family

4. **Future Perspectives**

The work This thesis has shed light about a novel mechanism of vesicular trafficking modulation exploited by tumor cells to metastasize: RAB7dependent rewiring of sphingolipid metabolism to increase ceramide production and secretion in exovesicles loaded with LRP2, that in turn promotes tumor progression in a paracrine way. Still, future work directed at better understanding the crosstalk between vesicular trafficking regulators and lipid metabolism and cancer will extend our knowledge of the contribution of these processes to human disease.

RAB proteins are general regulators of vesicular trafficking, acting as protein hubs for the binding of downstream interactors. Further analyses regarding the role of particular effectors downstream RAB7 are needed to understand how lysosomes move towards cell periphery and secrete their content into the extracellular space. Also, a deeper study of how is ceramide trafficked through the endolysosomal system, and its regulation on LRP2 protein levels, will broad our knowledge of the connection between vesicular trafficking and sphingolipid metabolism.

It should be noted that many groups have found associations between neural diseases such as Parkinson[382,383], Alzheimer[384] and melanoma. Importantly,

mutations in SOX10, the upstream regulator of RAB7 expression are also implicated in demyelinating peripheral neuropathies[385]. These diseases are characterized by the loss of the myelin sheath that insulates the nerves, of which sphingolipids are an essential component[386]. Our data link specific rewiring of vesicular trafficking pathways with altered sphingolipid metabolism, specifically, processes that take place in the lysosomes. Therefore, it would be interesting to explore whether GBA or SMPD1 have an implication in neuropathies or could play a driver role in in the progression of melanomas developed by patients suffering from Lysosomal storage diseases.

Regarding the rewiring of sphingolipid metabolism, there are other lipids and enzymes with important prometastatic functions such as Sphingosine 1 Phosphate (S1P)[387–389] or ASAH1[390]. Whether they might be playing a role in RAB7 dependent invasion is unknown. In order to obtain a more complete picture of the sphingolipid metabolism rewiring directed by RAB7 depletion. ASAH1, S1P and CERS activity should be taken into account.

Finally, there are many questions pending regarding LRP2 regulation, function and intracellular trafficking in melanoma. Therefore, a better understanding in all these topics will provide a meaningful insight about the mechanism of melanoma metastasis that might have the potential to be exploited as therapeutic target.

VIII.

CONCLUSIONS

CONCLUSIONES

In the light of the results presented in this PhD thesis, we can conclude the following:

1. RAB7 and RAB27 expression are essential for melanoma cell proliferation but have non-equivalent roles in cell invasion.

2. RAB7 and RAB27 depletion induce differential vesicular trafficking alterations: while RAB7 knockdown causes an increase in the number of lysosomes and their shift towards the cell periphery, RAB27 silencing induces membrane disruption and microvesicles formation.

3. An unbiased proteomic approach allowed for the identification of the sphingolipid metabolism rewiring towards ceramide production upon RAB7 depletion. This switch is characterized by an increase in SMPD1 and GBA protein levels.

4. In melanoma, the increase in ceramide content does not cause cell death but instead promotes cell invasion in a RAB7 dependent manner.

5. Proteomic analysis of the secreted fraction upon RAB7 depletion allowed for the identification of a cluster of lysosomal proteins specifically secreted (showing no changes in the intracellular levels).

6. LRP2, identified in the secreted lysosomal proteins cluster, is essential for melanoma proliferation and mediates RAB7 dependent invasion. It is secreted in exovesicles and colocalizes with ceramide-enriched domains.

Collectively the data presented in this PhD thesis deepens the knowledge of vesicular trafficking in melanoma and establish a novel crosstalk between sphingolipid metabolism and vesicle trafficking modulators.

A luz de los resultados presentados en esta tesis doctoral, se presentan las siguientes conclusiones:

1. La capacidad proliferativa de las células de melanoma es dependiente de la expresión tanto de RAB7 como de RAB27. Sin embargo, el silenciamiento de ambos genes tiene un efecto contrapuesto en la capacidad invasiva celular.

2. El silenciamiento de RAB7 o RAB27 desencadena una serie de alteraciones citoplásmicas. Una reducción en los niveles de RAB7 produce un incremento en la producción de lisosomas y su translocación a la periferia celular. Mientras que el silenciamiento de RAB27 presenta un cambio fenotípico caracterizado por la disrupción de la membrana y la formación de microvesículas.

3. Un análisis objetivo del proteoma celular tras el silenciamiento de RAB7 ha permitido la identificación de alteraciones en el metabolismo de esfingolípidos. Esta modulación está caracterizada por el incremento en los niveles tanto de SMPD1 como de GBA, ambas enzimas esenciales para la producción de ceramida.

4. El incremento en ceramida no modula la muerte celular, no obstante, conlleva a un aumento en la capacidad invasiva de las células de melanoma dependiente de la expresión de RAB7.

5. Mediante un análisis proteómico del medio condicionado controlado por la expresión de RAB7 se ha identificado un aumento en la secreción de un grupo de proteínas lisosomales. Dicho cambio no se observa sin embargo a nivel intracelular.

6. Análisis funcionales tras la identificación de LRP2 en el medio condicionado, revelan su papel indispensable en el mantenimiento de la

proliferación en melanoma. Además, postulan a LRP2 como nuevo factor de metástasis controlado por la expresión de RAB7.

Los datos presentados en esta tesis aumentan nuestro conocimiento del papel del tráfico vesicular en melanoma mediante el establecimiento de un nuevo punto de conexión entre el metabolismo de esfingolípidos y los moduladores del tráfico vesicular.

BIBLIOGRAPHY

IX.

BIBLIOGRAFÍA

1. Dupin, E. & Le Douarin, N. M. Development of melanocyte precursors from the vertebrate neural crest. *Oncogene* **22,** 3016–3023 (2003).
2. American Cancer Society. Key Statistics for Melanoma Skin Cancer. *2017-01-06* Available at: https://www.cancer.org/cancer/melanoma-skin-cancer/about/key-statistics.html. (Accessed: 22nd June 2017)
3. Garbe, C. *et al.* Diagnosis and treatment of melanoma. European consensus-based interdisciplinary guideline - Update 2016. *Eur. J. Cancer* **63,** 201–217 (2016).
4. Siegel, R. L., Miller, K. D. & Jemal, A. Cancer statistics, 2017. *CA. Cancer J. Clin.* **67,** 7–30 (2017).
5. Siegel, R., Naishadham, D. & Jemal, A. Cancer statistics, 2013. *CA. Cancer J. Clin.* **63,** 11–30 (2013).
6. Scoggins, C. R. *et al.* Gender-related differences in outcome for melanoma patients. *Ann Surg* **243,** 693–8; discussion 698–700 (2006).
7. Joosse, A. *et al.* Sex is an independent prognostic indicator for survival and relapse/progression-free survival in metastasized stage III to IV melanoma: a pooled analysis of five European organisation for research and treatment of cancer randomized controlled trials. *J. Clin. Oncol.* **31,** 2337–46 (2013).
8. Gupta, P. B. *et al.* The melanocyte differentiation program predisposes to metastasis after neoplastic transformation. *Nat. Genet.* **37,** 1047–1054 (2005).
9. Scott, K. L. *et al.* Proinvasion Metastasis Drivers in Early-Stage Melanoma Are Oncogenes. *Cancer Cell* **20,** 92–103 (2011).
10. Soengas, M. S. & Lowe, S. W. Apoptosis and melanoma chemoresistance. *Oncogene* **22,** 3138–3151 (2003).
11. Lawrence, M. S. *et al.* Mutational heterogeneity in cancer and the search for new cancer-associated genes. *Nature* **499,** 214–218 (2013).
12. Chin, L., Merlino, G. & DePinho, R. A. Malignant melanoma: modern black plague and genetic black box. *Genes Dev.* **12,** 3467–3481 (1998).
13. Luke, J. J., Flaherty, K. T., Ribas, A. & Long, G. V. Targeted agents and immunotherapies: optimizing outcomes in melanoma. *Nat. Rev. Clin. Oncol.* (2017). doi:10.1038/nrclinonc.2017.43
14. Wolchok, J. D. *et al.* Overall Survival with Combined Nivolumab and Ipilimumab in Advanced Melanoma. *N. Engl. J. Med.* **377,** 1345–1356 (2017).
15. Kawakami, A. & Fisher, D. E. Key Discoveries in Melanocyte Development. *J. Invest. Dermatol.* **131,** E2–E4 (2011).
16. Zabierowski, S. E. & Herlyn, M. Embryonic stem cells as a model for studying melanocyte development. *Methods Mol. Biol.* **584,** 301–16 (2010).
17. Nordlund, J. J. The Melanocyte and the Epidermal Melanin Unit: An Expanded Concept. *Dermatologic Clinics* **25,** 271–281 (2007).
18. Costin, G.-E. & Hearing, V. J. Human skin pigmentation: melanocytes modulate skin color in response to stress. *FASEB J.* **21,** 976–94 (2007).
19. Lopes, V. S., Wasmeier, C., Seabra, M. C. & Futter, C. E. Melanosome maturation defect in Rab38-deficient retinal pigment epithelium results in instability of immature melanosomes during transient melanogenesis. *Mol. Biol. Cell* **18,** 3914–27 (2007).

20. Fukuda, M. in *Encyclopedia of Cell Biology* 235–242 (Elsevier, 2016). doi:10.1016/B978-0-12-394447-4.20020-5
21. Brenner, M. & Hearing, V. J. The Protective Role of Melain Against UV Damage in Human Skin. *Photochem. Photobiol.* **84,** 539–49 (2008).
22. Lin, J. Y. & Fisher, D. E. Melanocyte biology and skin pigmentation. *Nature* **445,** 843–850 (2007).
23. Kaidbey, K. H., Agin, P. P., Sayre, R. M. & Kligman, A. M. Photoprotection by melanin--a comparison of black and Caucasian skin. *J. Am. Acad. Dermatol.* **1,** 249–60 (1979).
24. Jimbow, K., Roth, S. I., Fitzpatrick, T. B. & Szabo, G. Mitotic activity in non-neoplastic melanocytes in vivo as determined by histochemical, autoradiographic, and electron microscope studies. *J. Cell Biol.* **66,** 663–671 (1975).
25. Mintz, B. & Klein-Szanto, A. J. Malignancy of eye melanomas originating in the retinal pigment epithelium of transgenic mice after genetic ablation of choroidal melanocytes. *Proc. Natl. Acad. Sci. U. S. A.* **89,** 11421–5 (1992).
26. Brito, F. C. & Kos, L. Timeline and distribution of melanocyte precursors in the mouse heart. *Pigment Cell Melanoma Res.* **21,** 464–470 (2008).
27. Lin, C.-S. & Zak, F. G. Studies on Melanocytes: VI. Melanocytes in the Middle Ear. *Arch. Otolaryngol. - Head Neck Surg.* **108,** 489–490 (1982).
28. Goldgeier, M. H., Klein, L. E., Klein-Angerer, S., Moellmann, G. & Nordlund, J. J. The distribution of melanocytes in the leptomeninges of the human brain. *J. Invest. Dermatol.* **82,** 235–8 (1984).
29. Barrett, A. W. & Scully, C. Human oral mucosal melanocytes: a review. *J. Oral Pathol. Med.* **23,** 97–103 (1994).
30. Whiteman, D. C., Pavan, W. J. & Bastian, B. C. The melanomas: a synthesis of epidemiological, clinical, histopathological, genetic, and biological aspects, supporting distinct subtypes, causal pathways, and cells of origin. *Pigment Cell Melanoma Res.* **24,** 879–897 (2011).
31. Bastian, B. C. The Molecular Pathology of Melanoma: An Integrated Taxonomy of Melanocytic Neoplasia. *Annu. Rev. Pathol. Mech. Dis.* **9,** 239–271 (2014).
32. Bennett, D. C. Human melanocyte senescence and melanoma susceptibility genes. *Oncogene* **22,** 3063–3069 (2003).
33. Holly, E. A., Kelly, J. W., Shpall, S. N. & Chiu, S. H. Number of melanocytic nevi as a major risk factor for malignant melanoma. *J. Am. Acad. Dermatol.* **17,** 459–68 (1987).
34. English, J. S. *et al.* Site-specific melanocytic naevus counts as predictors of whole body naevi. *Br. J. Dermatol.* **118,** 641–4 (1988).
35. Zayour, M. & Lazova, R. Congenital melanocytic nevi. *Clinics in Laboratory Medicine* **31,** 267–280 (2011).
36. Kincannon, J. & Boutzale, C. The physiology of pigmented nevi. *Pediatrics* **104,** 1042–1045 (1999).
37. Clark, W. H. Origin of Familial Malignant Melanomas From Heritable Melanocytic Lesions. *Arch. Dermatol.* **114,** 732 (1978).
38. Shain, A. H. *et al.* The Genetic Evolution of Melanoma from Precursor Lesions. *N. Engl. J. Med.* **373,** 1926–1936 (2015).
39. Farber, M. J., Heilman, E. R. & Friedman, R. J. Dysplastic Nevi. *Dermatologic Clinics* **30,** 389–404 (2012).

40. Duffy, K. & Grossman, D. The dysplastic nevus: From historical perspective to management in the modern era. *J. Am. Acad. Dermatol.* **67,** 19.e1–19.e12 (2012).
41. LeBoit, P., Burg, G., Weedon, D. & Sarasain, A. *Pathology & Genetics of Skin Tumours. World Health Organization clasification of tumours*. (2006).
42. Bastian, B. C., LeBoit, P. E. & Pinkel, D. Mutations and copy number increase of HRAS in Spitz nevi with distinctive histopathological features. *Am. J. Pathol.* **157,** 967–972 (2000).
43. Puig, S. & Malvehy, J. Monitoring Patients with Multiple Nevi. *Dermatologic Clinics* **31,** 565–577 (2013).
44. Carrera, C. *et al.* Prognostic role of the histological subtype of melanoma on the hands and feet in Caucasians. *Melanoma Res.* 1 (2017). doi:10.1097/CMR.0000000000000340
45. Pollock, P. M. *et al.* High frequency of BRAF mutations in nevi. *Nat. Genet.* **33,** 19–20 (2002).
46. Carr, J. & Mackie, R. M. Point mutations in the N-ras oncogene in malignant melanoma and congenital naevi. *Br. J. Dermatol.* **131,** 72–7 (1994).
47. Van Raamsdonk, C. D. *et al.* Frequent somatic mutations of GNAQ in uveal melanoma and blue naevi. *Nature* **457,** 599–602 (2009).
48. Brenn, T. Pitfalls in the evaluation of melanocytic lesions. *Histopathology* **60,** 690–705 (2012).
49. Troxel, D. B. Pitfalls in the diagnosis of malignant melanoma: findings of a risk management panel study. *Am. J. Surg. Pathol.* **27,** 1278–83 (2003).
50. Clark, W. H., From, L., Bernardino, E. A. & Mihm, M. C. The Histogenesis and Biologic Behavior of Primary Human Malignant Melanomas of the Skin. *Cancer Res.* **29,** (1969).
51. Greenwald, H. S., Friedman, E. B. & Osman, I. Superficial spreading and nodular melanoma are distinct biological entities: A challenge to the linear progression model. *Melanoma Research* **22,** 1–8 (2012).
52. Cornelison, R. in *Dermatological Cryosurgery and Cryotherapy* 695–700 (2016). doi:10.1007/978-1-4471-6765-5_136
53. Durbec, F., Martin, L., Derancourt, C. & Grange, F. Melanoma of the hand and foot: Epidemiological, prognostic and genetic features. A systematic review. *British Journal of Dermatology* **166,** 727–739 (2012).
54. Shain, A. H. & Bastian, B. C. From melanocytes to melanomas. *Nat. Rev. Cancer* **16,** 345–358 (2016).
55. Hayward, N. K. *et al.* Whole-genome landscapes of major melanoma subtypes. *Nature* **545,** 175–180 (2017).
56. Singh, A. D., Turell, M. E. & Topham, A. K. Uveal Melanoma: Trends in Incidence, Treatment, and Survival. *Ophthalmology* **118,** 1881–1885 (2011).
57. Miller, A. J. & Mihm, M. C. Melanoma. *N. Engl. J. Med.* **355,** 51–65 (2006).
58. Clark, W. H. *et al.* A study of tumor progression: the precursor lesions of superficial spreading and nodular melanoma. *Hum. Pathol.* **15,** 1147–65 (1984).
59. Gimotty, P. A. *et al.* Biologic and prognostic significance of dermal Ki67 expression, mitoses, and tumorigenicity in thin invasive cutaneous melanoma. *J. Clin. Oncol.* **23,** 8048–8056 (2005).
60. Chin, L. *et al.* Cooperative effects of INK4a and ras in melanoma

susceptibility in vivo. *Genes Dev.* **11,** 2822–2834 (1997).
61. Dankort, D. *et al.* BrafV600E cooperates with Pten loss to induce metastatic melanoma. *Nat. Genet.* **41,** 544–552 (2009).
62. Maertens, O. *et al.* Elucidating distinct roles for NF1 in melanomagenesis. *Cancer Discov.* **3,** 338–349 (2013).
63. Dror, S. *et al.* Melanoma miRNA trafficking controls tumour primary niche formation. *Nat. Cell Biol.* **18,** 1006–1017 (2016).
64. Brychtova, S. *et al.* in *Research on Melanoma - A Glimpse into Current Directions and Future Trends* (InTech, 2011). doi:10.5772/22912
65. Karagiannis, P. *et al.* IgG4 subclass antibodies impair antitumor immunity in melanoma. *J. Clin. Invest.* **123,** 1457–1474 (2013).
66. Hoek, K. S. DNA microarray analyses of melanoma gene expression: A decade in the mines. *Pigment Cell Research* **20,** 466–484 (2007).
67. Haqq, C. *et al.* The gene expression signatures of melanoma progression. *Proc. Natl. Acad. Sci.* **102,** 6092–6097 (2005).
68. Stacker, S. A. *et al.* Lymphangiogenesis and lymphatic vessel remodelling in cancer. *Nat. Rev. Cancer* **14,** 159–172 (2014).
69. Karaman, S. & Detmar, M. Mechanisms of lymphatic metastasis. *J. Clin. Invest.* **124,** 922–928 (2014).
70. Damsky, W. E., Rosenbaum, L. E. & Bosenberg, M. Decoding melanoma metastasis. *Cancers* **3,** 126–163 (2011).
71. Olmeda, D. *et al.* Whole-body imaging of lymphovascular niches identifies pre-metastatic roles of midkine. *Nature* **546,** 676–680 (2017).
72. Bakalian, S. *et al.* Molecular Pathways Mediating Liver Metastasis in Patients with Uveal Melanoma. *Clin. Cancer Res.* **14,** (2008).
73. Demirsoy, S., Martin, S., Maes, H. & Agostinis, P. Adapt, Recycle, and Move on: Proteostasis and Trafficking Mechanisms in Melanoma. *Front. Oncol.* **6,** 240 (2016).
74. Peinado, H. *et al.* Melanoma exosomes educate bone marrow progenitor cells toward a pro-metastatic phenotype through MET. *Nat. Med.* **18,** 883–891 (2012).
75. Hoshino, A. *et al.* Tumour exosome integrins determine organotropic metastasis. *Nature* **527,** 329–335 (2015).
76. Damsky, W. E., Theodosakis, N. & Bosenberg, M. Melanoma metastasis: new concepts and evolving paradigms. *Oncogene* **33,** 2413–2422 (2014).
77. Gruber, S. B., Barnhill, R. L., Stenn, K. S. & Roush, G. C. Nevomelanocytic proliferations in association with cutaneous malignant melanoma: a multivariate analysis. *J. Am. Acad. Dermatol.* **21,** 773–80 (1989).
78. Bevona, C. *et al.* Cutaneous Melanomas Associated with Nevi. *Archives of Dermatology* **139,** 1620–1624 (2003).
79. Marks, R., Dorevitch, A. P. & Mason, G. DO ALL MELANOMAS COME FROM 'MOLES'? A STUDY OF THE HISTOLOGICAL ASSOCIATION BETWEEN MELANOCYTIC NAEVI AND MELANOMA. *Australas. J. Dermatol.* **31,** 77–80 (1990).
80. Crucioli, V. & Stilwell, J. The Histogenesis of malignant melanoma in relation to pre???existing pigmented lesions. *J. Cutan. Pathol.* **9,** 396–404 (1982).
81. Takata, M., Murata, H. & Saida, T. Molecular pathogenesis of malignant melanoma: A different perspective from the studies of melanocytic nevus

and acral melanoma. *Pigment Cell and Melanoma Research* **23,** 64–71 (2010).
82. Köhler, C. *et al.* Mouse Cutaneous Melanoma Induced by Mutant BRaf Arises from Expansion and Dedifferentiation of Mature Pigmented Melanocytes. *Cell Stem Cell* **21,** 679–693.e6 (2017).
83. Moon, H. *et al.* Melanocyte Stem Cell Activation and Translocation Initiate Cutaneous Melanoma in Response to UV Exposure. *Cell Stem Cell* **21,** 665–678.e6 (2017).
84. Van Akkooi, A. C. J. & Eggermont, A. M. M. Melanoma: MSLT-1 - SNB is a biomarker, not a therapeutic intervention. *Nat. Rev. Clin. Oncol.* **11,** 248–249 (2014).
85. Morton, D. L. *et al.* Final Trial Report of Sentinel-Node Biopsy versus Nodal Observation in Melanoma. *N. Engl. J. Med.* **370,** 599–609 (2014).
86. Lawrence, M. S. *et al.* Mutational heterogeneity in cancer and the search for new cancer-associated genes. *Nature* **499,** 214–218 (2013).
87. TCGA. Genomic Classification of Cutaneous Melanoma. *Cell* **161,** 1681–1696 (2015).
88. Chi, Z. *et al.* Clinical presentation, histology, and prognoses of malignant melanoma in ethnic Chinese: A study of 522 consecutive cases. *BMC Cancer* **11,** (2011).
89. Chang, A. E., Karnell, L. H. & Menck, H. R. The national cancer data base report on cutaneous and noncutaneous melanoma: A summary of 84,836 cases from the past decade. *Cancer* **83,** 1664–1678 (1998).
90. McLaughlin, C. C. *et al.* Incidence of noncutaneous melanomas in the U.S. *Cancer* **103,** 1000–1007 (2005).
91. Furney, S. J. *et al.* Genome sequencing of mucosal melanomas reveals that they are driven by distinct mechanisms from cutaneous melanoma. *J. Pathol.* **230,** 261–269 (2013).
92. Furney, S. J. *et al.* The mutational burden of acral melanoma revealed by whole-genome sequencing and comparative analysis. *Pigment Cell Melanoma Res.* **27,** 835–838 (2014).
93. Luo, J., Solimini, N. L. & Elledge, S. J. Principles of Cancer Therapy: Oncogene and Non-oncogene Addiction. *Cell* **136,** 823–837 (2009).
94. Garraway, L. A. & Sellers, W. R. Lineage dependency and lineage-survival oncogenes in human cancer. *Nat. Rev. Cancer* **6,** 742–742 (2006).
95. Flaherty, K. T., Hodi, F. S. & Fisher, D. E. From genes to drugs: targeted strategies for melanoma. *Nat. Rev. Cancer* **12,** 349–361 (2012).
96. Garraway, L. A. *et al.* Integrative genomic analyses identify MITF as a lineage survival oncogene amplified in malignant melanoma. *Nature* **436,** 117–122 (2005).
97. Chiaverini, C. *et al.* Microphthalmia-associated transcription factor regulates RAB27A gene expression and controls melanosome transport. *J Biol Chem* **283,** 12635–12642 (2008).
98. Widlund, H. R. & Fisher, D. E. Microphthalamia-associated transcription factor: a critical regulator of pigment cell development and survival. *Oncogene* **22,** 3035–3041 (2003).
99. Haq, R. *et al.* BCL2A1 is a lineage-specific antiapoptotic melanoma oncogene that confers resistance to BRAF inhibition. *Proc. Natl. Acad. Sci.* **110,** 4321–4326 (2013).

100. McGill, G. G. *et al.* Bcl2 regulation by the melanocyte master regulator Mitf modulates lineage survival and melanoma cell viability. *Cell* **109,** 707–718 (2002).
101. Akavia, U. D. *et al.* An integrated approach to uncover drivers of cancer. *Cell* **143,** 1005–1017 (2010).
102. Eichhoff, O. M. *et al.* The immunohistochemistry of invasive and proliferative phenotype switching in melanoma: a case report. *Melanoma Res.* **20,** 349–55 (2010).
103. Salti, G. I. *et al.* Micropthalmia transcription factor: A new prognostic marker in intermediate-thickness cutaneous malignant melanoma. *Cancer Res.* **60,** 5012–5016 (2000).
104. Alonso-Curbelo, D. *et al.* RAB7 Controls Melanoma Progression by Exploiting a Lineage-Specific Wiring of the Endolysosomal Pathway. *Cancer Cell* **26,** 61–76 (2014).
105. Goding, C. R. A picture of Mitf in melanoma immortality. *Oncogene* **30,** 2304–2306 (2011).
106. Cifdaloz, M. *et al.* Systems analysis identifies melanoma-enriched pro-oncogenic networks controlled by the RNA binding protein CELF1. *Nat. Commun.* **8,** 2249 (2017).
107. Pérez-Guijarro, E. *et al.* Lineage-specific roles of the cytoplasmic polyadenylation factor CPEB4 in the regulation of melanoma drivers. *Nat. Commun.* **7,** 13418 (2016).
108. Cifdaloz, M. New Oncogenic Networks Regulated by the RNA Binding Factor CUGBP1 in Melanoma. (Universidad Autónoma de Madrid, 2016).
109. Liersch, R., Hirakawa, S., Berdel, W. E., Mesters, R. M. & Detmar, M. Induced lymphatic sinus hyperplasia in sentinel lymph nodes by VEGF-C as the earliest premetastatic indicator. *Int. J. Oncol.* **41,** 2073–2078 (2012).
110. Wang, X., Moschos, S. J. & Becker, D. Functional analysis and molecular targeting of aurora kinases a and B in advanced melanoma. *Genes Cancer* **1,** 952–963 (2010).
111. Miaczynska, M. *et al.* APPL proteins link Rab5 to nuclear signal transduction via an endosomal compartment. *Cell* **116,** 445–56 (2004).
112. Biemesderfer, D. Regulated intramembrane proteolysis of megalin: Linking urinary protein and gene regulation in proximal tubule? *Kidney Int.* **69,** 1717–1721 (2006).
113. Bizzozero, L. *et al.* Acid sphingomyelinase determines melanoma progression and metastatic behaviour via the microphtalmia-associated transcription factor signalling pathway. *Cell Death Differ.* **21,** 507–520 (2013).
114. Beckett, C., Nalivaeva, N. N., Belyaev, N. D. & Turner, A. J. Nuclear signalling by membrane protein intracellular domains: The AICD enigma. *Cell. Signal.* **24,** 402–409 (2012).
115. Zou, Z. *et al.* Linking Receptor-mediated Endocytosis and Cell Signaling. *J. Biol. Chem.* **279,** 34302–34310 (2004).
116. Tokarev Alfonso, A. & Segev, N., A. A. Trafficking Inside Cells: Pathways, Mechanisms and Regulation. . *Landes Biosci. Springer Sci. Media* (2009).
117. Hanahan, D. & Weinberg, R. A. Review Hallmarks of Cancer : The Next Generation. *Cell* **144,** 646–674 (2011).
118. Colombo, M., Raposo, G. & Théry, C. Biogenesis, Secretion, and Intercellular

Interactions of Exosomes and Other Extracellular Vesicles. *Annu. Rev. Cell Dev. Biol.* **30,** 255–289 (2014).
119. Mosesson, Y., Mills, G. B. & Yarden, Y. Derailed endocytosis: an emerging feature of cancer. *Nat. Rev. Cancer* **8,** 835–850 (2008).
120. Jager, S. Role for Rab7 in maturation of late autophagic vacuoles. *J. Cell Sci.* **117,** 4837–4848 (2004).
121. Bucci, C. *et al.* The small GTPase rab5 functions as a regulatory factor in the early endocytic pathway. *Cell* **70,** 715–728 (1992).
122. Mu, F. T. *et al.* EEA1, an early endosome-associated protein. EEA1 is a conserved alpha-helical peripheral membrane protein flanked by cysteine "fingers" and contains a calmodulin-binding IQ motif. *J. Biol. Chem.* **270,** 13503–11 (1995).
123. Zerial, M., Christoforidis, S., McBride, H. M. & Burgoyne, R. D. The Rab5 effector EEA1 is a core component of endosome docking. *Nature* **397,** 621–625 (1999).
124. Bucci, C., Thomsen, P., Nicoziani, P., McCarthy, J. & van Deurs, B. Rab7: a key to lysosome biogenesis. *Mol. Biol. Cell* **11,** 467–80 (2000).
125. Gutierrez, M. G., Munafo, D. B., Beron, W. & Colombo, M. I. Rab7 is required for the normal progression of the autophagic pathway in mammalian cells. *J Cell Sci* **117,** 2687–2697 (2004).
126. Harrison, R. E., Bucci, C., Vieira, O. V, Schroer, T. A. & Grinstein, S. Phagosomes fuse with late endosomes and/or lysosomes by extension of membrane protrusions along microtubules: role of Rab7 and RILP. *Mol. Cell. Biol.* **23,** 6494–506 (2003).
127. Jaber, N. *et al.* Vps34 regulates Rab7 and late endocytic trafficking through recruitment of the GTPase-activating protein Armus. *J. Cell Sci.* **129,** 4424–4435 (2016).
128. Inoki, K., Kim, J. & Guan, K.-L. AMPK and mTOR in Cellular Energy Homeostasis and Drug Targets. *Annu. Rev. Pharmacol. Toxicol.* **52,** 381–400 (2012).
129. Hosokawa, N. *et al.* Nutrient-dependent mTORC1 Association with the ULK1 – Atg13 – FIP200 Complex Required for Autophagy. *Mol. Biol. Cell* **20,** 1981–1991 (2009).
130. Weidberg, H. *et al.* LC3 and GATE-16/GABARAP subfamilies are both essential yet act differently in autophagosome biogenesis. *EMBO J.* **29,** 1792–1802 (2010).
131. EL Andaloussi, S., Mäger, I., Breakefield, X. O. & Wood, M. J. A. Extracellular vesicles: biology and emerging therapeutic opportunities. *Nat. Rev. Drug Discov.* **12,** 347–357 (2013).
132. Thery, C., Ostrowski, M. & Segura, E. Membrane vesicles as conveyors of immune responses. *Nat Rev Immunol* **9,** 581–593 (2009).
133. Stenmark, H. Rab GTPases as coordinators of vesicle traffic. *Nat Rev Mol Cell Biol* **10,** 513–525 (2009).
134. Mosesson, Y., Mills, G. B. & Yarden, Y. Derailed endocytosis: an emerging feature of cancer. *Nat. Rev. Cancer* **8,** 835–850 (2008).
135. Ponnambalam, S. & Baldwin, S. A. Constitutive protein secretion from the trans-Golgi network to the plasma membrane. *Mol. Membr. Biol.* **20,** 129–39 (2003).
136. Rothman, J. E. & Orci, L. Molecular dissection of the secretory pathway.

Nature **355,** 409–415 (1992).
137. Vlassov, A. V., Magdaleno, S., Setterquist, R. & Conrad, R. Exosomes: Current knowledge of their composition, biological functions, and diagnostic and therapeutic potentials. *Biochim. Biophys. Acta - Gen. Subj.* **1820,** 940–948 (2012).
138. Cox, T. R. *et al.* The hypoxic cancer secretome induces pre-metastatic bone lesions through lysyl oxidase. *Nature* **522,** 106–110 (2015).
139. Yang, Z. & Klionsky, D. J. Eaten alive: a history of macroautophagy. *Nat. Cell Biol.* **12,** 814–822 (2010).
140. Galluzzi, L. *et al.* Autophagy in malignant transformation and cancer progression. *EMBO J.* **34,** 856–880 (2015).
141. Kroemer, G., Mariño, G. & Levine, B. Autophagy and the Integrated Stress Response. *Molecular Cell* **40,** 280–293 (2010).
142. Guo, J. Y., Xia, B. & White, E. Autophagy-Mediated tumor Promotion. *Cell* **155,** 1216–1219 (2013).
143. Degenhardt, K. *et al.* Autophagy promotes tumor cell survival and restricts necrosis, inflammation, and tumorigenesis. *Cancer Cell* **10,** 51–64 (2006).
144. Levy, J. M. M. & Thorburn, A. Targeting autophagy during cancer therapy to improve clinical outcomes. *Pharmacol. Ther.* **131,** 130–141 (2011).
145. Zhong, Z. *et al.* Autophagy, Inflammation, and Immunity: A Troika Governing Cancer and Its Treatment. *Cell* **166,** 288–298 (2016).
146. Checinska, A. & Soengas, M. S. The gluttonous side of malignant melanoma: Basic and clinical implications of macroautophagy. *Pigment Cell and Melanoma Research* **24,** 1116–1132 (2011).
147. Flemming, A. Cancer: Autophagy presents Achilles heel in melanoma. *Nat. Rev. Drug Discov.* **10,** 491–491 (2011).
148. Marino, M. L. *et al.* Autophagy is a protective mechanism for human melanoma cells under acidic stress. *J. Biol. Chem.* **287,** 30664–76 (2012).
149. Checinska, A. & Soengas, M. S. The gluttonous side of malignant melanoma: basic and clinical implications of macroautophagy. *Pigment Cell Melanoma Res.* **24,** 1116–1132 (2011).
150. Xie, X., Koh, J. Y., Price, S., White, E. & Mehnert, J. M. Atg7 Overcomes Senescence and Promotes Growth of BrafV600E-Driven Melanoma. *Cancer Discov.* **5,** 410–23 (2015).
151. Baenke, F., Peck, B., Miess, H. & Schulze, A. Hooked on fat: the role of lipid synthesis in cancer metabolism and tumour development. *Dis. Model. Mech.* **6,** 1353–63 (2013).
152. Beloribi-Djefaflia, S., Vasseur, S. & Guillaumond, F. Lipid metabolic reprogramming in cancer cells. *Oncogenesis* **5,** e189 (2016).
153. Trajkovic, K. *et al.* Ceramide Triggers Budding of Exosome Vesicles into Multivesicular Endosomes. *Science (80-.).* **319,** 1244–1247 (2008).
154. Gallala, H. D. & Sandhoff, K. Biological function of the cellular lipid BMP-BMP as a key activator for cholesterol sorting and membrane digestion. *Neurochem. Res.* **36,** 1594–600 (2011).
155. Truman, J.-P. *et al.* Differential regulation of acid sphingomyelinase in macrophages stimulated with oxidized low-density lipoprotein (LDL) and oxidized LDL immune complexes: role in phagocytosis and cytokine release. *Immunology* **136,** 30–45 (2012).
156. Kobayashi, T. *et al.* Late endosomal membranes rich in lysobisphosphatidic

acid regulate cholesterol transport. *Nat. Cell Biol.* **1,** 113–8 (1999).
157. Bianco, F. *et al.* Acid sphingomyelinase activity triggers microparticle release from glial cells. *EMBO J.* **28,** 1043–1054 (2009).
158. Cherfils, J. & Zeghouf, M. Regulation of Small GTPases by GEFs, GAPs, and GDIs. *Physiol. Rev.* **93,** 269–309 (2013).
159. Pfeffer, S. R. Rab GTPases: Specifying and deciphering organelle identity and function. *Trends in Cell Biology* **11,** 487–491 (2001).
160. Segev, N. Ypt and Rab GTPases: Insight into functions through novel interactions. *Current Opinion in Cell Biology* **13,** 500–511 (2001).
161. Guerra, F. & Bucci, C. Multiple Roles of the Small GTPase Rab7. *Cells* **5,** 34 (2016).
162. Rink, J., Ghigo, E., Kalaidzidis, Y. & Zerial, M. Rab Conversion as a Mechanism of Progression from Early to Late Endosomes. *Cell* **122,** 735–749 (2005).
163. Vonderheit, A. & Helenius, A. Rab7 Associates with Early Endosomes to Mediate Sorting and Transport of Semliki Forest Virus to Late Endosomes. *PLoS Biol.* **3,** e233 (2005).
164. Poteryaev, D., Datta, S., Ackema, K., Zerial, M. & Spang, A. Identification of the Switch in Early-to-Late Endosome Transition. *Cell* **141,** 497–508 (2010).
165. Kawamura, N. *et al.* Delivery of endosomes to lysosomes via microautophagy in the visceral endoderm of mouse embryos. *Nat. Commun.* **3,** 1071 (2012).
166. Horiuchi, H. *et al.* A Novel Rab5 GDP/GTP Exchange Factor Complexed to Rabaptin-5 Links Nucleotide Exchange to Effector Recruitment and Function. *Cell* **90,** 1149–1159 (1997).
167. Barr, F. & Lambright, D. G. Rab GEFs and GAPs. *Curr. Opin. Cell Biol.* **22,** 461–470 (2010).
168. Lippé, R., Miaczynska, M., Rybin, V., Runge, A. & Zerial, M. Functional synergy between Rab5 effector Rabaptin-5 and exchange factor Rabex-5 when physically associated in a complex. *Mol. Biol. Cell* **12,** 2219–28 (2001).
169. Jovic, M., Sharma, M., Rahajeng, J. & Caplan, S. The early endosome: a busy sorting station for proteins at the crossroads. *Histol. Histopathol.* **25,** 99–112 (2010).
170. Christoforidis, S. *et al.* Phosphatidylinositol-3-OH kinases are Rab5 effectors. *Nat. Cell Biol.* **1,** 249–252 (1999).
171. Cabrera, M. *et al.* The Mon1-Ccz1 GEF activates the Rab7 GTPase Ypt7 via a longin-fold-Rab interface and association with PI3P-positive membranes. *J. Cell Sci.* **127,** 1043–1051 (2014).
172. Nordmann, M. *et al.* The Mon1-Ccz1 Complex Is the GEF of the Late Endosomal Rab7 Homolog Ypt7. *Curr. Biol.* **20,** 1654–1659 (2010).
173. Yasuda, S. *et al.* Mon1-Ccz1 activates Rab7 only on late endosomes and dissociates from the lysosome in mammalian cells. *J. Cell Sci.* **129,** 329–340 (2016).
174. Shinde, S. R. & Maddika, S. PTEN modulates EGFR late endocytic trafficking and degradation by dephosphorylating Rab7. *Nat. Commun.* **7,** 10689 (2016).
175. Numrich, J. & Ungermann, C. Endocytic Rabs in membrane trafficking and

signaling. *Biol. Chem.* **395,** 327–33 (2014).
176. Solinger, J. A. & Spang, A. Tethering complexes in the endocytic pathway: CORVET and HOPS. *FEBS J.* **280,** 2743–57 (2013).
177. van der Kant, R. *et al.* Characterization of the Mammalian CORVET and HOPS Complexes and Their Modular Restructuring for Endosome Specificity. *J. Biol. Chem.* **290,** 30280–30290 (2015).
178. van der Kant, R. *et al.* Late endosomal transport and tethering are coupled processes controlled by RILP and the cholesterol sensor ORP1L. *J. Cell Sci.* **126,** 3462–3474 (2013).
179. Lin, X. *et al.* RILP interacts with HOPS complex via VPS41 subunit to regulate endocytic trafficking. *Sci. Rep.* **4,** 7282 (2015).
180. Khatter, D. *et al.* The small GTPase Arl8b regulates assembly of the mammalian HOPS complex on lysosomes. *J. Cell Sci.* **128,** 1746–1761 (2015).
181. Johansson, M. *et al.* Activation of endosomal dynein motors by stepwise assembly of Rab7–RILP–p150 ^{Glued} , ORP1L, and the receptor βlll spectrin. *J. Cell Biol.* **176,** 459–471 (2007).
182. Huotari, J. & Helenius, A. Endosome maturation. *EMBO J.* **30,** 3481–3500 (2011).
183. Storrie, B. & Desjardins, M. The biogenesis of lysosomes: Is it a kiss and run, continuous fusion and fission process? *BioEssays* **18,** 895–903 (1996).
184. Feng, Y., Press, B. & Wandinger-Ness, A. Rab 7: an important regulator of late endocytic membrane traffic. *J. Cell Biol.* **131,** 1435–52 (1995).
185. Press, B., Feng, Y., Hoflack, B. & Wandinger-Ness, A. Mutant Rab7 causes the accumulation of cathepsin D and cation-independent mannose 6-phosphate receptor in an early endocytic compartment. *J. Cell Biol.* **140,** 1075–89 (1998).
186. Ceresa, B. P. & Bahr, S. J. rab7 Activity Affects Epidermal Growth Factor:Epidermal Growth Factor Receptor Degradation by Regulating Endocytic Trafficking from the Late Endosome. *J. Biol. Chem.* **281,** 1099–1106 (2006).
187. Vanlandingham, P. A. & Ceresa, B. P. Rab7 regulates late endocytic trafficking downstream of multivesicular body biogenesis and cargo sequestration. *J Biol Chem* **284,** 12110–12124 (2009).
188. Arighi, C. N., Hartnell, L. M., Aguilar, R. C., Haft, C. R. & Bonifacino, J. S. Role of the mammalian retromer in sorting of the cation-independent mannose 6-phosphate receptor. *J. Cell Biol.* **165,** 123–133 (2004).
189. Carlton, J. *et al.* Sorting Nexin-1 Mediates Tubular Endosome-to-TGN Transport through Coincidence Sensing of High- Curvature Membranes and 3-Phosphoinositides. *Curr. Biol.* **14,** 1791–1800 (2004).
190. Seaman, M. N. J. Cargo-selective endosomal sorting for retrieval to the Golgi requires retromer. *J. Cell Biol.* **165,** 111–122 (2004).
191. Rojas, R. *et al.* Regulation of retromer recruitment to endosomes by sequential action of Rab5 and Rab7. *J. Cell Biol.* **183,** 513–526 (2008).
192. de Duve, C. & Wattiaux, R. Functions of Lysosomes. *Annu. Rev. Physiol.* **28,** 435–492 (1966).
193. Mellman, I., Fuchs, R. & Helenius, A. Acidification of the Endocytic and Exocytic Pathways. *Annu. Rev. Biochem.* **55,** 663–700 (1986).
194. Forgac, M. Vacuolar ATPases: rotary proton pumps in physiology and

pathophysiology. *Nat. Rev. Mol. Cell Biol.* **8,** 917–929 (2007).
195. Maxson, M. E. & Grinstein, S. The vacuolar-type H+-ATPase at a glance - more than a proton pump. *J. Cell Sci.* **127,** 4987–4993 (2014).
196. De Luca, M. & Bucci, C. A new V-ATPase regulatory mechanism mediated by the Rab interacting lysosomal protein (RILP). *Commun. Integr. Biol.* **7,** e971572 (2014).
197. De Luca, M. *et al.* RILP regulates vacuolar ATPase through interaction with the V1G1 subunit. *J. Cell Sci.* **127,** 2697–2708 (2014).
198. Johnson, D. E., Ostrowski, P., Jaumouillé, V. & Grinstein, S. The position of lysosomes within the cell determines their luminal pH. *J. Cell Biol.* **212,** 677–692 (2016).
199. Eskelinen, E.-L. in *International review of cell and molecular biology* **266,** 207–247 (2008).
200. Mullock, B. M., Bright, N. A., Fearon, C. W., Gray, S. R. & Luzio, J. P. Fusion of lysosomes with late endosomes produces a hybrid organelle of intermediate density and is NSF dependent. *J. Cell Biol.* **140,** 591–601 (1998).
201. Wang, T., Ming, Z., Xiaochun, W. & Hong, W. Rab7: Role of its protein interaction cascades in endo-lysosomal traffic. *Cell. Signal.* **23,** 516–521 (2011).
202. Wu, B. *et al.* Aldehyde dehydrogenase 2 activation in aged heart improves the autophagy by reducing the carbonyl modification on SIRT1. *Oncotarget* **7,** 2175–88 (2016).
203. Su, H. *et al.* Perturbation of Cullin Deneddylation via Conditional Csn8 Ablation Impairs the Ubiquitin-Proteasome System and Causes Cardiomyocyte Necrosis and Dilated Cardiomyopathy in Mice. *Circ. Res.* **108,** 40–50 (2011).
204. Zhou, J. *et al.* Activation of lysosomal function in the course of autophagy via mTORC1 suppression and autophagosome-lysosome fusion. *Cell Res.* **23,** 508–523 (2013).
205. Yu, L. *et al.* Termination of autophagy and reformation of lysosomes regulated by mTOR. *Nature* **465,** 942–946 (2010).
206. Rong, Y. *et al.* Spinster is required for autophagic lysosome reformation and mTOR reactivation following starvation. *Proc. Natl. Acad. Sci.* **108,** 7826–7831 (2011).
207. Zhang, J. *et al.* Autophagic lysosomal reformation depends on mTOR reactivation in H2O2-induced autophagy. *Int. J. Biochem. Cell Biol.* **70,** 76–81 (2016).
208. Jimenez-Orgaz, A. *et al.* Control of RAB7 activity and localization through the retromer-TBC1D5 complex enables RAB7-dependent mitophagy. *EMBO J.* e201797128 (2017). doi:10.15252/embj.201797128
209. Wong, Y. C., Ysselstein, D. & Krainc, D. Mitochondria–lysosome contacts regulate mitochondrial fission via RAB7 GTP hydrolysis. *Nature* (2018). doi:10.1038/nature25486
210. Yamano, K., Fogel, A. I., Wang, C., van der Bliek, A. M. & Youle, R. J. Mitochondrial Rab GAPs govern autophagosome biogenesis during mitophagy. *Elife* **3,** e01612 (2014).
211. Pankiv, S. *et al.* FYCO1 is a Rab7 effector that binds to LC3 and PI3P to mediate microtubule plus end–directed vesicle transport. *J. Cell Biol.* **188,**

253–269 (2010).
212. Cogli, L. *et al.* Charcot–Marie–Tooth type 2B disease-causing RAB7A mutant proteins show altered interaction with the neuronal intermediate filament peripherin. *Acta Neuropathol.* **125,** 257–272 (2013).
213. Cogli, L., Progida, C., Bramato, R. & Bucci, C. Vimentin phosphorylation and assembly are regulated by the small GTPase Rab7a. *Biochim. Biophys. Acta - Mol. Cell Res.* **1833,** 1283–1293 (2013).
214. Frasa, M. A. M. *et al.* Armus Is a Rac1 Effector that Inactivates Rab7 and Regulates E-Cadherin Degradation. *Curr. Biol.* **20,** 198–208 (2010).
215. Sun, Y., Büki, K. G., Ettala, O., Vääräniemi, J. P. & Väänänen, H. K. Possible Role of Direct Rac1-Rab7 Interaction in Ruffled Border Formation of Osteoclasts. *J. Biol. Chem.* **280,** 32356–32361 (2005).
216. Mascia, A. *et al.* Rab7 Regulates CDH1 Endocytosis, Circular Dorsal Ruffles Genesis, and Thyroglobulin Internalization in a Thyroid Cell Line. *J. Cell. Physiol.* **231,** 1695–1708 (2016).
217. Palokangas, H., Mulari, M. & Vaananen, H. K. Endocytic pathway from the basal plasma membrane to the ruffled border membrane in bone-resorbing osteoclasts. *J Cell Sci* **110 (Pt 1,** 1767–1780 (1997).
218. Stuart, L. M. & Ezekowitz, R. A. Phagocytosis and comparative innate immunity: learning on the fly. *Nat. Rev. Immunol.* **8,** 131–141 (2008).
219. Ravichandran, K. S. & Lorenz, U. Engulfment of apoptotic cells: signals for a good meal. *Nat. Rev. Immunol.* **7,** 964–974 (2007).
220. Vieira, O. V *et al.* Modulation of Rab5 and Rab7 recruitment to phagosomes by phosphatidylinositol 3-kinase. *Mol. Cell. Biol.* **23,** 2501–14 (2003).
221. Flannagan, R. S., Cosío, G. & Grinstein, S. Antimicrobial mechanisms of phagocytes and bacterial evasion strategies. *Nat. Rev. Microbiol.* **7,** 355–366 (2009).
222. Via, L. E. *et al.* Arrest of mycobacterial phagosome maturation is caused by a block in vesicle fusion between stages controlled by rab5 and rab7. *J. Biol. Chem.* **272,** 13326–31 (1997).
223. Chandra, P. *et al.* Mycobacterium tuberculosis Inhibits RAB7 Recruitment to Selectively Modulate Autophagy Flux in Macrophages. *Sci. Rep.* **5,** 16320 (2015).
224. Saxena, S., Bucci, C., Weis, J. & Kruttgen, A. The Small GTPase Rab7 Controls the Endosomal Trafficking and Neuritogenic Signaling of the Nerve Growth Factor Receptor TrkA. *J. Neurosci.* **25,** 10930–10940 (2005).
225. Raiborg, C. *et al.* Repeated ER–endosome contacts promote endosome translocation and neurite outgrowth. *Nature* **520,** 234–238 (2015).
226. Shirane, M. & Nakayama, K. I. Protrudin Induces Neurite Formation by Directional Membrane Trafficking. *Science (80-.).* **314,** 818–821 (2006).
227. Deinhardt, K. *et al.* Rab5 and Rab7 Control Endocytic Sorting along the Axonal Retrograde Transport Pathway. *Neuron* **52,** 293–305 (2006).
228. Kawauchi, T. *et al.* Rab GTPases-Dependent Endocytic Pathways Regulate Neuronal Migration and Maturation through N-Cadherin Trafficking. *Neuron* **67,** 588–602 (2010).
229. Auer-Grumbach, M. *et al.* Ulcero-mutilating neuropathy in an Austrian kinship without linkage to hereditary motor and sensory neuropathy IIB and hereditary sensory neuropathy I loci. *Neurology* **54,** 45–52 (2000).
230. Bucci, C. & De Luca, M. Molecular basis of Charcot-Marie-Tooth type 2B

disease. *Biochem. Soc. Trans.* **40,** 1368–72 (2012).
231. Hirosaki, K., Yamashita, T., Jin, H.-Y., Jimbow, K. & Wada, I. Tyrosinase and Tyrosinase-Related Protein 1 Require Rab7 for Their Intracellular Transport. *J. Invest. Dermatol.* **119,** 475–480 (2002).
232. Jordens, I. *et al.* Rab7 and Rab27a control two motor protein activities involved in melanosomal transport. *Pigment Cell Res.* **19,** 412–423 (2006).
233. Gilot, D. *et al.* A non-coding function of TYRP1 mRNA promotes melanoma growth. *Nat. Cell Biol.* **19,** 1348–1357 (2017).
234. Wang, T. *et al.* A role of Rab7 in stabilizing EGFR-Her2 and in sustaining Akt survival signal. *J. Cell. Physiol.* **227,** 2788–2797 (2012).
235. Williams, K. C. & Coppolino, M. G. Phosphorylation of membrane type 1-matrix metalloproteinase (MT1-MMP) and its vesicle-associated membrane protein 7 (VAMP7)-dependent trafficking facilitate cell invasion and migration. *J. Biol. Chem.* **286,** 43405–43416 (2011).
236. Edinger, A. L., Cinalli, R. M. & Thompson, C. B. Rab7 Prevents Growth Factor-Independent Survival by Inhibiting Cell-Autonomous Nutrient Transporter Expression. *Dev. Cell* **5,** 571–582 (2003).
237. Steffan, J. J. *et al.* Supporting a role for the GTPase rab7 in prostate cancer progression. *PLoS One* **9,** (2014).
238. Steffan, J. J. & Cardelli, J. A. Thiazolidinediones Induce Rab7-RILP-MAPK-Dependent Juxtanuclear Lysosome Aggregation and Reduce Tumor Cell Invasion. *Traffic* **11,** 274–286 (2010).
239. Steffan, J. J., Williams, B. C., Welbourne, T. & Cardelli, J. A. HGF-induced invasion by prostate tumor cells requires anterograde lysosome trafficking and activity of Na+-H+ exchangers. *J. Cell Sci.* **123,** 1151–9 (2010).
240. Romero Rosales, K., Peralta, E. R., Guenther, G. G., Wong, S. Y. & Edinger, A. L. Rab7 Activation by Growth Factor Withdrawal Contributes to the Induction of Apoptosis. *Mol. Biol. Cell* **20,** 2831–2840 (2009).
241. Zhao, T., Ding, X., Yan, C. & Du, H. Endothelial Rab7 GTPase mediates tumor growth and metastasis in lysosomal acid lipase–deficient mice. *J. Biol. Chem.* **292,** 19198–19208 (2017).
242. Alonso-Curbelo, D. *et al.* RAB7 counteracts PI3K-driven macropinocytosis activated at early stages of melanoma development. *Oncotarget* **6,** 11848–62 (2015).
243. Ostrowski, M. *et al.* Rab27a and Rab27b control different steps of the exosome secretion pathway. *Nat. Cell Biol.* **12,** 19–30 (2010).
244. Bahadoran, P. *et al.* Characterization of the molecular defects in Rab27a, caused by RAB27A missense mutations found in patients with Griscelli syndrome. *J. Biol. Chem.* **278,** 11386–92 (2003).
245. Pastural, E. *et al.* Griscelli disease maps to chromosome 15q21 and is associated with mutations in the Myosin-Va gene. *Nat. Genet.* **16,** 289–292 (1997).
246. Fukuda, M. & Kuroda, T. S. Slac2-c (synaptotagmin-like protein homologue lacking C2 domains-c), a novel linker protein that interacts with Rab27, myosin Va/VIIa, and actin. *J. Biol. Chem.* **277,** 43096–103 (2002).
247. Fukuda, M., Kuroda, T. S. & Mikoshiba, K. Slac2-a/Melanophilin, the Missing Link between Rab27 and Myosin Va. *J. Biol. Chem.* **277,** 12432–12436 (2002).
248. Kuroda, T. S. & Fukuda, M. Rab27A-binding protein Slp2-a is required for

peripheral melanosome distribution and elongated cell shape in melanocytes. *Nat. Cell Biol.* **6,** 1195–1203 (2004).
249. Wang, H. *et al.* The Rab27a effector exophilin7 promotes fusion of secretory granules that have not been docked to the plasma membrane. *Mol. Biol. Cell* **24,** 319–330 (2013).
250. Fukuda, M. Slp4-a/Granuphilin-a Inhibits Dense-core Vesicle Exocytosis through Interaction with the GDP-bound Form of Rab27A in PC12 Cells. *J. Biol. Chem.* **278,** 15390–15396 (2003).
251. Kimura, T. *et al.* The GDP-dependent Rab27a effector coronin 3 controls endocytosis of secretory membrane in insulin-secreting cell lines. *J. Cell Sci.* **121,** 3092–8 (2008).
252. Wang, Q. *et al.* High expression of RAB27A and TP53 in pancreatic cancer predicts poor survival. *Med. Oncol.* **32,** 372 (2015).
253. Dong, W.-W. *et al.* Differential expression of Rab27A/B correlates with clinical outcome in hepatocellular carcinoma. *World J. Gastroenterol.* **18,** 1806–13 (2012).
254. Wang, H. *et al.* Rab27a Was Identified as a Prognostic Biomaker by mRNA Profiling, Correlated with Malignant Progression and Subtype Preference in Gliomas. *PLoS One* **9,** e89782 (2014).
255. Wang, J.-S., Wang, F.-B., Zhang, Q.-G., Shen, Z.-Z. & Shao, Z.-M. Enhanced Expression of Rab27A Gene by Breast Cancer Cells Promoting Invasiveness and the Metastasis Potential by Secretion of Insulin-Like Growth Factor-II. *Mol. Cancer Res.* **6,** 372–382 (2008).
256. Liu, J. *et al.* Rab27A overexpression promotes bladder cancer proliferation and chemoresistance through regulation of NF-κB signaling. *Oncotarget* **8,** 75272–75283 (2017).
257. Worst, T. S. *et al.* RAB27A, RAB27B and VPS36 are downregulated in advanced prostate cancer and show functional relevance in prostate cancer cells. *Int. J. Oncol.* **50,** 920–932 (2017).
258. Dong, W. *et al.* Decreased expression of Rab27A and Rab27B correlates with metastasis and poor prognosis in colorectal cancer. *Discov. Med.* **20,** 357–67 (2015).
259. Qu, L. *et al.* Exosome-Transmitted lncARSR Promotes Sunitinib Resistance in Renal Cancer by Acting as a Competing Endogenous RNA. *Cancer Cell* **29,** 653–668 (2016).
260. Bobrie, A. *et al.* Rab27a supports exosome-dependent and -independent mechanisms that modify the tumor microenvironment and can promote tumor progression. *Cancer Res.* **72,** 4920–4930 (2012).
261. Ostenfeld, M. S. *et al.* Cellular Disposal of miR23b by RAB27-Dependent Exosome Release Is Linked to Acquisition of Metastatic Properties. *Cancer Res.* **74,** 5758–5771 (2014).
262. Dornier, E. *et al.* Glutaminolysis drives membrane trafficking to promote invasiveness of breast cancer cells. *Nat. Commun.* **8,** 2255 (2017).
263. Denoyelle, C. *et al.* Anti-oncogenic role of the endoplasmic reticulum differentially activated by mutations in the MAPK pathway. *Nat. Cell Biol.* **8,** 1053–1063 (2006).
264. Gil, S. Y. *et al.* Clusterin and LRP2 are critical components of the hypothalamic feeding regulatory pathway. *Nat. Commun.* **4,** 1862 (2013).
265. Gratzner, H. G., Leif, R. C., Ingram, D. J. & Castro, A. The use of antibody

specific for bromodeoxyuridine for the immunofluorescent determination of DNA replication in single cells and chromosomes. *Exp. Cell Res.* **95,** 88–94 (1975).
266. Thery, C., Amigorena, S., Raposo, G. & Clayton, A. Isolation and characterization of exosomes from cell culture supernatants and biological fluids. *Curr Protoc Cell Biol* **Chapter 3,** Unit 3 22 (2006).
267. Pennacchi, P. C. *et al.* Glycated Reconstructed Human Skin as a Platform to Study the Pathogenesis of Skin Aging. *Tissue Eng. Part A* **21,** 2417–25 (2015).
268. Faião-Flores, F. *et al.* Targeting the hedgehog transcription factors GLI1 and GLI2 restores sensitivity to vemurafenib-resistant human melanoma cells. *Oncogene* **36,** 1849–1861 (2017).
269. Sandri, S. *et al.* Vemurafenib resistance increases melanoma invasiveness and modulates the tumor microenvironment by MMP-2 upregulation. *Pharmacol. Res.* **111,** 523–533 (2016).
270. Massaro, R. R. *et al.* Inhibition of proliferation and invasion in 2D and 3D models by 2-methoxyestradiol in human melanoma cells. *Pharmacol. Res.* **119,** 242–250 (2017).
271. Wisniewski, J. R., Zougman, A., Nagaraj, N., Mann, M. & Wi, J. R. Universal sample preparation method for proteome analysis. *Nat. Methods* **6,** 377–362 (2009).
272. Cox, J. & Mann, M. MaxQuant enables high peptide identification rates, individualized p.p.b.-range mass accuracies and proteome-wide protein quantification. *Nat. Biotechnol.* **26,** 1367–1372 (2008).
273. Cox, J. *et al.* Andromeda: A peptide search engine integrated into the MaxQuant environment. *J. Proteome Res.* **10,** 1794–1805 (2011).
274. Breitwieser, F. P. *et al.* General statistical modeling of data from protein relative expression isobaric tags. *J. Proteome Res.* **10,** 2758–2766 (2011).
275. Hundertmark, C. *et al.* MS-specific noise model reveals the potential of iTRAQ in quantitative proteomics. *Bioinformatics* **25,** 1004–11 (2009).
276. Subramanian, A. *et al.* Gene set enrichment analysis: A knowledge-based approach for interpreting genome-wide expression profiles. *Proc. Natl. Acad. Sci.* **102,** 15545–15550 (2005).
277. Jensen, L. J. *et al.* STRING 8--a global view on proteins and their functional interactions in 630 organisms. *Nucleic Acids Res* **37,** D412–6 (2009).
278. Oliveros, J. C. VENNY. An interactive tool for comparing lists with Venn Diagrams. *BioinfoGP of CNB-CSIC* http://bioinfogp.cnnb.csic.es/tools/venny/index.ht (2007). doi:10.1017/S0266267108002022
279. Kriebel, P. W., Barr, V. A., Rericha, E. C., Zhang, G. & Parent, C. A. Collective cell migration requires vesicular trafficking for chemoattractant delivery at the trailing edge. *J. Cell Biol.* **183,** 949–61 (2008).
280. Caswell, P. T. & Norman, J. C. Integrin Trafficking and the Control of Cell Migration. *Traffic* **7,** 14–21 (2006).
281. Jones, M. C., Caswell, P. T. & Norman, J. C. Endocytic recycling pathways: emerging regulators of cell migration. *Curr. Opin. Cell Biol.* **18,** 549–557 (2006).
282. Mosesson, Y., Mills, G. B. & Yarden, Y. Derailed endocytosis: an emerging feature of cancer. *Nat Rev Cancer* **8,** 835–850 (2008).

283. Caswell, P. T., Vadrevu, S. & Norman, J. C. Integrins: Masters and slaves of endocytic transport. *Nature Reviews Molecular Cell Biology* **10,** 843–853 (2009).
284. Astudillo, L. *et al.* Glucosylceramidases and malignancies in mammals. *Biochimie* **125,** 267–280 (2016).
285. Marchesini, N. & Hannun, Y. A. Acid and neutral sphingomyelinases: roles and mechanisms of regulation. *Biochem. Cell Biol.* **82,** 27–44 (2004).
286. Hannun, Y. A. & Obeid, L. M. Principles of bioactive lipid signalling: lessons from sphingolipids. *Nat. Rev. Mol. Cell Biol.* **9,** 139–150 (2008).
287. Obeid, L. M., Linardic, C. M., Karolak, L. A. & Hannun, Y. A. Programmed cell death induced by ceramide. *Science* **259,** 1769–71 (1993).
288. Carpinteiro, A. *et al.* Regulation of hematogenous tumor metastasis by acid sphingomyelinase. *EMBO Mol. Med.* **7,** 714–34 (2015).
289. Petersen, N. H. T. *et al.* Transformation-Associated Changes in Sphingolipid Metabolism Sensitize Cells to Lysosomal Cell Death Induced by Inhibitors of Acid Sphingomyelinase. *Cancer Cell* **24,** 379–393 (2013).
290. Hara, A. & Radin, N. S. Destruction and resynthesis of mouse beta-glucosidases. *Biochim. Biophys. Acta* **582,** 412–22 (1979).
291. Chang, Y.-C. *et al.* Secretory RAB GTPase 3C modulates IL6-STAT3 pathway to promote colon cancer metastasis and is associated with poor prognosis. *Mol. Cancer* **16,** 135 (2017).
292. Tsai, C.-H. *et al.* Small GTPase Rab37 targets tissue inhibitor of metalloproteinase 1 for exocytosis and thus suppresses tumour metastasis. *Nat. Commun.* **5,** 4804 (2014).
293. Mohamed, M. M. & Sloane, B. F. Cysteine cathepsins: multifunctional enzymes in cancer. *Nat. Rev. Cancer* **6,** 764–75 (2006).
294. Marzolo, M.-P. & Farfán, P. New Insights into the Roles of Megalin/LRP2 and the Regulation of its Functional Expression. *Biol. Res.* **44,** 89–105 (2011).
295. Willnow, T. E. *et al.* Defective forebrain development in mice lacking gp330/megalin. *Proc. Natl. Acad. Sci. U. S. A.* **93,** 8460 (1996).
296. Andersen, R. K. *et al.* Melanoma tumors frequently acquire *LRP2* /megalin expression, which modulates melanoma cell proliferation and survival rates. *Pigment Cell Melanoma Res.* **28,** 267–280 (2015).
297. Gonias, S. L., Karimi-Mostowfi, N., Murray, S. S., Mantuano, E. & Gilder, A. S. Expression of LDL receptor-related proteins (LRPs) in common solid malignancies correlates with patient survival. *PLoS One* **12,** (2017).
298. Brasoveanu, L. I. *et al.* Melanoma cells constitutively release an anchor-positive soluble form of protectin (sCD59) that retains functional activities in homologous complement-mediated cytotoxicity. *J. Clin. Invest.* **100,** 1248–1255 (1997).
299. Maelandsmo, G. M. *et al.* Differential expression patterns of S100A2, S100A4 and S100A6 during progression of human malignant melanoma. *Int. J. cancer* **74,** 464–9 (1997).
300. Ivanov, S. V *et al.* Diagnostic SOX10 gene signatures in salivary adenoid cystic and breast basal-like carcinomas. *Br. J. Cancer* **109,** 444–451 (2013).
301. Dong, D. *et al.* A Critical Role for GRP78/BiP in the Tumor Microenvironment for Neovascularization during Tumor Growth and Metastasis. *Cancer Res.* **71,** 2848–2857 (2011).

302. Riker, A. I. *et al.* The gene expression profiles of primary and metastatic melanoma yields a transition point of tumor progression and metastasis. *BMC Med. Genomics* **1,** 13 (2008).
303. Sorlie, T. *et al.* Gene expression patterns of breast carcinomas distinguish tumor subclasses with clinical implications. *Proc. Natl. Acad. Sci.* **98,** 10869–10874 (2001).
304. Sorlie, T. *et al.* Repeated observation of breast tumor subtypes in independent gene expression data sets. *Proc. Natl. Acad. Sci. U. S. A.* **100,** 8418–23 (2003).
305. Wigle, D. A. *et al.* Molecular profiling of non-small cell lung cancer and correlation with disease-free survival. *Cancer Res.* **62,** 3005–8 (2002).
306. Garraway, L. A. *et al.* Integrative genomic analyses identify MITF as a lineage survival oncogene amplified in malignant melanoma. *Nature* **436,** 117–122 (2005).
307. Müller, J. *et al.* Low MITF/AXL ratio predicts early resistance to multiple targeted drugs in melanoma. *Nat. Commun.* **5,** 5712 (2014).
308. Noguchi, S. *et al.* Analysis of microRNA-203 function in CREB/MITF/RAB27a pathway: comparison between canine and human melanoma cells. *Vet. Comp. Oncol.* **14,** 384–394 (2016).
309. Ostalecki, C. *et al.* Multiepitope tissue analysis reveals SPPL3-mediated ADAM10 activation as a key step in the transformation of melanocytes. *Sci. Signal.* **10,** eaai8288 (2017).
310. Kawakami, A. *et al.* Rab7 Regulates Maturation of Melanosomal Matrix Protein gp100/Pmel17/Silv. *J. Invest. Dermatol.* **128,** 143–150 (2008).
311. HIDA, T. *et al.* Rab7 is a critical mediator in vesicular transport of tyrosinase-related protein 1 in melanocytes. *J. Dermatol.* **38,** 432–441 (2011).
312. Fukuda, M. Rab27 Effectors, Pleiotropic Regulators in Secretory Pathways. *Traffic* **14,** 949–963 (2013).
313. Carpinteiro, A., Dumitru, C., Schenck, M. & Gulbins, E. Ceramide-induced cell death in malignant cells. *Cancer Lett.* **264,** 1–10 (2008).
314. Ogretmen, B. Sphingolipid metabolism in cancer signalling and therapy. *Nat. Rev. Cancer* **18,** 33–50 (2018).
315. Raisova, M. *et al.* Resistance to CD95/Fas-induced and ceramide-mediated apoptosis of human melanoma cells is caused by a defective mitochondrial cytochrome c release. *FEBS Lett.* **473,** 27–32 (2000).
316. Morad, S. A. F. & Cabot, M. C. Ceramide-orchestrated signalling in cancer cells. *Nat. Rev. Cancer* **13,** 51–65 (2013).
317. Schiffmann, S. *et al.* Ceramide synthases and ceramide levels are increased in breast cancer tissue. *Carcinogenesis* **30,** 745–752 (2009).
318. Senkal, C. E. *et al.* Alteration of Ceramide Synthase 6/C $_{16}$ -Ceramide Induces Activating Transcription Factor 6-mediated Endoplasmic Reticulum (ER) Stress and Apoptosis via Perturbation of Cellular Ca $^{2+}$ and ER/Golgi Membrane Network. *J. Biol. Chem.* **286,** 42446–42458 (2011).
319. Mesicek, J. *et al.* Ceramide synthases 2, 5, and 6 confer distinct roles in radiation-induced apoptosis in HeLa cells. *Cell. Signal.* **22,** 1300–1307 (2010).
320. Park, M. A. *et al.* Vorinostat and sorafenib increase ER stress, autophagy and apoptosis via ceramide-dependent CD95 and PERK activation. *Cancer*

Biol. Ther. **7,** 1648–62 (2008).
321. Jiang, W. & Ogretmen, B. Autophagy paradox and ceramide. *Biochim. Biophys. Acta* **1841,** 783–92 (2014).
322. Menuz, V. *et al.* Protection of C. elegans from Anoxia by HYL-2 Ceramide Synthase. *Science (80-.).* **324,** 381–384 (2009).
323. Record, M., Carayon, K., Poirot, M. & Silvente-Poirot, S. Exosomes as new vesicular lipid transporters involved in cell-cell communication and various pathophysiologies. *Biochimica et Biophysica Acta - Molecular and Cell Biology of Lipids* **1841,** 108–120 (2014).
324. Schuchman, E. H. The pathogenesis and treatment of acid sphingomyelinase-deficient Niemann–Pick disease. *J. Inherit. Metab. Dis.* **30,** 654–663 (2007).
325. Froehlich, S. J. *et al.* in *Encyclopedia of Molecular Mechanisms of Disease* 1479–1480 (Springer Berlin Heidelberg, 2009). doi:10.1007/978-3-540-29676-8_1286
326. Hruska, K. S., LaMarca, M. E., Scott, C. R. & Sidransky, E. Gaucher disease: mutation and polymorphism spectrum in the glucocerebrosidase gene (GBA). *Hum. Mutat.* **29,** 567–583 (2008).
327. Lidove, O., Sedel, F., Charlotte, F., Froissart, R. & Vanier, M. T. in *JIMD reports* **15,** 117–21 (2014).
328. Cox, T. M., Rosenbloom, B. E. & Barker, R. A. Gaucher disease and comorbidities: B-cell malignancy and parkinsonism. *Am. J. Hematol.* **90,** S25–S28 (2015).
329. Cullen, V. *et al.* Acid β-glucosidase mutants linked to gaucher disease, parkinson disease, and lewy body dementia alter α-synuclein processing. *Ann. Neurol.* **69,** 940–953 (2011).
330. Landgren, O., Turesson, I., Gridley, G. & Caporaso, N. E. Risk of malignant disease among 1525 adult male US veterans with Gaucher disease. *Arch. Intern. Med.* **167,** 1189–1194 (2007).
331. Greene, M. H., Mead, G. D., Reimer, R. R., Bergfeld, W. F. & Fraumeni Jr., J. F. Malignant melanoma and Charcot-Marie-Tooth disease. *Am J Med Genet* **5,** 69–71 (1980).
332. Saini, R., Lehrhoff, S. & Sarnoff, D. S. Charcot-Marie-tooth disease and multiple malignant melanomas: a case report. *J. Drugs Dermatol.* **9,** 164–6 (2010).
333. Kirkegaard, T. & Jäättelä, M. Lysosomal involvement in cell death and cancer. *Biochim. Biophys. Acta - Mol. Cell Res.* **1793,** 746–754 (2009).
334. Aits, S. & Jaattela, M. Lysosomal cell death at a glance. *J. Cell Sci.* **126,** 1905–1912 (2013).
335. Schramm, M., Herz, J., Haas, A., Krönke, M. & Utermöhlen, O. Acid sphingomyelinase is required for efficient phago-lysosomal fusion. *Cell. Microbiol.* **10,** 1839–1853 (2008).
336. Utermöhlen, O., Herz, J., Schramm, M. & Krönke, M. Fusogenicity of membranes: The impact of acid sphingomyelinase on innate immune responses. *Immunobiology* **213,** 307–314 (2008).
337. Kirkegaard, T. *et al.* Hsp70 stabilizes lysosomes and reverts Niemann–Pick disease-associated lysosomal pathology. *Nature* **463,** 549–553 (2010).
338. Gabandé-Rodríguez, E., Boya, P., Labrador, V., Dotti, C. G. & Ledesma, M. D. High sphingomyelin levels induce lysosomal damage and autophagy

dysfunction in Niemann Pick disease type A. *Cell Death Differ.* **21,** 864–875 (2014).
339. Zhu, L. *et al.* Acid sphingomyelinase is required for cell surface presentation of Met receptor tyrosine kinase in cancer cells. *J. Cell Sci.* **129,** 4238–4251 (2016).
340. Mascarenhas, J. B. *et al.* PAX3 and SOX10 activate MET receptor expression in melanoma. *Pigment Cell Melanoma Res.* **23,** 225–237 (2010).
341. Kubic, J. D., Little, E. C., Lui, J. W., Iizuka, T. & Lang, D. PAX3 and ETS1 synergistically activate MET expression in melanoma cells. *Oncogene* **34,** 4964–4974 (2015).
342. Organ, S. L. & Tsao, M.-S. An overview of the c-MET signaling pathway. *Ther. Adv. Med. Oncol.* **3,** S7–S19 (2011).
343. Moon, Y. W. *et al.* LAMC2 enhances the metastatic potential of lung adenocarcinoma. *Cell Death Differ.* **22,** 1341–1352 (2015).
344. Yu, Z. *et al.* microRNA 17/20 inhibits cellular invasion and tumor metastasis in breast cancer by heterotypic signaling. *Proc. Natl. Acad. Sci. U. S. A.* **107,** 8231–6 (2010).
345. Casazza, A. *et al.* Sema3E–Plexin D1 signaling drives human cancer cell invasiveness and metastatic spreading in mice. *J. Clin. Invest.* **120,** 2684–2698 (2010).
346. Podhajcer, O. L. *et al.* Expression of cathepsin D in primary and metastatic human melanoma and dysplastic nevi. *J. Invest. Dermatol.* **104,** 340–4 (1995).
347. Gemoll, T. *et al.* Increased cathepsin D protein expression is a biomarker for osteosarcomas, pulmonary metastases and other bone malignancies. *Oncotarget* **6,** 16517–26 (2015).
348. Ohnishi, Y., Tajima, S. & Ishibashi, A. Coordinate expression of membrane type-matrix metalloproteinases-2 and 3 (MT2-MMP and MT3-MMP) and matrix metalloproteinase-2 (MMP-2) in primary and metastatic melanoma cells. *Eur. J. Dermatol.* **11,** 420–3
349. Shin, J. *et al.* Identification of ganglioside GM2 activator playing a role in cancer cell migration through proteomic analysis of breast cancer secretomes. *Cancer Sci.* **107,** 828–835 (2016).
350. Spoelgen, R. *et al.* LRP2/megalin is required for patterning of the ventral telencephalon. *Development* **132,** 405–414 (2005).
351. Christ, A. *et al.* LRP2 Is an Auxiliary SHH Receptor Required to Condition the Forebrain Ventral Midline for Inductive Signals. *Dev. Cell* **22,** 268–278 (2012).
352. Rg-, J. *et al.* Animal Model Megalin Knockout Mice as an Animal Model of Low Molecular Weight Proteinuria. *Am. J. Pathol.* **155,** 1361–1370 (1999).
353. LEHESTE, J. R. *et al.* Hypocalcemia and osteopathy in mice with kidney-specific megalin gene defect. *FASEB J.* **17,** 247–249 (2003).
354. Pisitkun, T., Shen, R.-F. & Knepper, M. A. Identification and proteomic profiling of exosomes in human urine. *Proc. Natl. Acad. Sci.* **101,** 13368–13373 (2004).
355. Terryn, S. *et al.* Tubular proteinuria in patients with HNF1α mutations: HNF1α drives endocytosis in the proximal tubule. *Kidney Int.* **89,** 1075–1089 (2016).
356. De, S. *et al.* Exocytosis-mediated urinary full-length megalin excretion is

linked with the pathogenesis of diabetic nephropathy. *Diabetes* **66,** 1391–1404 (2017).
357. Zhang, B. *et al.* MicroRNA-146a represses LRP2 translation and leads to cell apoptosis in Alzheimer's disease. *FEBS Lett.* **590,** 2190–2200 (2016).
358. Spuch, C., Ortolano, S. & Navarro, C. LRP-1 and LRP-2 receptors function in the membrane neuron. Trafficking mechanisms and proteolytic processing in Alzheimer's disease. *Front. Physiol.* **3,** 269 (2012).
359. Nielsen, R. *et al.* Endocytosis provides a major alternative pathway for lysosomal biogenesis in kidney proximal tubular cells. *Proc. Natl. Acad. Sci.* **104,** 5407–5412 (2007).
360. Jensen, L. L. *et al.* Lack of megalin expression in adult human terminal ileum suggests megalin-independent cubilin/amnionless activity during vitamin B12 absorption. *Physiol. Rep.* **2,** 824–831 (2014).
361. Fernandez-Banet, J. *et al.* Decoding complex patterns of genomic rearrangement in hepatocellular carcinoma. *Genomics* **103,** 189–203 (2014).
362. Schuetz, A. N. *et al.* Molecular classification of renal tumors by gene expression profiling. *J. Mol. Diagn.* **7,** 206–218 (2005).
363. Holt, S. K. *et al.* Association of megalin genetic polymorphisms with prostate cancer risk and prognosis. *Clin. Cancer Res.* **14,** 3823–31 (2008).
364. Peinado, H. *et al.* Pre-metastatic niches: organ-specific homes for metastases. *Nat. Rev. Cancer* **17,** 302–317 (2017).
365. Hood, J. L., San Roman, S. & Wickline, S. A. Exosomes released by melanoma cells prepare sentinel lymph nodes for tumor metastasis. *Cancer Res.* **71,** 3792–3801 (2011).
366. Baietti, M. F. *et al.* Syndecan-syntenin-ALIX regulates the biogenesis of exosomes. *Nat. Cell Biol.* **14,** 677–685 (2012).
367. Lazar, I. *et al.* Adipocyte Exosomes Promote Melanoma Aggressiveness through Fatty Acid Oxidation: A Novel Mechanism Linking Obesity and Cancer. *Cancer Res.* **76,** 4051–4057 (2016).
368. Felicetti, F. *et al.* Exosome-mediated transfer of miR-222 is sufficient to increase tumor malignancy in melanoma. *J. Transl. Med.* **14,** 56 (2016).
369. Boelens, M. C. *et al.* Exosome transfer from stromal to breast cancer cells regulates therapy resistance pathways. *Cell* **159,** 499–513 (2014).
370. Lazar, I. *et al.* Proteome characterization of melanoma exosomes reveals a specific signature for metastatic cell lines. *Pigment Cell Melanoma Res.* **28,** 464–475 (2015).
371. Gonzales, P. A. *et al.* Large-Scale Proteomics and Phosphoproteomics of Urinary Exosomes. *J. Am. Soc. Nephrol.* **20,** 363–379 (2009).
372. Raj, D. A. A., Fiume, I., Capasso, G. & Pocsfalvi, G. A multiplex quantitative proteomics strategy for protein biomarker studies in urinary exosomes. *Kidney Int.* **81,** 1263–1272 (2012).
373. Vyas, N. *et al.* Vertebrate Hedgehog is secreted on two types of extracellular vesicles with different signaling properties. *Sci. Rep.* **4,** 7357 (2015).
374. Marzolo, M.-P. *et al.* Differential Distribution of Low-Density Lipoprotein-Receptor-Related Protein (LRP) and Megalin in Polarized Epithelial Cells is Determined by Their Cytoplasmic Domains. *Traffic* **4,** 273–288 (2003).
375. Sezgin, E., Levental, I., Mayor, S. & Eggeling, C. The mystery of membrane

organization: composition, regulation and roles of lipid rafts. *Nat. Rev. Mol. Cell Biol.* **18,** 361–374 (2017).
376. Megha & London, E. Ceramide selectively displaces cholesterol from ordered lipid domains (rafts): Implications for lipid raft structure and function. *J. Biol. Chem.* **279,** 9997–10004 (2004).
377. Silva, L. C., De Almeida, R. F. M., Castro, B. M., Fedorov, A. & Prieto, M. Ceramide-domain formation and collapse in lipid rafts: Membrane reorganization by an apoptotic lipid. *Biophys. J.* **92,** 502–516 (2007).
378. Ebinu, J. O. & Yankner, B. A. A RIP Tide in Neuronal Signal Transduction. *Neuron* **34,** 499–502 (2002).
379. Zou, Z. *et al.* Linking receptor-mediated endocytosis and cell signaling: evidence for regulated intramembrane proteolysis of megalin in proximal tubule. *J. Biol. Chem.* **279,** 34302–10 (2004).
380. May, P., Reddy, Y. K. & Herz, J. Proteolytic Processing of Low Density Lipoprotein Receptor-related Protein Mediates Regulated Release of Its Intracellular Domain. *J. Biol. Chem.* **277,** 18736–18743 (2002).
381. Gorovoy, M., Gaultier, A., Campana, W. M., Firestein, G. S. & Gonias, S. L. Inflammatory mediators promote production of shed LRP1/CD91, which regulates cell signaling and cytokine expression by macrophages. *J. Leukoc. Biol.* **88,** 769–778 (2010).
382. Liu, R., Gao, X., Lu, Y. & Chen, H. Meta-analysis of the relationship between Parkinson disease and melanoma. *Neurology* **76,** 2002–2009 (2011).
383. Disse, M., Reich, H., Lee, P. K. & Schram, S. S. A Review of the Association Between Parkinson Disease and Malignant Melanoma. *Dermatol. Surg.* **42,** 141–6 (2016).
384. Escamez, M. J. *et al.* Capturing the biological impact of CDKN2A and MC1R genes as an early predisposing event in melanoma and non melanoma skin cancer. *Oncotarget* **5,** 1439–51 (2014).
385. Jones, E. A. *et al.* Interactions of Sox10 and Egr2 in myelin gene regulation. *Neuron Glia Biol.* **3,** 377–87 (2007).
386. O'Brien, J. S. & Sampson, E. L. Fatty acid and fatty aldehyde composition of the major brain lipids in normal human gray matter, white matter, and myelin. *J. Lipid Res.* **6,** 545–551 (1965).
387. Weyden, L. van der *et al.* Genome-wide in vivo screen identifies novel host regulators of metastatic colonization. *Nature* **541,** 233–236 (2017).
388. Kunkel, G. T., Maceyka, M., Milstien, S. & Spiegel, S. Targeting the sphingosine-1-phosphate axis in cancer, inflammation and beyond. *Nat. Rev. Drug Discov.* **12,** 688–702 (2013).
389. Visentin, B. *et al.* Validation of an anti-sphingosine-1-phosphate antibody as a potential therapeutic in reducing growth, invasion, and angiogenesis in multiple tumor lineages. *Cancer Cell* **9,** 225–238 (2006).
390. Seelan, R. S. *et al.* Human acid ceramidase is overexpressed but not mutated in prostate cancer. *Genes, Chromosom. Cancer* **29,** 137–146 (2000).

X. *APPENDIX*

APÉNDICES

UPREGULATED PROTEINS shRAB7/shControl		

PROTEIN	SK-Mel-103 log_2FC	UACC-62 log_2FC
ACADVL	0,42	0,48
ALDH4A1	0,44	0,42
ANXA4	0,31	0,52
ASPH	0,54	0,42
CALR	0,33	0,51
CANX	0,67	0,39
CCDC90B	0,47	0,44
CD151	0,31	0,55
CD59	0,48	0,49
CDK6	0,36	0,46
CLPTM1L	0,48	0,33
COMT	0,46	0,41
CRELD1	0,62	0,69
CTSA	0,49	0,31
CYB5R1	0,35	0,45
DEGS1	0,38	0,36
DNAJC25	0,31	0,46
ECE1	0,54	0,79
ENDOD1	0,55	1,05
EPDR1	0,33	0,40
FDXR	0,32	0,35
FKBP11	0,41	0,38
FNDC3B	0,34	0,43
FUNDC2	0,55	0,69
GAA	0,36	0,45
GALNT7	0,34	0,43
GBA	0,32	0,53
GGCX	0,35	0,77
HLA-A	0,47	0,45
HLA-A	0,45	0,42
IGF2BP3	0,34	0,63
KDELR1	0,61	0,43
KIAA0319L	0,61	0,89
LAMP1	0,58	0,74
LNP	0,39	0,76
LNX2	0,35	0,48
MAPRE3	0,31	0,56
MBOAT7	0,39	0,40
MFSD10	1,04	0,78
MLEC	0,40	0,48
MOGS	0,32	0,38
NAT14	0,59	0,48
NPEPPS	0,58	0,62
NRP1	0,39	0,60
P4HB	0,33	0,59
PBXIP1	0,42	0,90
PGM5	0,50	0,31
PI4KB	0,68	0,64
PLD3	0,35	0,53
PLIN2	0,57	0,35
PPCS	0,35	0,35
PRAF2	0,37	0,56
PRKCDBP	0,36	0,45
PTRF	0,53	0,34
QPCTL	0,62	0,69
RFT1	0,48	0,50
SCCPDH	0,39	0,42
SCFD1	0,31	0,43
SGSH	0,54	0,48
SIAE	0,38	0,52
SLC26A2	0,37	0,31
SMPD1	0,40	0,63
SSR3	0,74	0,31
STX18	0,34	0,31
SYNJ2BP	0,76	0,58
TCEAL3	0,46	0,73
TMBIM6	1,09	0,85
TMEM126A	0,57	0,43
TMEM2	0,92	0,63
TMEM245	0,43	0,45
TMEM43	0,52	0,32
TMEM59	0,59	0,42
TSPO	0,44	0,33
ZNF185	0,36	0,39

DOWNREGULATED PROTEINS shRAB7/shControl

PROTEIN	SK-Mel-103 log_2FC	UACC-62 log_2FC
ACLY	-0,38	-0,48
ASF1A	-0,37	-0,45
CANT1	-0,76	-0,81
COX15	-0,33	-0,48
COX17	-0,77	-0,66
DYNLT1	-0,43	-0,53
G6PD	-0,33	-0,79
GART	-0,32	-0,50
GATC	-0,75	-0,53
HELLS	-0,37	-1,89
HIRIP3	-0,41	-0,49
IDH1	-0,38	-0,50
LRWD1	-0,37	-0,35
MAD2L1	-0,32	-0,55
MRFAP1	-0,65	-0,60
NCAPH	-0,35	-0,48
NFYB	-0,46	-0,61
NUDT19	-0,39	-0,66
ORC2	-0,35	-0,37
PHGDH	-0,51	-0,41
QRICH1	-0,36	-0,37
RAB7A	-0,79	-1,76
RBFOX2	-0,32	-0,33
RRM2	-0,43	-0,50
SGTA	-0,54	-0,79
SLC1A5	-0,47	-0,51
SLC7A5	-0,42	-0,63
SMUG1	-0,44	-0,56
TCEA1	-0,31	-0,38
TCOF1	-0,81	-0,83
TGOLN2	-0,32	-0,36
TMPO	-0,38	-0,60
TXLNA	-0,34	-0,40
WBP2	-0,50	-0,66

Annex 1. List of proteins regulated in melanoma cell lines upon RAB7 (in both cell lines, SK-MEL-103 UACC-62) with fold change values. Pink: upregulated genes, green: downregulated genes.

UPREGULATED PROTEINS shRAB27/shControl

PROTEIN	SK-Mel-103 log_2FC	UACC-62 log_2FC
AACS	0,58	0,31
AGO2	0,59	0,71
AK1	0,58	0,37
ALB	0,87	1,15
ALG5	0,50	0,36
AMPD2	0,34	0,74
AP2B1	0,34	0,41
ARFGAP1	0,44	0,43
ASCC1	0,43	0,33
ATP6V0D1	0,73	0,36
ATP7A	0,66	0,96
ATXN3	0,32	0,38
BAG3	0,34	0,68
BET1	0,38	0,46
BIN1	0,48	0,57
BPNT1	0,32	0,33
C19orf10	0,37	0,88
C6orf211	0,59	0,78
CA13	0,59	0,50
CAMK2G	0,53	0,34
CAPZA1	0,32	0,42
CARHSP1	0,37	0,84
CASP6	0,63	0,48
CCDC47	0,32	0,34
CCNDBP1	0,65	0,64
CDK5	0,56	0,32
CDK6	0,50	1,07
CFL2	0,45	0,32
CHM	0,45	0,46
CHMP1A	0,44	0,40
CHMP4B	0,64	0,31
CLIC1	0,37	0,38
CLTB	0,31	0,51
CLTC	0,36	0,40
CMAS	0,41	0,46
CPOX	0,55	0,46
CPPED1	0,60	0,50
CRTAP	0,34	0,34
CTSD	0,88	0,67
CYB5R1	0,86	0,52
CYCS	0,42	0,58
DAPK3	1,30	0,57
DPCD	0,71	0,53
DYNC1LI1	0,31	0,40
EEA1	0,38	0,51
EFTUD1	0,31	0,59
EHD1	0,53	0,38
EOGT	0,34	0,95
ERP44	0,57	0,74
FAF2	0,40	0,36
FAM177A1	0,39	0,36
FNTA	0,40	0,36
FRYL	0,32	0,39
FSCN1	0,52	0,62
GAK	0,39	0,42
GALNT2	0,37	0,43
GAN	0,59	0,45
GDI1	0,44	0,44
GLO1	0,48	0,37
GLOD4	0,41	0,33
GLRX	0,40	0,79
GNA15	0,76	0,44
GNPDA1	0,68	0,33
GOLGA1	0,35	0,50
GOPC	0,57	0,51
GSTO1	0,32	0,37
HOMER3	0,31	0,50
HSPB8	0,91	0,66
IDH1	0,35	0,36
IGF2BP1	0,43	0,47
IL1RAP	0,67	0,34
IRGQ	0,52	0,39
ISG15	0,54	0,70
JMJD6	0,33	0,44
KATNAL1	0,76	0,49
KIAA1598	0,32	0,41
KIF1B	0,60	0,52
KTN1	0,35	0,32
LAMTOR2	0,72	0,41
LIMS3L	0,38	0,32
LMAN1	0,33	0,39
LRP1	0,76	0,39
LYPLA2	0,79	0,62
MAN1B1	0,56	0,55
MAPKAPK2	0,35	0,63
MAPRE3	0,89	0,70
MON2	0,43	0,37
NAPG	0,52	0,36
NAT1	0,36	0,52
NCEH1	0,79	0,66
NCKAP5L	0,82	0,79
NPEPPS	0,64	0,57
NRBP1	0,74	0,82
NSFL1C	0,44	0,56
OS9	0,33	0,32
P4HB	0,38	0,39
PCTP	0,79	0,37
PCYOX1	0,50	0,62
PEX13	0,84	0,42
PGAM1	0,33	0,47
PIP4K2C	0,61	0,37
PKN1	0,37	0,33
PLIN2	2,06	1,29
PLIN3	0,52	0,90
PPP3CC	0,35	0,56
PROSC	0,41	0,34
PSMB6	0,33	0,57
PSMD11	0,32	0,53
PSMD12	0,34	0,50
PSMD13	0,34	0,49
PSMD7	0,32	0,31
PTRHD1	0,41	0,55
RAB11FIP1	1,08	0,31
RAB18	0,72	0,35
RAB1A	0,80	0,39
RAB31	0,36	0,36
RAP2B	0,99	0,35
RASA2	0,62	0,67
REEP5	0,49	0,36
REXO2	0,44	0,76
RGS10	0,52	0,46
RINT1	0,51	0,60
RNPEP	0,32	0,39
RRAGC	0,49	0,31
RRM2B	0,49	0,63
RTKN	0,32	0,71
S100A11	0,40	0,38
S100A3	0,69	1,92
SCAMP2	0,54	0,37
SCAMP4	0,60	0,39
SCFD1	0,40	0,60
SEC22B	0,63	0,49
SEC62	0,83	0,32
SERPINE1	1,37	1,31
SERPINH1	0,84	0,87
SH3GL1	0,51	0,57
SLC25A24	0,51	0,43
SNX29	0,62	0,69
SSR1	0,40	0,51
STX12	0,90	0,49
STX18	0,68	0,41
TDG	0,94	0,48
TGOLN2	0,45	0,44
TMBIM6	1,23	0,92
TMCO1	0,84	0,43
TMED8	0,33	0,56
TMEM165	0,45	0,36
TMEM57	0,48	0,36
TOM1	0,58	0,76
TPD52L2	0,39	0,35
TRAFD1	0,32	0,53
TRPV2	0,81	0,70
TSC1	0,88	1,09
TSC22D2	0,36	0,33
TSTA3	0,32	0,55
TTC5	0,38	0,32
TUBB3	0,66	0,49
UBE2G1	0,48	0,56
UBE2H	0,41	0,32
UBXN4	0,32	0,35
UGGT1	0,51	0,32
VAMP3	0,48	0,36
VKORC1	0,35	0,33
WFS1	0,52	0,63
YIF1A	0,41	0,56
YIPF5	0,54	0,54
YKT6	0,56	0,42
YRDC	0,59	0,57
YWHAG	0,37	0,39
ZFAND5	0,59	1,03
ZMPSTE24	0,67	0,40

DOWNREGULATED PROTEINS shRAB27/shControl

PROTEIN	SK-Mel-103 log_2FC	UACC-62 log_2FC
AASS	-0,40	-0,41
ACADVL	-0,54	-0,77
ACOT2	-0,47	-0,39
ADCK4	-0,45	-0,60
ADI1	-0,34	-0,34
ANAPC7	-0,36	-0,31
APOBEC3B	-0,86	-0,75
ARHGDIA	-0,40	-0,42
ARPP19	-0,55	-0,45
ATP5SL	-0,50	-0,54
BBX	-0,52	-0,40
BET1L	-0,51	-0,49
BICD2	-0,48	-0,39
BYSL	-0,36	-0,32
BZW2	-0,45	-1,06
C14orf159	-0,83	-0,32
CADM1	-0,69	-0,33
CALR	-0,35	-0,31
CARS2	-0,43	-0,35
CAST	-0,51	-0,33
CCDC12	-0,38	-0,32
CCDC43	-0,55	-0,42
CCNK	-0,51	-0,48
CD151	-0,57	-0,83
CDK8	-0,49	-0,38
CELF1	-0,78	-0,46
CHTF18	-0,52	-0,73
CMSS1	-0,34	-0,42
CNOT2	-0,32	-0,32
COMMD6	-0,39	-0,37
COQ6	-0,53	-0,39
COX5B	-0,59	-0,36
COX6C	-0,43	-0,69
CSE1L	-0,34	-0,32
CUL4B	-0,49	-0,40
CUX1	-0,34	-0,31
DAP3	-0,53	-0,41
DCK	-0,71	-0,33
DECR2	-0,33	-0,65
DHRS11	-0,61	-0,54
DIAPH1	-0,68	-0,40
DIMT1	-0,47	-0,64
DNLZ	-0,37	-0,58
DUS3L	-0,48	-0,42
EARS2	-0,44	-0,62
EHMT1	-0,61	-0,36
EIF2A	-0,68	-0,44
ENSA	-1,13	-0,51
ERAL1	-0,34	-0,40
ERBB2IP	-0,64	-0,33
ERI1	-0,74	-0,51
ETV6	-0,42	-0,41
EXOC6	-0,70	-1,04
EXOSC1	-0,59	-0,48
FADS1	-0,60	-0,80
FAH	-0,62	-0,34
FAM136A	-0,53	-0,52
FAM213A	-0,38	-0,67
FANCI	-1,15	-0,81
FEN1	-0,36	-0,31
FTH1	-1,41	-0,44
FUT8	-0,79	-0,35
GADD45GIP1	-0,74	-0,60
GAPVD1	-0,78	-0,49
GATC	-0,57	-0,78
GNAQ	-0,35	-0,42
GOT1	-0,52	-0,42
H1FX	-1,09	-0,50
HADH	-0,92	-0,53
HAX1	-0,32	-0,40
HDAC1	-0,91	-0,64
HELLS	-1,42	-0,82
HIRA	-0,46	-0,58
HIRIP3	-0,97	-0,44
HIST1H1D	-0,93	-0,47
HIST1H4A	-0,39	-0,50
HIST2H2BD	-0,64	-0,50
HK2	-0,36	-0,37
HLA-A	-0,57	-0,39
HLTF	-0,37	-0,48
HMGB3	-0,81	-0,46
HMGCS1	-0,52	-0,49
HSPA9	-0,70	-0,72
IQGAP3	-0,78	-0,63
ITGA4	-0,36	-0,53
ITGA6	-0,42	-0,67
ITGB1	-0,40	-0,37
JUND	-0,46	-0,40
KIAA1524	-0,54	-0,44
KIF2C	-0,73	-0,54
KLF16	-0,35	-0,41
KPNA2	-0,64	-0,56
L3HYPDH	-0,65	-0,69
LARP1	-0,54	-0,57
LIG1	-0,55	-0,47
LIMCH1	-0,61	-0,37
LMO7	-0,36	-0,51
LPCAT1	-0,33	-0,41
LRRFIP2	-0,70	-0,44
MAD2L1	-0,63	-0,64
MBLAC2	-0,57	-0,78
MCM2	-1,23	-0,40
MCM3	-1,20	-0,44
MCM5	-0,89	-0,55
MCM6	-1,17	-0,47
MCMBP	-0,75	-0,49
MCU	-0,39	-0,39
MGEA5	-0,91	-0,54
MORF4L1	-0,73	-0,64
MP68	-0,79	-1,53
MRPL10	-0,66	-0,72
MRPL11	-0,76	-0,44
MRPL14	-0,56	-0,33
MRPL18	-0,54	-0,36
MRPL19	-0,62	-0,37
MRPL21	-0,62	-0,42
MRPL22	-0,47	-0,32
MRPL24	-0,59	-0,36
MRPL27	-0,49	-0,32
MRPL28	-0,73	-0,46
MRPL3	-0,54	-0,36
MRPL32	-0,35	-0,42
MRPL33	-0,58	-0,53
MRPL37	-0,64	-0,43
MRPL4	-0,47	-0,32
MRPL41	-0,80	-0,53
MRPL43	-0,51	-0,34
MRPL47	-0,70	-0,44
MRPL48	-0,54	-0,32
MRPL53	-0,46	-0,46
MRPL57	-0,87	-0,46
MRPL9	-0,45	-0,46
MRPS12	-0,37	-0,48
MRPS16	-0,44	-0,69
MRPS18A	-0,51	-0,54
MRPS18B	-0,38	-0,61
MRPS2	-0,35	-0,41
MRPS23	-0,43	-0,36
MRPS25	-0,51	-0,44
MRPS27	-0,42	-0,31
MRPS28	-0,75	-0,69
MRPS30	-0,75	-0,54
MRPS34	-0,60	-0,39
MRPS9	-0,33	-0,50
MT-ATP6	-0,38	-0,66
MTHFS	-0,34	-0,36
MTMR1	-0,56	-0,73
MT-ND2	-0,65	-1,00
MT-ND5	-0,48	-0,37
NAGK	-0,48	-0,72
NCAPD2	-0,84	-0,32
NCAPG	-0,69	-0,33
NCAPH	-1,00	-0,39
NDUFA10	-0,54	-0,39
NDUFA12	-0,76	-0,60
NDUFA2	-0,83	-0,54
NDUFA7	-0,65	-0,37
NDUFA8	-0,50	-0,43
NDUFA9	-0,43	-0,42
NDUFAF7	-0,60	-0,48
NDUFB3	-0,59	-0,33
NDUFB6	-0,46	-0,49
NDUFC2	-0,69	-0,67
NDUFS1	-0,61	-0,31
NDUFS4	-0,67	-0,54
NDUFS5	-0,43	-0,47
NDUFS6	-0,58	-0,42
NDUFS7	-0,40	-0,45
NDUFV1	-0,66	-0,43
NDUFV2	-0,61	-0,42
NFIC	-1,24	-0,75

DOWNREGULATED PROTEINS shRAB27/shControl

PROTEIN	SK-Mel-103 log_2FC	UACC-62 log_2FC
NOA1	-0,64	-0,50
NOLC1	-1,00	-0,90
NOVA2	-1,11	-0,43
NQO1	-1,21	-0,76
NRAS	-0,47	-0,48
NT5C2	-0,50	-0,34
NT5DC3	-0,66	-0,33
NUDT1	-0,49	-0,62
NUF2	-1,07	-1,25
NUP188	-0,45	-0,36
NUP43	-0,41	-0,32
NUP85	-0,33	-0,46
OARD1	-0,45	-0,78
OLA1	-0,76	-0,83
ORC4	-0,57	-0,32
ORC5	-0,50	-0,48
PARN	-0,40	-0,46
PBK	-0,54	-0,51
PDCD5	-0,39	-0,39
PDPR	-0,59	-0,43
PEF1	-0,46	-0,42
PFDN1	-0,51	-0,50
PFN2	-0,97	-0,70
PHF6	-0,79	-0,90
PITPNB	-0,75	-0,55
PLSCR1	-0,80	-1,65
PM20D2	-0,58	-0,36
PNKP	-0,37	-0,61
POLR1E	-0,53	-0,71
PPP1CC	-0,70	-0,82
PRAME	-0,68	-0,33
PRIM2	-0,70	-0,55
PRKAR1A	-0,32	-0,41
PRKAR2B	-0,44	-0,41
PRPS2	-0,49	-0,36
PRTFDC1	-0,38	-0,44
PSIP1	-0,48	-0,43
PSMB9	-0,40	-0,60
PSMG1	-0,31	-0,39
QKI	-0,66	-0,78
RAB38	-0,37	-0,69
RAB8A	-0,45	-0,54
RABGAP1	-0,48	-0,39
RARS2	-0,77	-0,45
RASSF8	-0,39	-0,42
RBBP7	-0,65	-0,44
RBBP9	-0,67	-0,73
RBMXL1	-0,54	-0,36
RCC1	-0,70	-0,57
RFC4	-0,78	-0,52
RFC5	-0,68	-0,41
RHOA	-0,33	-0,51
ROCK1	-0,45	-0,48
RPGRIP1	-0,86	-0,97
RPS15A	-0,34	-0,52
RPS3	-0,37	-0,32
RQCD1	-0,48	-0,36

PROTEIN	SK-Mel-103 log_2FC	UACC-62 log_2FC
RRM2	-1,35	-0,43
SAMHD1	-0,62	-0,53
SARM1	-0,35	-0,82
SARS2	-0,37	-0,38
SCARB1	-0,32	-1,47
SCD	-0,61	-1,26
SELENBP1	-0,35	-0,61
SH3BP4	-0,51	-0,33
SHCBP1	-0,96	-0,43
SHMT1	-0,38	-0,35
SLC1A5	-0,99	-0,42
SLC25A11	-0,36	-0,73
SLC39A1	-0,64	-0,76
SLC3A2	-1,00	-0,75
SLFN11	-0,59	-0,54
SMARCC1	-1,13	-0,43
SMC2	-0,98	-0,35
SNF8	-0,51	-0,76
SPATS2L	-1,08	-0,92
SPC25	-0,66	-0,64
SRPK1	-0,48	-0,65
SSBP1	-0,74	-0,45
STAT5B	-0,38	-0,56
STMN1	-0,51	-0,33
TFAM	-0,40	-0,47
TFB1M	-0,58	-0,60
TMEM2	-0,88	-1,01
TMPO	-1,17	-1,03
TOP2A	-0,70	-0,91
TRAP1	-0,56	-0,72
TRIP13	-0,63	-0,46
TTL	-0,40	-0,38
TXLNG	-0,47	-0,43
TXN	-0,44	-0,31
TYMS	-0,62	-0,55
UBAP2	-0,37	-0,61
UBR7	-0,80	-0,34
UBTF	-0,49	-0,34
UCHL3	-0,61	-0,74
UQCC2	-0,48	-0,44
USMG5	-0,64	-0,85
USP48	-0,40	-0,36
VILL	-1,39	-1,72
VPS25	-0,40	-0,51
VPS36	-0,50	-0,37
VRK1	-0,38	-0,70
WDFY1	-0,52	-1,07
WRNIP1	-0,62	-0,31
WWTR1	-1,12	-0,49
XPO7	-0,44	-0,35
XPOT	-0,39	-0,32
YARS2	-0,66	-0,44
ZAK	-0,57	-0,43
ZMAT2	-0,62	-0,41

Annex 2. List of proteins regulated in melanoma cell lines upon RAB27 (in both cell lines, SK-MEL-103 UACC-62) with fold change values. Pink: upregulated genes, green: downregulated genes.

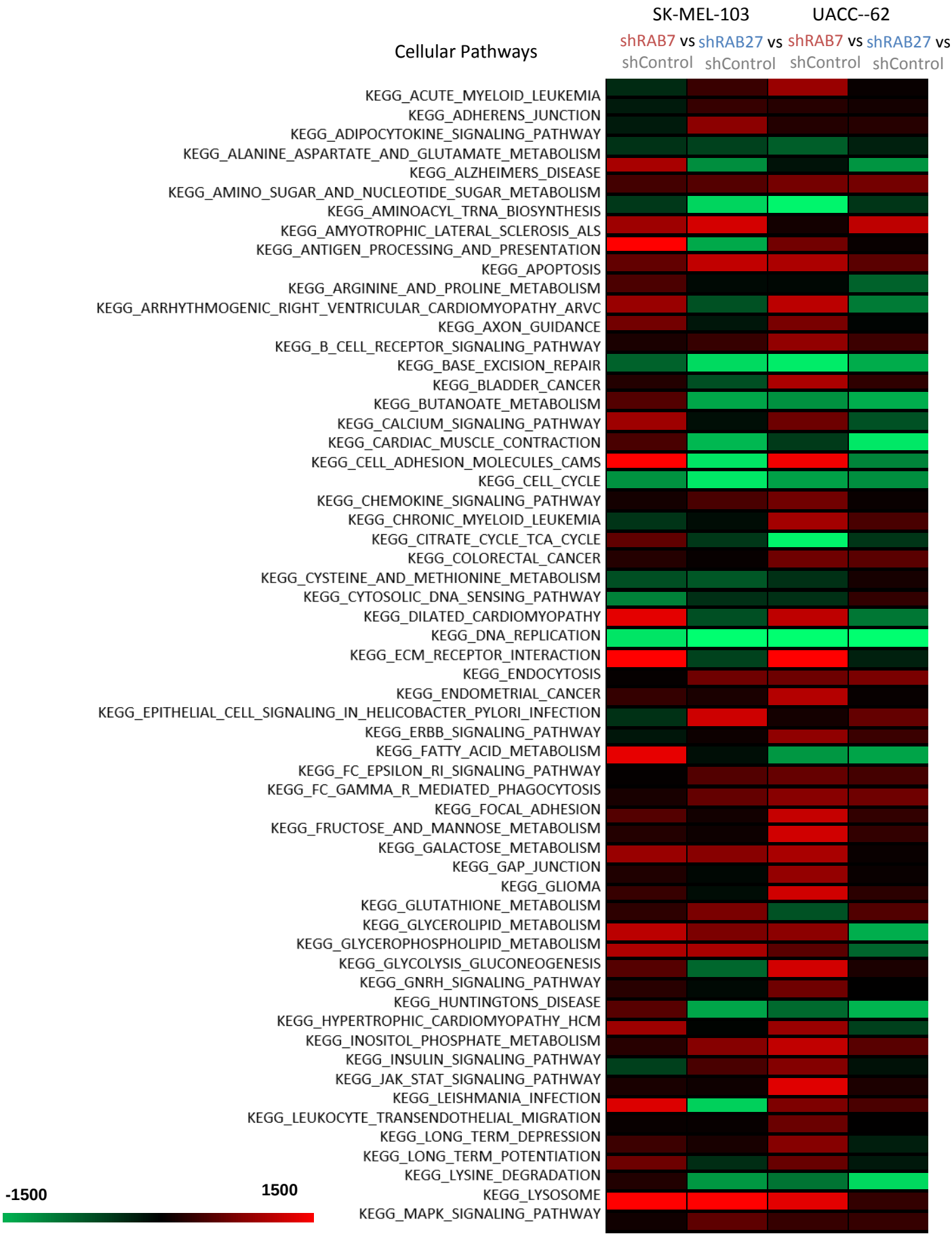
SK-MEL-103
UACC--62
Cellular Pathways
shRAB7 vs shControl
shRAB27 vs shControl
shRAB7 vs shControl
shRAB27 vs shControl
KEGG_ACUTE_MYELOID_LEUKEMIA
KEGG_ADHERENS_JUNCTION
KEGG_ADIPOCYTOKINE_SIGNALING_PATHWAY
KEGG_ALANINE_ASPARTATE_AND_GLUTAMATE_METABOLISM
KEGG_ALZHEIMERS_DISEASE
KEGG_AMINO_SUGAR_AND_NUCLEOTIDE_SUGAR_METABOLISM
KEGG_AMINOACYL_TRNA_BIOSYNTHESIS
KEGG_AMYOTROPHIC_LATERAL_SCLEROSIS_ALS
KEGG_ANTIGEN_PROCESSING_AND_PRESENTATION
KEGG_APOPTOSIS
KEGG_ARGININE_AND_PROLINE_METABOLISM
KEGG_ARRHYTHMOGENIC_RIGHT_VENTRICULAR_CARDIOMYOPATHY_ARVC
KEGG_AXON_GUIDANCE
KEGG_B_CELL_RECEPTOR_SIGNALING_PATHWAY
KEGG_BASE_EXCISION_REPAIR
KEGG_BLADDER_CANCER
KEGG_BUTANOATE_METABOLISM
KEGG_CALCIUM_SIGNALING_PATHWAY
KEGG_CARDIAC_MUSCLE_CONTRACTION
KEGG_CELL_ADHESION_MOLECULES_CAMS
KEGG_CELL_CYCLE
KEGG_CHEMOKINE_SIGNALING_PATHWAY
KEGG_CHRONIC_MYELOID_LEUKEMIA
KEGG_CITRATE_CYCLE_TCA_CYCLE
KEGG_COLORECTAL_CANCER
KEGG_CYSTEINE_AND_METHIONINE_METABOLISM
KEGG_CYTOSOLIC_DNA_SENSING_PATHWAY
KEGG_DILATED_CARDIOMYOPATHY
KEGG_DNA_REPLICATION
KEGG_ECM_RECEPTOR_INTERACTION
KEGG_ENDOCYTOSIS
KEGG_ENDOMETRIAL_CANCER
KEGG_EPITHELIAL_CELL_SIGNALING_IN_HELICOBACTER_PYLORI_INFECTION
KEGG_ERBB_SIGNALING_PATHWAY
KEGG_FATTY_ACID_METABOLISM
KEGG_FC_EPSILON_RI_SIGNALING_PATHWAY
KEGG_FC_GAMMA_R_MEDIATED_PHAGOCYTOSIS
KEGG_FOCAL_ADHESION
KEGG_FRUCTOSE_AND_MANNOSE_METABOLISM
KEGG_GALACTOSE_METABOLISM
KEGG_GAP_JUNCTION
KEGG_GLIOMA
KEGG_GLUTATHIONE_METABOLISM
KEGG_GLYCEROLIPID_METABOLISM
KEGG_GLYCEROPHOSPHOLIPID_METABOLISM
KEGG_GLYCOLYSIS_GLUCONEOGENESIS
KEGG_GNRH_SIGNALING_PATHWAY
KEGG_HUNTINGTONS_DISEASE
KEGG_HYPERTROPHIC_CARDIOMYOPATHY_HCM
KEGG_INOSITOL_PHOSPHATE_METABOLISM
KEGG_INSULIN_SIGNALING_PATHWAY
KEGG_JAK_STAT_SIGNALING_PATHWAY
KEGG_LEISHMANIA_INFECTION
KEGG_LEUKOCYTE_TRANSENDOTHELIAL_MIGRATION
KEGG_LONG_TERM_DEPRESSION
KEGG_LONG_TERM_POTENTIATION
KEGG_LYSINE_DEGRADATION
KEGG_LYSOSOME
KEGG_MAPK_SIGNALING_PATHWAY
-1500
1500

Annex 3. Enriched biological processes identified from changes in the Proteome of the indicated cell lines defined by KEGG database

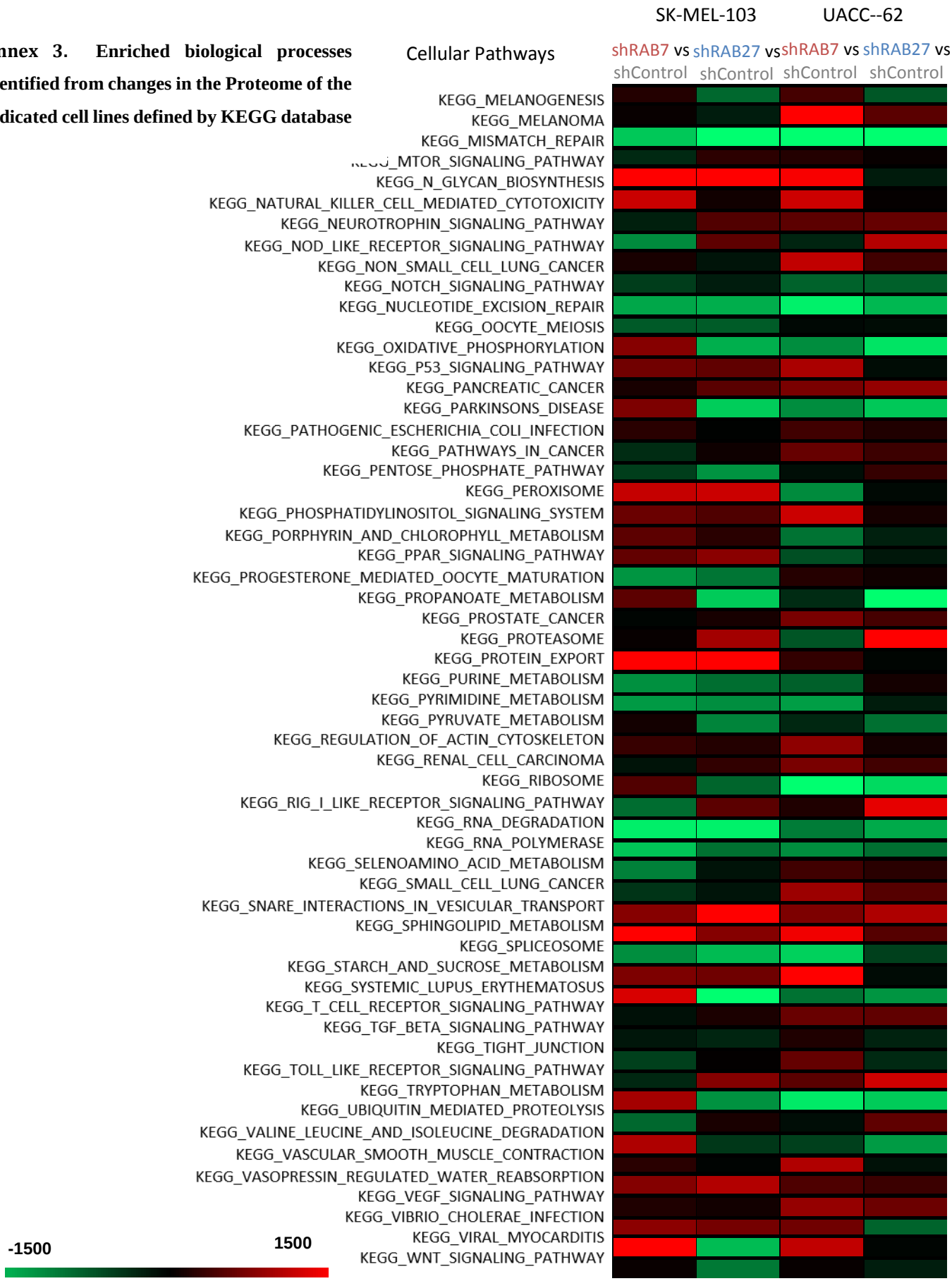

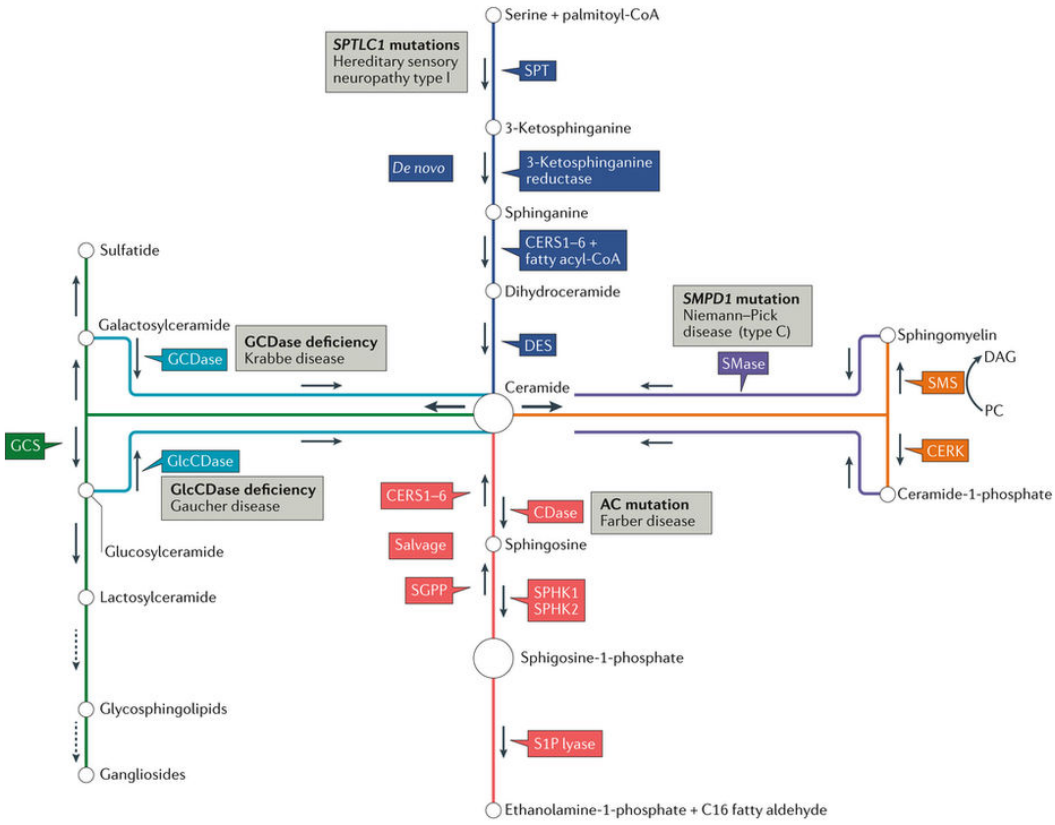

Figure S1. Schematic representation of sphingolipid metabolism. De novo synthesis pathway of ceramide, (blue). Synthesis/degradation of glucosylceramides (green/light blue) and sphingomyelin (orange/purple). Ceramide degradation (red). Diseases associated with enzymes mutations are depicted in gray boxes. Ref[314]

GO	GO Term	GO ID	Proteins	FDR	Proteins identified
Biological Process	vesicle-mediated transport	GO.0016192	12	0.0429	IGF2R,LGI3,LMAN1,LMAN2,**LRP2**,MCFD2,PPT1,PSAP,SCG3, TXNDC5,VEGFA,VLDLR
	single-organism catabolic process	GO.0044712	11	0.0429	COL7A1,CSPG4,CTSD,FUCA1,GM2A,LIPA,MMP15,MMP8, PLBD2,PPT1,PXDN
Molecular Function	hydrolase activity, hydrolyzing O-glycosyl compounds	GO.0004553	5	0.00797	FUCA1,GANAB,GM2A,MAN2B1,NAGLU
	carbohydrate binding	GO.0030246	7	0.00797	GANAB,IGF2R,LGALS1,LMAN1,LMAN2,MAN2B1,PAM
	mannose binding	GO.0005537	3	0.00899	IGF2R,LMAN1,LMAN2
	endonuclease activity, active with either ribo- or deoxyribonucleic acids and producing 3 -phosphomonoesters	GO.0016894	3	0.00899	DNASE2,RNASE1,RNASET2
	monosaccharide binding	GO.0048029	4	0.0116	IGF2R,LMAN1,LMAN2,PAM
Cellular Composition	extracellular region part	GO.0044421	35	2.24e-13	CADM4,COL7A1,CREG1,CSPG4,CTSC,CTSD,DNASE2,ERAP1, FAM3C,FKBP2,FUCA1,GANAB,GM2A,IGF2R,LGALS1,LIPA, LMAN1,LMAN2,**LRP2**,MAN2B1,MMP8,NAGLU,PAM,PLBD2, PSAP,PTPRZ1,PXDN,RNASE1,RNASET2,S100B,SEMA3E,STC1, TXNDC5,VEGFA,VLDLR
	extracellular region	GO.0005576	37	2.47e-13	CADM4,COL7A1,CREG1,CSPG4,CTSC,CTSD,DNASE2,ERAP1, FAM3C,FKBP2,FUCA1,GANAB,GM2A,IGF2R,ISM2,ITIH6,LGALS1, LGI3,LIPA,LMAN1,LMAN2,**LRP2**,MAN2B1,MMP8,NAGLU,PAM, PLBD2,PSAP,PTPRZ1,PXDN,RNASE1,RNASET2,SCG3,SEMA3E, TXNDC5,VEGFA,VLDLR
	membrane-bounded vesicle	GO.0031988	33	1.14e-12	CADM4,CREG1,CSPG4,CTSC,CTSD,DNASE2,ERAP1,FAM3C, FKBP2,FREM2,FUCA1,GANAB,GM2A,IGF2R,LGALS1,LGI3,LIPA, LMAN1,LMAN2,MAN2B1,MCFD2,MFI2,NAGLU,PAM,PLBD2, PPT1,PSAP,PXDN,RNASE1,RNASET2,SCG3,TXNDC5,VEGFA
	extracellular exosome	GO.0070062	30	1.31e-12	CADM4,CREG1,CSPG4,CTSC,CTSD,DNASE2,ERAP1,FAM3C, FKBP2,FREM2,FUCA1,GANAB,GM2A,IGF2R,LGALS1,LIPA, LMAN1,LMAN2,**LRP2**,MAN2B1,MFI2,NAGLU,PAM,PLBD2, PPT1,PSAP,PXDN,RNASE1,RNASET2,TXNDC5
	lysosome	GO.0005764	16	1.56e-12	CSPG4,CTSC,CTSD,DNASE2,FUCA1,GM2A,IGF2R,LIPA,**LRP2**, MAN2B1,NAGLU,PLBD2,PPT1,PSAP,RNASET2,TXNDC5
	lysosomal lumen	GO.0043202	9	3.59e-11	CSPG4,CTSD,GM2A,NAGLU,PLBD2,PPT1,PSAP,RNASET2, TXNDC5
	vacuolar part	GO.0044437	11	7.79e-08	CSPG4,CTSD,GM2A,IGF2R,**LRP2**,NAGLU,PLBD2,PPT1,PSAP, RNASET2,TXNDC5
	extracellular space	GO.0005615	17	1.62e-07	COL7A1,CTSC,CTSD,ERAP1,LGALS1,LMAN2,MFI2,MMP8,PPT1, PSAP,PXDN,RNASET2,S100B,SEMA3E,STC1,VEGFA,VLDLR
	extracellular matrix	GO.0031012	8	0.000216	COL7A1,FREM2,LGALS1,MMP15,MMP8,PTPRZ1,PXDN,VEGFA
	endoplasmic reticulum lumen	GO.0005788	6	0.000627	COL7A1,ERAP1,GANAB,RCN2,RNASET2,TXNDC5
	proteinaceous extracellular matrix	GO.0005578	7	0.00116	COL7A1,FREM2,LGALS1,MMP8,PTPRZ1,PXDN,VEGFA
	cytoplasmic membrane-bounded vesicle	GO.0016023	11	0.00128	CTSD,FAM3C,GANAB,IGF2R,LGI3,LMAN1,**LRP2**,MCFD2,PPT1, SCG3,VEGFA
	cell surface	GO.0009986	9	0.00236	CSPG4,DCBLD2,IGF2R,LGALS1,LMAN2,MFI2,SEMA7A,VEGFA, VLDLR
	endoplasmic reticulum	GO.0005783	12	0.0123	COL7A1,CTSC,ERAP1,FKBP2,LMAN1,LMAN2,**LRP2**,MCFD2, PXDN,RCN2,RNASET2,TXNDC5
	Golgi apparatus	GO.0005794	11	0.0178	CSPG4,CTSC,FAM3C,GANAB,IGF2R,LMAN1,LMAN2,**LRP2**, MCFD2,PPT1,PSAP
	endomembrane system	GO.0012505	18	0.0312	COL7A1,CSPG4,CTSC,ERAP1,FAM3C,FKBP2,LMAN1,LMAN2, MCFD2,PPT1,PSAP,PXDN,RCN2,RNASET2,SCG3,TXNDC5, VEGFA,VLDLR
	transport vesicle	GO.0030133	4	0.0401	IGF2R,LMAN1,MCFD2,SCG3
	transport vesicle membrane	GO.0030658	3	0.0404	LMAN1,MCFD2,SCG3
	endoplasmic reticulum-Golgi intermediate compartment	GO.0005793	3	0.0497	LMAN1,LMAN2,MCFD2

Annex 5. List of genes regulated in each Gene Ontology Terms found to be significantly enriched in UACC-62 shRAB7 specifically secreted proteins.